Final Technical Report

An Industry/Academe Consortium for Achieving 20% wind by 2030 through Cutting-Edge Research and Workforce Training.

December 2013

DOE Award Number: DE-E0002980

Project Period: January 15, 2010 – August 31, 2013

Submitted by:
Eolos Wind Energy Research Consortium
University of Minnesota

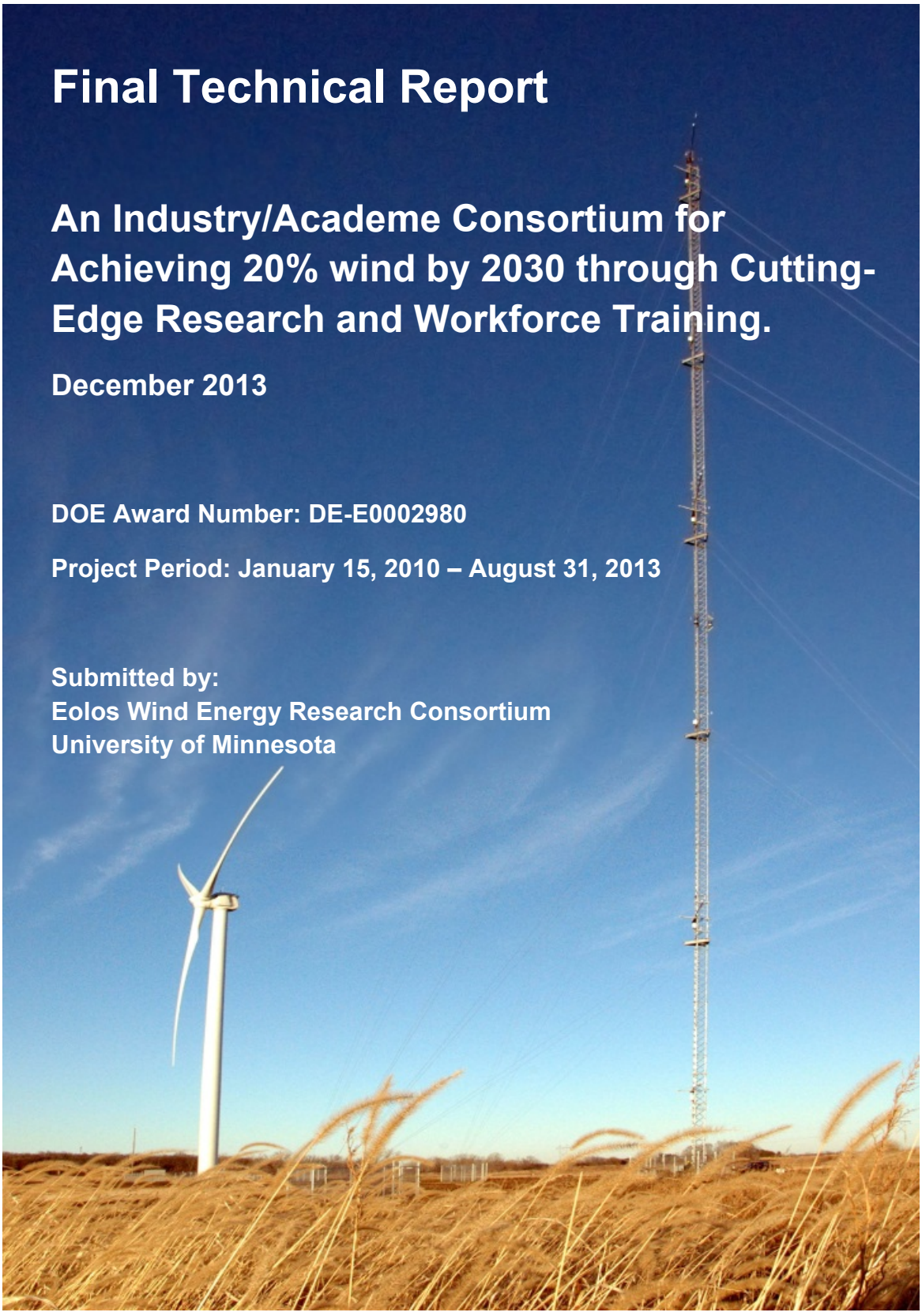

(This page intentionally left blank)

Final Technical Report

Project Title: An Industry/Academe Consortium for Achieving 20% Wind by 2030 through Cutting-Edge Research and Workforce Training

DOE Award Number: DE-EE0002980

Project Period: January 15, 2010 – August 31, 2013

Primary Award Recipient:
University of Minnesota
Saint Anthony Falls Laboratory
2 3rd Ave SE
Minneapolis, MN 55414

Principle Investigator: Fotis Sotiropoulos, Professor of Civil Engineering and Director of St. Anthony Falls Laboratory, fotis@umn.edu, 612-624-2022

Report Prepared by:
Fotis Sotiropoulos
Jeff Marr
Chris Milliren
Mos Kaveh
Ned Mohan
Henryk Stolarski
Mark Glauser
Roger Arndt
And other co-authors

Working Partners:
3M – Memo Izzi
Clipper Windpower – Tony Chobot
Lockheed Martin – Robert Monson
Syracuse University – Mark Glauser
WindLogics – Jennifer Leise

Cost Sharing Support provide by:
College of Science and Engineering, University of Minnesota
Initiative for Renewable Energy and the Environment, University of Minnesota,
Lockheed Martin
St. Anthony Falls Laboratory, University of Minnesota
Syracuse University
UMore Park, University of Minnesota
WindLogics
Xcel Energy

DOE Project Team:

DOE HQ Program Manager – Jose Zayas
DOE Field Contract Officer – Pamela Brodie
DOE Field Grants Management Specialist – Laura Merrick
DOE Field Project Officer – Gary Nowakowski
DOE/CNJV Project Monitor – Melissa (Luken) Callaway

Date of Report: December 15, 2013

Table of Contents

(This page intentionally left blank)

List of Acronyms

AAAS	American Association for the Advancement of Science
ADS	Azimuth-Doppler Spectrum
AIAA	American Institute of Aeronautics and Astronautics
AMS	American Meteorological Society
ASME	American Society of Mechanical Engineers
BEM	Blade Element Momentum
CBR	California Bearing Ratio
CEU	Continuing Education Credits
CFD	Computational Fluid Dynamics
CPPM	Capital Planning and Project Management
CT	Current Transducer
CURVIB	Curvilinear immersed boundary method
CUSP	Consortium of Universities for Sustainable Power
DAQ	Data Acquisition
dBA	Decibel A-weighted
DC	Direct current
DFT	Discrete Fourier Transforms
DOE	Department of Energy
dof	Degree of freedom
EA	Environmental Assessment
E-MCP	Enhanced measure-correlate-predict
FAA	Federal Aviation Administration
FOA	Funding Opportunity Announcement.
FONSI	Finding of No Significant Impact
FSI	Fluid-Structure Interaction
GMRES	Generalized minimal residual method
GOW	Gopher Ordinance Works
IEC	International Electrotechnical Commission
IEEE	Institute of Electrical and Electronics Engineers
I/Q	in-phase/quadrature
Ksf	kilo pounds per square foot
kV	kiloVolt
LES	Large Eddy Simulation
LIDAR	Light Detection and Ranging
LM	Lockheed Martin
LMP	Locational Marginal Price
MPI	Message Passing Interface
MRC	Mesabi Range College
MTI	Moving Target Indicator
NEPA	National Environmental Policy Act
NREL	National Renewable Energy Laboratory
NRHP	National Registry of Historic Places
MTI	Moving target indicator

MW	Megawatt
OMS	Operation and Maintenance Service Agreement
OEM	Original Equipment Manufacturer
pcf	Pounds per cubic foot
PDD	Phase Difference Detector
PDP	Power Distribution Panel
PIV	Particle Image Velocimetry
PPA	Power Purchase Agreement
PT	Power Transducer
PWM	Pulse Width Modulator
R&D	Research and Development
RANS	Reynolds-averaged Navier–Stokes
RMS	root mean square
ROC	Receiver operator characteristics
SAFL	St. Anthony Falls Laboratory, University of Minnesota
SCADA	Supervisory Control and Data Acquisition
SHPO	State Historic Preservation Office
SOPO	Statement of Project Objectives
SPD	Standard Proctor Density
SWA	Sliding Window Average
TSA	Turbine Supply Agreement
UMN	University of Minnesota
VWiS	Virtual Wind Simulator
WRF	Weather Research and Forecasting
WTG	Wind turbine generator

Lists of Figures

List of Tables

(This page intentionally left blank)

List of Appendices

(This page intentionally left blank)

Acknowledgment, Disclaimer and Proprietary Data Notice

Acknowledgment: This report is based upon work supported by the U. S. Department of Energy under Award No. DE-EE0002980

(This page intentionally left blank)

Executive Summary

In January 2010, the University of Minnesota, along with academic and industry project partners, began work on a four year project to establish new facilities and research in strategic areas of wind energy necessary to move the nation towards a goal of 20% wind energy by 2030. The project was funded by the U.S. Department of Energy with funds made available through the American Recovery and Reinvestment Act of 2009. $7.9M of funds were provided by DOE and $3.1M was provided through matching funds. The project was organized into three Project Areas. Project Area 1 focused on design and development of a utility scale wind energy research facility to support research and innovation. The project commissioned the Eolos Wind Research Field Station in November of 2011. The site, located 20 miles from St. Paul, MN operates a 2.5MW Clipper Liberty C-96 wind turbine, a 130-ft tall sensored meteorological tower and a robust sensor and data acquisition network. The site is operational and will continue to serve as a site for innovation in wind energy for the next 15 years. Project Areas 2 involved research on six distinct research projects critical to the 20% Wind Energy by 2030 goals. The research collaborations involved faculty from two universities, over nine industry partners and two national laboratories. Research outcomes include new knowledge, patents, journal articles, technology advancements, new computational models and establishment of new collaborative relationships between university and industry. Project Area 3 focused on developing educational opportunities in wind energy for engineering and science students. The primary outcome is establishment of a new graduate level course at the University of Minnesota called *Wind Engineering Essentials*. The seminar style course provides a comprehensive analysis of wind energy technology, economics, and operation. The course is highly successful and will continue to be offered at the University. The vision of U.S. DOE to establish unique, open-access research facilities and creation of university-industry research collaborations in wind energy were achieved through this project. The University of Minnesota, through the establishment of the Eolos Wind Energy Consortium and the Eolos Wind Research Field Station continue to develop new research collaborations with industry partners.

(This page intentionally left blank)

Introduction

In January 2010, the University of Minnesota began work on a multi-year project to establish new national research collaborations in Wind Energy. The Eolos Wind Energy Research Consortium was established with funding support provided by the U.S. Department of Energy through the 2009 American Recovery and Reinvestment Act. The project titled, An Industry/Academe Consortium for Achieving 20% Wind by 2030 Through Cutting-Edge Research and Workforce Training, was completed in August of 2013 and successfully achieved all stated project objectives. The project has also established a solid foundation of research collaboration and unique research facilities that will support U.S.-based wind energy research and development into the future.

The University of Minnesota established the **Eolos Wind Energy Research Consortium** to stimulate collaboration between industry and academia to accelerate the wind energy industry toward meeting the Department of Energy's 20% Wind Energy by 2030 goals. The objectives of the project were: 1) to develop a mix of full-scale and laboratory-scale wind energy research facilities enabling cost-effective development and real-world testing and demonstration, including collection of field-scale data; 2) to utilize the facilities to develop and execute a research agenda driven by industry need; and 3) to develop new curricula and educational initiatives to train next generation wind industry leaders. The total cash funding from the Department of Energy was $7,981,677.00 and included an additional $3,077,816 in project cost share.

The project developed and commissioned the **Eolos Wind Research Field Station**, a utility scale wind energy research facility located 20 miles from the University of Minnesota, Twin Cities campus and 14 miles (as the crow flies) from the Minneapolis/St. Paul International Airport. The centerpiece of the field station is a paired 2.5 Megawatt (MW) horizontal axis turbine and ~130-meter tall meteorological tower. The field station allows university and industry partners the opportunity to research, develop and deploy technologies at full-scale and utilize an advanced sensor and data acquisition network. The field station, operating since October 2011, serves as a highly accessible and visible demonstration facility that is now available to the U.S. Wind Energy Industry for research innovation for the next 15 years.

In addition to establishing the Eolos Wind Research Field Station, the University of Minnesota carried out six research tasks focused on improving wind turbine energy output, decreasing maintenance costs, and removing barriers to development. The research programs are described in detail in the research section of this report. Over 20 academic and industry partners participated in the construction, research and curriculum development over the course of the project. Two Patents were obtained as a result of one of the projects. In addition, the academic course developed as part of the educational goals of the project, Wind Engineering Essentials, will continue to be offered at the University of Minnesota as well as online in several formats for years to come.

In the sections below, the establishment of the Eolos Research Field Station, the research tasks, and the educational initiatives are described in detail.

Background

The impetus for the project solicitation was largely based on barriers identified in the "20% Wind Energy by 2030" report issued by the U.S. Department of Energy (DOE) in July of 2008. The report found that the nation possesses wind energy resources sufficient to meet the 20% wind energy by 2030 scenario. The major challenges identified in the report include availability of electric transmission and ability to integrate large amounts of wind energy, continued reduction in wind capital costs and improvement in turbine performance through technology advancement, and improved domestic supply chain and manufacturing capabilities. A surge in wind capacity will require a trained and educated workforce that can manufacture, install, operate and maintain wind turbines and operate the Nation's electricity transmission infrastructure.

The stated goal of this Funding Opportunity Announcement (FOA 0000090) was to, "fund consortia between institutions of higher learning and industry that will perform focused research on critical wind energy challenges" and suggested that proposals must address specific challenges identified in the 2030 report. The FOA sought proposals in two topic areas listed below. The University proposal focused on topic area 1.

1) **Partnerships for Wind Research and Turbine Reliability**: Universities in regions of the country in a Power Class 3 at 50 meters or greater wind region with consistent wind resources throughout the year are encouraged to team with industry partners to establish facilities/equipment and a research agenda necessary to study major challenges facing today's wind industry. Proposals must address one or more challenges described in the "20% Wind Energy by 2030" report and shall include descriptions of how the wind hardware and software will be acquired. DOE highly encourages research in "turbine reliability" as a topic in any consortia proposal.

2) **Wind Energy Research & Development**: University R&D to advance material design, performance measurements, analytical models, and leveraging partnerships with industry to improve power systems operations, maintenance or repair operations, wind turbine and/or component manufacturing, and interdisciplinary system integration. Fellowships, internships, etc. may be used to support the research agenda. Universities are encouraged to partner with the wind industry in defining their R&D agenda, developing their curriculum, and intern partnerships.

The funding for this program was appropriated by the American Recovery and Reinvestment Act of 2009 (Pub.L. 111-5). The Recovery Act's purposes were to stimulate the economy and to create and retain jobs. The DOE Funding Opportunity Announcement was issued on May 29, 2009 with letter of intent due on July 7, 2009 and full proposals due on July 29, 2009. The University of Minnesota developed a letter of intent and full proposal with an established team of academic and private partners and was successful in winning one of three grants awarded through this competitive solicitation.

Project Results and Discussion

During the pre-award phase of the project, a Statement of Project Objectives (SOPO) was developed and approved by the U.S. Department of Energy. The SOPO is provided in Appendix A. Divided into three sections or Program Areas, the SOPO provided the roadmap for the project. This section reports on results from each of the three program areas.

Program Area 1: Development of Field Scale Research Facility

Program Area 1 focused on design, construction, and commissioning of the Eolos Research Field Station. The first phase of the station development was the successful completion of a National Environmental Policy Act (NEPA) Environmental Assessment by the DOE.

Phase 1: Preconstruction Tasks

Preconstruction activities included all site development activities up to final design, construction and commissioning. Construction could not be started until the NEPA process was completed.

1.1 Procurement of Design-Build Services

The University procured design-build services to assist in design and construction of the Eolos Field Station. The procurement method used was a Best Value Competitive Bid process that was facilitated by the University's Department of Capital Planning and Project Management (CPPM). A solicitation was issued in January 2010 for design-bid firms for the design and construction of the MW-scale turbine facility. Four entities submitted proposals. At the conclusion of the selection process, the proposal team of Ryan Companies & Barr Engineering was selected as the design-build contractors for the construction of the Eolos Field Station. The Ryan-Barr team provided highly competent design-build services throughout the life of the project.

1.2 NEPA and Section 106 Assessments

The National Environmental Policy Act requires all federally funded projects to conduct an environmental review of the project (either an Environmental Assessment or Environmental Impact Statement) and demonstrate a Finding of No Significant Impact prior to commencing with the project. For this particular project, it was determined that an Environmental Assessment was required. The University assisted the U.S. Department of Energy in conducting this study. Details are provided below.

1.2.1 Environmental Assessment

The Environmental Assessment (EA) was a major task in the development of the Eolos Field Station. The task took approximately 13 months to complete and the assessment involved close collaboration between DOE, the University, and several contractors. The DOE was responsible for conducting the EA and making the determinations on project impacts, however, the DOE requested University assistance in developing the EA as part of the project scope.

The University elected to retain a contractor to assist in developing the EA and selected HDR, Inc to lead the EA development. HDR was a pre-approved DOE NEPA contractor and has offices in Minneapolis. HDR's scope on the project was to synthesize field reports, generated by specialty consultants, into a comprehensive Environmental Assessment of the project.

The draft EA was published to a public website for public review and comment. All comments received on the project were addressed in the final EA report.

In addition to the comment period, the project team held a public forum on the project at a community center near the turbine site. The meeting, held July 29, 2010, was publicized in the local papers, city webpages, and email lists. Comments made by the audience during the forum were recorded and follow-up was provided as necessary. The meeting was well attended and the project had positive support from attendees.

In March of 2011, The U.S. Department of Energy's Office of Energy Efficiency Golden Field Office issued a final environmental assessment for the Eolos project. Some categories of potential environmental impact were evaluated and dismissed from further analysis. These include: air quality, water resources, recreational resources, shadow flicker, ice throw, natural resources and energy supply, and intentional destructive acts.

The following categories of potential impact were evaluated, and the results are summarized:

Geology and soil resources: The foundations for the turbine and met tower would be 7 to 10 feet below surface grade and would not be deep enough to impact geologic resources, including groundwater and sand and gravel deposits. The soil on the site is in the Waukegan silt loam group. Soil could potentially be contaminated by construction machinery and would be physically disturbed by compaction, reducing the hydraulic conductivity of the soil. A total of 0.05 acres of the project is on soil designated as prime farmland.

Land use: Existing land use on the project area includes 177 acres of cultivated crops, 13 acres of open space, 6 acres of pasture, and 6 acres of low- and medium-intensity development. However, the agricultural leases are expiring and the land will become unmaintained open space. Twenty-one farmsteads and single family residences are within 1 mile of the project area, but the nearest home is over 3,000 feet away. The University of Minnesota owns the land and plans to develop the property. The land immediately surrounding the wind turbine is committed to wind energy research for the next 15 years. Future land use plans for the "UMore Park" community are conceptual and the City of Rosemount and the University will have to evaluate proposed future land uses; some residential development may be prohibited from the immediate vicinity of the turbine.

Biological resources: The project area does not contain high-quality habitat for wildlife, as it lacks large areas of forest or grassland, lakes, wetlands, or streams. However, a total of 103 breeding bird species have been identified in the project area and a 5-mile vicinity, including two state-threatened species and two special concern species. The project area is located within the Mississippi River corridor for migratory waterfowl. However, it is unlikely that waterfowl would pass through the area at an altitude that would subject them to collision risk with the turbine because there is no suitable stopover habitat in the project site. In general, avian mortality rates during operation of the wind turbine would be estimated at 1-2 birds per year, plus some additional mortalities caused by a met tower. Birds could also collide with the new power lines, causing electrocution, but Xcel Energy plans to implement strategies to reduce this impact; for example, increasing the separation between grounded lines. The number of mortalities would

not have significant, population-level effects on the avian species. Six species of bats may be found in the project area. Some bats could be killed by the wind turbine or met tower, but because only one turbine will be constructed, the impact is expected to be minor. One of the bat species that has habitat in Minnesota, the Eastern Pipistrelle, is a species of concern, but it has never been recorded as occurring in Dakota County. The only state-threatened species of animal known to occur within 1 mile of the project area is the loggerhead shrike. Surveys were conducted to find these shrikes at the project site but none were identified, and because the species prefers grasslands with shrubs, the proposed project site does not provide good habitat.

Cultural resources: Surveys of archaeological and architectural historical and cultural resources were conducted to determine if they would be affected by the project. The review of the proposed fiber optic lines determined that because the lines would be near the right-of-way of an existing road, they were unlikely to impact other structures, and the issue was not further evaluated. Several phases of archaeological and architectural history surveys took place. Results included the identification of two former Gopher Ordinance works structures from the Rosemount Aeronautical Research Laboratory, but they were found to lack historic integrity and were not eligible for listing in the National Register of Historic Places (NRHP). It was also determined that there were no structures or features associated with the Minnesota Agricultural Experiment Station within 1.0 mile of the turbine location. The architectural history review also identified 36 properties 50 years of age or older within the Area of Potential Effect. All but one was determined ineligible for listing in the national register of historic places because of a lack of significance or loss of integrity. However, further evaluation was given to the Edmund H. Knodt Farm, which is 0.67 miles from the proposed turbine location and includes a farmstead built in 1867 and several outbuildings. It was found that the visibility of the turbine might affect the setting and feeling of the farm's landscape. The resolution of this issue is discussed in Section 1.2.2.

Socioeconomics and environmental justice: It was found that the project would not have a direct influence on population in Dakota County but would have a minor short-term economic benefit during construction. It will not affect the tax revenue because it is located on University property. Overall, environmental impacts from the proposed projects would be minor and beneficial, so there would not be any adverse and disproportional impacts to these populations.

Noise: Background levels of sound near the site were assumed to be 55 dBA because of the traffic along County Road 42 and Highway 52; on the site, further from the roads, existing background noise was only 40. A model was created to determine the sound levels from the proposed turbine. Expected sound levels at the nearest receptor, a house on the UMore property, was found to be 42 dBA, resulting in a modeled increase of 4 dBA. Generally, sound increases of 3 dBA are the smallest that are noticeable. However, because sound attenuation due to trees was not accounted for in the model, actual sound levels would be less.

Aesthetics and visual resources: The views of the project site were dominated by five remnant chimney stacks, the Pine Bend Refinery, and businesses near the city of Coates. The turbine would be visible from Highway 52, County Road 42, and nearby residential areas. A variety of human responses are expected to the sight of the turbine, but because there are already a

number of tall modern structures in the area such as water towers, antennae, and power lines, the visual impact of the turbine project is minimal.

Transportation: The project would not result in a detectable increase in vehicular traffic or new roads except gravel access roads on the site. Notices of the proposed construction for the tower were submitted to the Federal Aviation Administration (FAA) on June 3, 2010. The FAA determined that the turbine and met tower would not obstruct air navigation and would not interfere with long range radar, so a No Hazard notification was issued on June 15, 2010. Minnesota Department of Transportation also confirmed that the structures would not impact the operation of the nearest VOR station.

Utilities: The project will involve a new 34.5-kV underground feeder and new low-voltage above-ground line along Blaine Avenue. Fourteen existing microwave paths were identified that traverse the UMore Park property, but the turbine and met tower would not obstruct the paths nor emit electromagnetic interference. Finally, the Department of Commerce communicated that no federal agencies identified concerns over blockage of radio frequency impact.

Hazardous Materials: Several of the existing buildings on the project site contain asbestos, so workers affiliated with the project had to take asbestos training. Barr Engineering developed an emission control plan containing guidelines in case asbestos was encountered during construction. Lubricants, fuel, coolant, antifreeze, and other hazardous materials that are used with construction equipment present the opportunity for accidental emission. Best management practices regarding spills and cleanup helped to prevent the release of these materials.

Health and safety: It was estimated that the project would have a very low incident rate during the construction phase. A wind turbine has the potential to collapse due to mechanical failure or extreme weather. However, because the turbine is isolated from occupied structures, there would be little risk of harm in the case of a collapse.

Unavoidable adverse impacts: Trees will be removed from a 25-acre area surrounding the project and 0.6 acres of land would be permanently lost to construct the turbine. Some birds are expected to be killed each year by the operating turbine. Use of a strobe light on the tower might reduce the fatalities. The views from nearby property will also be altered.

Local short-term use vs. maintenance and enhancement of long term productivity: The use of the environment for the turbine project will have a negligible effect on long-term productivity, because the University plans to remove and decommission the site at the end of the project.

Irreversible and irretrievable commitment of resources: There will be an irretrievable commitment of land required for construction and operation of the projects during its 15-year life. Also, some materials and energy will be irreversibly committed to construct and operate the facility.

As the University of Minnesota further develops UMore Park, it will have to cooperate with the City of Rosemount to evaluate proposed land uses in the vicinity of the turbine to ensure that they are compatible with turbine operation. Urban and suburban development in the vicinity of UMore Park is currently increasing as well. The environmental assessment found that the

project would contribute negligibly to the cumulative impacts on most resources, even in combination with reasonably foreseeable future events and developments in the area.

1.2.2 Cultural Resources Assessments

As mentioned in section 1.2.1 Environmental Assessment, the Eolos project site was evaluated for both architectural and archaeological historic and cultural resources. The following reports were written and submitted to the Minnesota State Historic Preservation Office (SHPO):

- Cultural Resources Literature Review of Proposed Fiber Optic Lines for the UMore Park Research Wind Turbine Project, Dakota County, Minnesota.
- Phase IA Archeological and Architectural History Survey for the UMore Park Research Wind Turbine Project, Dakota County, Minnesota.
- Phase I and II Architectural History Survey for the UMore Park Research Wind Turbine Project, Dakota County, Minnesota.
- Phase I Architectural History Review for the Minnesota Agricultural Experiment Station for the UMore Park Research Wind Turbine Project, Dakota County, Minnesota.

In the archaeological and historical surveys, the Edmund H. Knodt Farm was determined eligible for listing on the National Register of Historic Places (NRHP). At that time (October 2010), the Department of Energy determined that the turbine would not affect the Knodt Farm because (1) it would not affect the integrity of the buildings or structures on the farm, which were its characteristic features; (2) the met tower and turbine structures would be visible but would not dominate the landscape because they would only be 8 degrees from the horizon; and (3) there were two other existing non-historic vertical features already visible from the farmstead, as well as other non-historic features such as Highway 52.

In a letter dated November 30, 2010, the State Historic Preservation Office approved most of the reports and findings of the archaeological and historical surveys. However, SHPO disagreed with the finding of no effect regarding the Knodt Farm, and requested that the Farm be documented according to the Historic Property Record guidelines (Level II).

A memorandum of agreement was created to execute the documentation. The University of Minnesota was tasked with collecting and submitting all necessary information for documentation within 30 days of the agreement. The SHPO was to review the submittal and, within 15 days, advise on whether or not the documentation was satisfactory. In a letter dated March 1, 2011, Kelly Gragg-Johnson stated that the State Historic Preservation Office had received and reviewed the final Minnesota Historical Property Record for the Edmund H. Knodt Farm and found the materials acceptable, fulfilling the stipulations set forth in the Memorandum of Agreement.

1.2.3 Finding of No Significant Impact

The Finding of No Significant Impact is signed Carol J. Battershell, Golden Field Office Manager, and dated March 9, 2011. The Department of Energy determined that the proposed action of constructing the turbine research facility would not constitute a major Federal action significantly affecting the quality of the human environment within the context of NEPA, and an environmental impact statement would not be required.

1.3 Preliminary Design

Ryan Companies/Barr Engineering led the project management of the design and construction phase of the project in collaboration with University staff at the St. Anthony Falls Laboratory (SAFL) and the Department of Capital Planning and Project Management. Throughout the design process, representatives from SAFL, HDR Engineering, Barr Engineering, and Ryan Companies met weekly. A total of 59 meetings spanned from May 2010 to August 2011. Preliminary design focused on all aspects of the field station site including civil, electrical, transportation, structural, turbine delivery and construction, commissioning planning, turbine interconnection and power purchase agreements. The pre-construction phase involved design through 80% complete. Once the FONSI was established by DOE, the project moved to Phase 2 - final design and construction. The details of design are included in the section below.

Phase 2: Construction Tasks

1.4 Turbine Acquisition

Four legal documents were developed around the procurement of the turbine. These documents are briefly described below.

1.4.1 Research Agreement

On June 3, 2011, a Research Agreement was executed between the University and Clipper Windpower. This document establishes a framework for mutually beneficial research collaboration between the two entities. The agreement obligated Clipper to share certain technical information about the turbine necessary for the University to achieve the research goals of the grant. The agreement also described Clipper's participation in Eolos research and the Eolos Wind Energy Consortium. The term of the research agreement was two years from the executed date, or for the entire duration of the 2010 Department of Energy award, and remains intact thereafter until it is terminated by either party. After termination, the University of Minnesota's confidentiality and use obligations and covenants remain intact.

1.4.2 Turbine Supply Agreement

The initial plan for turbine procurement involved purchase of a turbine from a major U.S. wind developer. Early in the project, it became clear that this mechanism to acquire the research turbine was not feasible and so, in consultation with DOE project officers, the University initiated a competitive proposal process for supply of the Eolos turbine. The University invited proposals from several major turbine original equipment manufacturers (OEMs). The evaluation metrics for the proposal were based on costs, value, and potential for research collaboration with the OEM. In May 2010, The University selected Clipper Windpower to join as a research partner in the Eolos consortium and to supply the turbine for the Eolos Field Station. Upon completion of the selection process, Clipper immediately joined the design and construction tasks within the project; supporting design of foundation, transportation, electrical and civil engineering. Clipper also provided information required to complete the NEPA EA such as information required to complete visual and noise assessments.

A Turbine Supply Agreement (TSA), established between Clipper Windpower, Ryan Companies, Inc. and the University of Minnesota, was executed on June 3, 2011. The TSA

agreement provided all necessary information for supply, delivery, construction, and commissioning of the Liberty C96 turbine at the University of Minnesota site.

1.4.3 Warranty Agreement

A Warranty Agreement for the turbine was also negotiated and executed on June 3, 2011. This agreement, established between Ryan Companies, Clipper Windpower and the University of Minnesota, provided details of the warranty obligations of Clipper Windpower and the University of Minnesota. A 2-year warranty period was established through the agreement. Over this period, the University was obligated to use Clipper Windpower Operation and Maintenance Services through a separate OMS agreement. In general, the warranty covered all parts and labor on the turbine for over the warranty period. Annual warranty payments were required from the University for warranty services.

1.4.3 Operation and Maintenance Service Agreement

As part of the requirements of the Warranty Agreement, the University and Clipper negotiated an Operations and Maintenance Service (OMS) Agreement. The period of the agreement was two years with the option to continue into the future. This agreement outlined the obligation and responsibilities for both Clipper and UMN for safe and responsible operation of the turbine. Details on maintenance schedule, non-warranty parts and labor, parts supply obligations, and maintenance facilities required at the site were also included in the document.

1.5 Power Utility Interconnection and Power Purchasing Agreements

This task involved developing the legal agreements necessary to connect and operate the turbine in Xcel Energy's transmission system. Agreements included an Interconnection Agreement and a Power Purchase Agreement.

1.5.1 Interconnection Agreement

The Interconnection Agreement allows for the point of common coupling between the generation system in the turbine and the transmission grid. Under the agreement, Xcel has right of access to disconnect the generation system if necessary during routine maintenance as well as during an emergency. The agreement bears the signatures of Jerome A. Malmquist, Direct of Energy management at the University of Minnesota, and William Kaphing, Vice President of the Control Center at Xcel Energy. It became effective on October 24, 2011 and will remain effective until both parties agree to terminate it. James Nash from Xcel Energy and Kevin DeRuyscher from the University of Minnesota are correspondents responsible for notices, demands, and requests authorized by the agreement.

A license agreement is attached to the Interconnection agreement that grants Xcel Energy a license to construct and install power lines, towers, poles, foundations, and other devices on the property where the turbine is located for 180 days after the effective date of the agreement, and to operate, use, maintain, repair and remove the utilities for a 50-year duration beginning April 1, 2011. The license was negotiated by the Real Estate Office of the Regents of the University of Minnesota and the Siting & Land Rights department of Northern States Power.

1.5.2 Power Purchase Agreement (PPA)

The Power Purchase Agreement ensures that Xcel Energy will purchase net power from the University of Minnesota (the "Seller") at a Guaranteed Price. The Guaranteed Price is a percentage of the integrated, hourly real-time Locational Marginal Price (LMP) as determined by MISO. The PPA bears the signature of the CFO of the Regents of the University of Minnesota, R. H. Pfutzenreuter, and the Managing Director of Xcel Energy, Eric W. Pierce. The PPA became effective on the day of the first Commercial Operation and continued until December 31, 2012, then on continued month-to-month until either party terminated it by giving 60 days of written notice.

It is important to note that the DOE provided guidance to the University that the field station's first priority is research operation and not generation of energy revenue. In other words, the site, once operational, must be operated to maximize research availability over energy and revenue production. Further, DOE suggested that the site could not generate income from the sale of energy produced by the turbine. For this reason, the PPA negotiations focused on provide operational flexibility at the site versus maximizing price for energy. Presently, a new power purchase agreement is in negotiation. The update PPA will be tailored to meet the research and sustainability needs of the Eolos Field Station.

1.6 Construction Cost Estimation and Subcontractor Team Development

With the issuance of the FONSI and approval by DOE to move to the construction phase of the project, the Design-Build team developed final subcontractor team to complete design and carry out the field station construction. This process was led by Ryan Companies and included establishing subcontracts with a range of vendors. Additionally, final negotiation with Clipper Windpower on TSA terms and condition and schedule of delivery were completed resulting in a final project costs and schedule estimate. This task was completed in June 2011.

1.7 Final Design

This task involved completing design of all aspect of the Eolos Field Station. Details are provided below.

1.7.1 Surveying

Site Surveys were conducted by Hakansan Anderson. The survey is of the access road and feedline line along Blaine Avenue and of the turbine site location. Drawings were submitted on July 28, 2010 and are included in Appendix C.

1.7.2 Geotechnical Study

Barr Engineering conducted a geotechnical analysis of the project site and submitted a draft report on July 30, 2010. The following field and laboratory procedures were conducted as part of the analysis, with their results summarized:

- Cone Penetration Test
- Marchetti Dilatometer Test
- Soil borings with a hollow stem auger
- Standard Penetration Tests
- Lab tests including:

- Sieve and hydrometer analysis
- Standard Proctor Density determinations
- Thermal resistivity
- Soil pH tests
- Soluble chloride and soluble sulfate tests

Results from the various tests are summarized in the table:

Table 1.1.Summary of geotechnical/soil properties at turbine site.

Geotechnical Analysis Results		**Notes**
Classification	Poorly graded sand or poorly graded sand with a little gravel	
Percent fines	< 2%	
Friction angle	39%	Based on direct shear test at depths of 10 and 15 feet
Groundwater depth	74 feet	
Shear wave velocity	859 ft/s	
Compression wave velocity	2833 ft/s	
Poisson's ratio	0.45	
Constrained modulus	218 – 2,232 ksf	At depths ranging from 9 feet to the bottom of the sounding; indicates low compressibility
Maximum dry density	101.8 pcf with moisture content of 174% 102.5 pcf with moisture content of 17.2 %	Dry density of 100 pcf or 95% of maximum dry density, whichever is greater, should be used for backfill
California Bearing Ratio (CBR)	2.5 %	Depth of 12-24 inches, compacted to 95% of SPD at optimum water content.

Based on the soil testing results, recommendations were made for road, turbine tower, and met tower construction. Recommendations for road design began with clearing vegetation and root zone and compaction of the exposed subgrade with one pass of a non-vibrating sheepsfoot or drum compactor. Ultimately the subgrade would need to be compacted to 95% of its maximum dry density. Roadway surface was to be granular, made from crushed native gravel and compacted with a smooth roller in loose lifts of less than 9".

It was expected that the turbine would bear on sand, which was to be compacted to 98% of its maximum dry density. Native material could be used as backfill if it was placed in lifts that are 1' or shallower, was compacted to the appropriate dry density and checked periodically for compaction, and if it was graded at ¼" per foot to ensure that water drains away. The frost depth at the site of the turbine is approximately 60", and so the site was suitable for a spread footing foundation at a depth below grade of nine feet. The allowable bearing capacities were determined to be:

Table 1.2. Summary of soil bearing capacity.

	Bearing Capacity	Factor of Safety
Extreme loading	5,500 psf	2.26
Normal loading	4,000 psf	3.0

Recommendations for the foundation of the meteorological tower were less specific because of a lack of design information. A drilled shaft was assumed as the primary support with guy wires and anchors for lateral support. It was recommended that frost heave, which would be a threat to any foundation shallower than 5 feet, be taken into consideration for the shaft design. For design purposes, the density of the soil was taken as 110 pcf moist. The shear strength was estimated at 500 psf at depths shallower than 5ft and as cohesionless sand with a friction angle of 35 degrees between 5 and 10 feet deep. The allowable bearing capacity was estimated at 4,000 psf, increasing to 5,000 psf for a shaft more than 10 feet below the ground. Lateral load resistance was recommended at 90 lbs/in^3 and settlement was estimated at 1 inch total. The lateral earth pressure was estimated at 650 psf in the clayey soils and 270 psf in the sand below. Fill recommendations include compacting to 95% of the standard Proctor maximum dry density for shallow fills, and 98% for deep fills more than 5 feet below ground surface. Lifts of 12 inches or less and grading to direct water away from the foundation were also recommended.

1.7.3 Electrical

Electrical design of switch gear, transformers and grounding was performed by Barr Engineering. The drawings include:

- Drawing E-01: List of abbreviations and symbols
- Drawing E-02: Fence post and gate post grounding detail, antenna pole detail, and pullbox detail
- Drawing E-03: Plan view of turbine tower, Power Distribution Panel, and Transformer
- Drawing E-04: Section view of tower foundation, detail section of the foundation grounding, and detail section view of conduit layout between cable access pit and box pad.
- Drawing E-05: Plan view of the 35kV switchgear
- Drawing E-06: One-line diagram of interconnection
- Drawing E-07: Detail of Met Tower and Wind Tower service boxes, detail of station service, and one-line diagram of station service

1.7.4 Foundation

Structural foundation design for the wind turbine was performed by Barr Engineering Company. Drawings were issued for construction on May 26, 2011. The drawings consist of two sheets.

- Drawing *UMore Park S-01 Rev1:* Plan view of the tower foundation, elevation of the tower foundation, section view of tower foundation, detail of the tower bottom flange, detail of the embedment ring, and detail of top and bottom reinforcement.

- Drawing *UMore Park S-02 Rev 1:* The document contains written details on foundation construction including:
    - Excavation, subgrade preparation, backfill & compaction
    - Cast-in-place concrete and steel reinforcing requirements
    - Anchor bolts and embedment ring

1.7.5 Site Civil Assessment

Civil design was completed by Barr Engineering on April 1, 2011. C-01 and C-04 are contained in Appendix D.

- C-01: This document is a site map. It contains an aerial photograph of the site with major features drawn in and highlighted. Some basic dimensions are provided.
- C-02: This document provides a plan view of the intersections that needed improvement for turbine component delivery. It also provides details of the bus turn around area that was constructed near the wind turbine.
- C-03: This document provides road construction specifications. These include design parameters; road excavation, backfill, and compaction requirements; and testing and inspection requirements.
- C-04: Tree removal plan. A 25-acre area around the turbine, met tower, and control building were to be cleared of trees.

1.7.6 Abatement

An asbestos hazard assessment was conducted as a requirement of a stipulation agreement between the University of Minnesota and the Minnesota Pollution Control Agency on land formerly part of Gopher Ordinance Works (GOW). The assessment included visual inspection of the surface area that would be cleared of brush and trees, and of land currently being farmed in the area. There were some structures built by GOW in the proposed turbine area, but none were extant in the turbine area. However, some areas may have been used as temporary dumping grounds and others could have been contaminated by asbestos-containing pipe insulation that was used in an above-ground piping system by GOW and whose fate was poorly documented during demolition.

No Asbestos-containing materials were observed during the visual inspections, which took place over a series of days between June 14th and July 2nd, 2010. However, a representative from the University of Minnesota's Facilities Management-Hazardous Material Program was present during tree and shrub removal to document procedures and address Asbestos-containing materials if they are uncovered. Notifications were filed with the Minnesota Pollution Control Agency 14 working days prior to disturbance of the area, to prevent prolonged work stoppage in the event of a discovery. The University of Minnesota UMore Park established specific tree removal procedures that were followed during clearing. The asbestos inspector on site was Sean J. Gabor.

1.7.7 Wind Resource Assessment

WindLogics, Inc., prepared an assessment of wind resources at the UMore Park site, issued June 30, 2010. The WindLogics modeling process included a mesoscale model for larger-scale

weather patterns and a wind flow model for smaller-scale terrain and land features. The final resolution of the model was 50 meters. WindLogics used E-MCP to normalize the model output to long-term climatic means. The report found that the long-term wind resource at the proposed tower location is 7.19 m/s. Applying the long-term wind resource to the power curve of the Clipper Windpower C-96 Class IIB 2.5-MW turbine results in an estimated gross capacity factor of 35%.

1.8 Construction

1.8.1 Turbine and Met tower.

Construction of the Meteorological tower and wind turbine was performed by Ryan Companies and their subcontractor team. Below is a timeline of construction events for the wind turbine and met tower.

March 9, 2011—FONSI is issued. Construction related activities can now begin.

March 25, 2011—Tree clearing in the areas surrounding the wind turbine begins.

April 20, 2011 —Xcel begins to place power-line poles that lead to the wind turbine. Tree clearing is ongoing.

July 11, 2011 – Grading and excavation for the foundation of the wind turbine and met tower begins.

July 18, 2011 – Excavation completes and the mud mat at the bottom of the excavation is poured.

July 19, 2011—Foundation settlement plates are installed in the native soil beneath the wind turbine for later research purposes.

July 20, 2011—Rebar placement for the wind turbine and met tower foundations begins.

July 26, 2011—Main foundation concrete pour begins at 6:00am. Both wind turbine and met tower foundations are poured.

July 27, 2011—Foundation pedestal concrete is poured for both met tower and wind turbine.

August 2, 2011—Backfilling and compaction of soil begins on wind turbine and met tower foundations and electrical/lightning grounding rings are installed in the soil.

August 24, 2011—The crane begins to arrive on site. Nearly 27 trucks were required for delivery. Crane assembly begins.

August 29, 2011—Turbine components begin to arrive at UMore Park in Rosemount, MN.

August 30, 2011—UMN staff technicians begin to install sensors in the wind turbine blades.

September 7, 2011—First tower section of the wind turbine is lifted into place. UMN staff technicians begin to install strain gauges on the interior wall of the wind turbine tower.

September 8, 2011—Second and third tower sections of the wind turbine are lifted into place.

September 16, 2011—Fourth Tower section of the wind turbine is lifted into place. Nacelle, gearbox, and generators are lifted and installed on the same day.

September 19, 2011—Met tower installation begins.

September 23, 2011—Rotor is lifted into place and attached to the gearbox of the turbine.

October 24, 2011—Met tower sensors arrive at the site from Campbell Scientific.

October 25, 2011—Wind Turbine Commissioning ceremony.

November 11, 2011 – Met tower sensor network becomes operational.

Figure 1.1: Photo of the survey stake marking the location of the wind turbine on the first day of construction. A bulldozer is shown grading the site in preparation for excavation for the foundation.

Figure 1.2: The rebar cage of the wind turbine foundation nears completion in July, 2011.

Figure 1.3: Concrete is poured for the foundation of the wind turbine.

Figure 1.4: University of Minnesota research technician Dick Christopher prepares the inside surface of a wind turbine blade for the installation of fiber optic strain gauges and temperature probes.

Figure 1.5: The second of four wind turbine tower sections is lifted into place.

Figure 1.6: The wind turbine rotor is lifted into place on September 23, 2011.

Figure 1.7: Jose Zayas (Department of Energy) addresses the audience at the commissioning ceremony of the Eolos Wind Energy Field Research Station on October 25. 2011.

1.8.2 Custom Research Sensor Network

To enable current and future research on the Eolos 2.5MW wind turbine, the University of Minnesota team designed and installed a number of custom research sensor systems. These systems were designed to perform state-of-the-art measurements on critical wind turbine components. Custom blade sensors, foundation and tower sensors, power sensors and a specialized meteorological tower were designed and installed by University of Minnesota. These systems are described below.

Windcube LIDAR:

On June 9, 2010 the University of Minnesota purchased a Windcube LIDAR system from NRG Systems Inc. using funds from this project. The Windcube LIDAR is a portable wind profiling device that uses a laser to measure wind speed and direction at 10 user defined elevations from 40m to 100m with a sample rate of 1 measurement per second. Capable of being deployed at any location Eolos researchers would like to collect data, the Windcube is especially useful for wake studies on the Eolos 2.5MW wind turbine. While the met tower (described below) can provide very detailed and accurate measurements of the wind velocity profile, it is stationary and cannot be placed in areas of interest in the wind turbine wake. The Windcube is very mobile and can be deployed nearly anywhere, allowing researchers to choose precisely the location at which they would like to collect data. To enable the Windcube to be deployed for long durations

at locations where grid power is not available, a custom generator system was designed and constructed by University of Minnesota research engineers.

Meteorological Tower:

An instrumented meteorological (met) tower, first made operational on November 11, 2011, provides key wind and atmospheric information at the Eolos site. The design of the Eolos met tower was strongly patterned after those in existence at NREL's National Wind Technology Center near Boulder, Colorado. Guidance on tower design and instrument selection, installation, and operation was also taken from IEC 61400-12-1 Ed.1: "Wind turbines - Part 12-1: Power performance measurements of electricity producing wind turbines".

The met tower height of 425ft (129.5m) was selected to correspond to the upper extent of turbine rotor swept area (130m). Instrumentation is located at roughly the limits of the rotor swept area (30m and 130m), hub height (80m), rotor blade mid span (55m and 105m) and 10m for a total of 6 instrumented elevations designated 1 through 6, Elev. 1 being at the top. Elev. 6, the 10m elevation, was added to allow comparison of Eolos data with other more commonly available meteorological data. Wind measurement instruments are located on 12ft and 18ft booms. Sonic Anemometers are located at Elev. 1, 3, 5, and 6 at the ends of 18ft booms. Accelerometers capable of static and dynamic measurement are attached to these anemometers to assess tower sway and boom arm vibration. Cup anemometers and wind vanes are mounted on cross arms at the ends of 12ft boom arms at all 6 instrumented elevations. Air temperature and relative humidity are measured at all 6 instrumented elevations; the probes being housed in gill radiation shields attached to the tower itself. A barometric pressure sensor is located on the tower at hub height (80m, Elev. 3).

Power to and signals from all instrumentation are routed through junction boxes located on the tower at each of the 6 instrumented elevations, through "homerun" cables secured to tower legs and leading to ground level, and finally through subsurface conduits to 2 datalogger enclosures (Enclosure A and Enclosure B) located at ground level adjacent to the tower. These enclosures house 2 Campbell Scientific CR3000 data loggers each of which as an NL115 network interface and 2GB SD memory card. The NL115s have assigned IP addresses and provide Ethernet connectivity to the Eolos data center. The data from all loggers are time stamped. Clock synchronicity between the 2 met tower loggers, as well as the other loggers at Eolos including the two monitoring strain and movement in the turbine tower foundation, and the one monitoring turbine power output, is maintained to an accuracy of about 10μSec by GPS based clock setting that occurs once per second.

Data acquisition rates are 20Hz for the sonic anemometer and associated accelerometer data and 1Hz for the cup anemometer, wind vane, air temperature, relative humidity, and barometric pressure data.

The Eolos met tower, having sonic and cup anemometers and wind vanes at 4 of the 6 elevations, allows a somewhat unique data quality assessment method - one need simply compare sonic and cup/vane data at the same elevation where available. It should be noted that the sonic anemometers are located on different boom arms 3m above the cup anemometers

and vanes but for this purpose, the difference can be considered negligible. On June 3, 2013 the cup anemometers were replaced with new MEASNET calibrated Class One anemometers.

Wind Turbine SCADA System

The Clipper 2.5MW wind turbine that was constructed at the Eolos field research station has a complex control system. The wind turbine is constantly making measurements of hundreds of parameters. Most of these measurements are saved for a short amount of time and are averaged to 10 minute records to be archived. In typical Clipper wind turbines, the 1 Hz data stream is not archived. Seeing this data stream as extremely useful, University of Minnesota researchers installed systems to capture this 1Hz data before it is averaged. This data is part of Eolos data archive.

Clipper's datastream enters a SQL database after being collected by the monitoring systems on the wind turbine. To capture this datastream, the University established their own SQL database on a separate server rack and then replicates the Clipper SQL database as it is updated. The result is a searchable database of essential turbine parameters collected at 1Hz. The system is capable of collecting continuous 1 Hz data on many turbine parameters. Below is a list of some of these parameters.

Table 1.3. Summary of measured parameters from the Eolos research turbine.

Service Status	Yaw Position	Generator 1 Temp
TurbineState	Yaw Error	Generator 2 Temp
Wind Speed	Air Density	Generator 3 Temp
Real Power	Barometric Pressure	Generator 4 Temp
Reactive Power	Nacelle Temperature	Yaw Mode
Pitch Position Blade 1	Ambient Temperature	Yaw State
Pitch Position Blade 2	Gearbox Oil Temperature	Fault Code
Pitch Position Blade 3	Hydraulic Oil Temp	Fault Count
Generator Speed	Gearbox bearing 1 Temp	Nacelle Direction
Hub Speed	Gearbox bearing 2 Temp	Wind Direction
Rotor Position	Gearbox bearing 3 Temp	
Tower Acceleration	Gearbox bearing 4 Temp	

Wind Turbine Blade Sensors

The blade sensor system on the turbine at the Eolos wind research station provides a continuous data set of blade strain and blade acceleration. The system was installed with support from Sandia National Laboratories and the Micron Optics, Inc. and with funding from the U.S. Department of Energy.

The system continuously logs data at 20 Hz and is time stamped very accurately using GPS so that the data can be compared to other datasets collected at the Eolos wind research station. The data is automatically archived into a SQL database for easy access by researchers. The system utilizes a National Instruments cRIO paired with Micron Optics sm130 interrogator for data collection. The sensors include the following:

- One triaxial accelerometer in the hub,
- Data Acquisition (DAQ) enclosure at the center of the rotation used for blade position and hub movement,
- Three triaxial accelerometers in each of the three blades (totaling nine),
- Ten fiber optic strain gauges mounted in each of the three blades (totaling 30),
- Ten fiber optic temperature sensors mounted near each strain gauge in each of the three blades (totaling 30),
- One GPS antenna used for accurate time stamping.

An innovative installation solution was developed to install some of the accelerometers deep inside the already assembled blades on the construction site just before rotor assembly and installation.

Power Sensors

In order to verify the turbine net power and current output and to generate a power curve to determine turbine efficiency, it was necessary to install a third party power transducer, current transformers and a data acquisition system in accordance with in IEC standard 61400-12-1 Ed.1: "Wind turbines - Part 12-1: Power performance measurements of electricity producing wind turbines."

The devices were initially to be installed in the turbine power distribution panel. The three current transformers (CT's) were to be installed around the buss bars of each phase in the Power Distribution Panel (PDP). The power transducer (PT) was also to be installed in the 690VAC compartment of the PDP. Upon further investigation it was found that the PDP could not accommodate the CT's due to their physical size. It was decided that the CT's and PT would be housed in the pad mounted transformer enclosure.

In October 2011, a Camille Bauer DMT-1000 multifunction programmable power transducer and three current transformers, CT-125 were purchased from Ohio Semitronics, Inc. and installed in the cabinet of the pad mounted transformer (PMT). Additionally, a CR-800 data logger, battery backup and radio transmitter were purchased from Campbell Scientific and installed in a water tight enclosure on the side of the pad mounted transformer.

The standard digital data acquisition system is capable of continuous sampling at a rate of 1 Hz and has the ability to store unprocessed data. The accuracy of the data acquisition system has been verified and the uncertainty of the DAQ system is negligible compared to that of the sensors.

Foundation Sensors

The tower and foundation of the Eolos wind turbine have been instrumented to provide measurements of tower loads and foundation movement. The system was designed by Barr Engineering Company in close collaboration with the research engineers at the St. Anthony Falls Laboratory. The primary measurements that the system is design to take are: 1) overturning moment applied by the tower to the foundation and 2) foundation rotation.

Combining these two measurements allows researchers to compute the “rotational stiffness” of the foundation, or how much the foundation rotates in response to a load. A minimum rotational stiffness for wind turbine foundations is given to foundation design engineers as criteria to foundation design. The foundation and tower sensor system at the Eolos wind turbine allows researchers to obtain an actual measurement of how well the foundation design meets the turbine OEM’s design criteria.

To obtain a measurement of the overturning moment, 20 uni-axial strain gauges were applied to the interior of the wind turbine tower wall. The gauges were applied to the interior of the tower to protect them from the elements and were installed at a height of 2 feet above the bottom flange to ensure that they were sufficiently out of the way of anchor bolts that require maintenance every 12 months. 10 thermocouples were also attached to the turbine tower so that thermal expansion of the tower steel could be accounted for. To obtain measurements of the foundation rotation, 3, 2G tri-axial DC accelerometers were initially used. However, it was determined that these sensors, mounted to the foundation pedestal of the wind turbine, were not sensitive enough to measure the very slight rotation of the foundation. In February 2013, the accelerometers were replaced with a bi-axial tiltmeter mounted on the surface of the foundation pedestal.

Measurements are collected on two Campbell Scientific CR3000s. The strain gauges and the tiltmeter are sampled continuously at 20Hz while the thermocouples are sampled at 1 measurement per minute. Each datalogger is connected to the Eolos research network via an NL115 Ethernet module and has a 2GB compact flash card that can store data in the event of a network outage. To ensure synchronous data collection, both between the two foundation dataloggers and the other sensor networks at the Eolos field station, a GPS module updates the clocks on the dataloggers once every second.

In addition to the sensor network, 24 settlement plates were installed through the foundation of the wind turbine. These settlement plates were designed to allow a survey team to perform periodic measurements of the foundation settlement over time. Before the concrete for the foundation was poured, 6” diameter steel plates were buried in the native soil beneath the foundation. Once the rebar had been placed, 10 foot long steel rods were attached to the buried plates. These rods extend through the concrete foundation encased in PVC pipe so that they can move independently of the foundation itself. The top of the rods are protected by sewer clean-out covers that allow trucks and other equipment to drive around the base of the wind turbine without damaging the settlement plates. A survey crew with standard survey equipment can remove the sewer clean out covers and survey the elevations of the settlement plates, tying the measurements into 3 brass survey monuments that are installed in concrete a distance from the wind turbine.

1.9 Construction Project Closeout

In October 2011, Ryan Companies provided the University of Minnesota with a 1,080 page “Turnover Manual” for the UMore Park Wind Turbine. This manual provides details of permitting, construction and inspection of the wind turbine. The following is the table of contents of this document.

A. Permits
B. Special Inspection Final Report
C. Geotechnical Engineering Report
D. Foundation
E. Civil
F. WTG Transformer
G. Station Service Transformer
H. Switchgear
I. WTG Components
J. WTG Tower Assembly
K. Mechanical Completion
L. Commissioning
M. Met Tower
N. Site Photos
O. Record Drawings

As a part of project closeout and wind turbine commissioning, a number of assessments were performed on the wind turbine to verify that the wind turbine had been installed correctly and was ready for operation. This process is detailed in Section L: Commissioning of the Ryan Companies turnover manual. The assessments were performed as checklists. The following assessments were performed prior to wind turbine commissioning and project closeout.

A. Installation Quality Checklist
B. Pre-Commissioning Checklist
C. Final Commissioning Checklist
D. SCADA Turbine Pre-Commissioning Checklist
E. SCADA Turbine Final Commissioning Checklist
F. SCADA Rack Pre-Commissioning Checklist
G. SCADA Rack Final Commissioning Checklist

The final payment to Ryan Companies was made on February 1, 2012.

Program Area 2: Research

Each of the research projects described below carried its own set of objectives and outcomes.

Task 2.1: Increasing Wind Turbine Output Using Vortex Generators and Riblets

Literature Review and Background

Achieving skin friction drag reduction through the use of riblets has been a topic of intensive research throughout the last several decades. Riblet structures are typically in the range of a couple micrometers to several hundred micrometers in height and work to suppress the lateral migration of coherent turbulent structures.

Despite several valuable efforts to date, the fundamental mechanisms that induce drag reduction have not been well established and the potential benefits associated with the use of riblets applied to wind turbines are unclear. Two pertinent conclusions have been established: the drag reduction mechanism arises from a decrease in shear stress on the riblet sidewalls near the trough; and the effectiveness of a given riblet size is dependent on Reynolds number and angle of attack. In this context, there are a number of important questions that still cannot be answered in the context of wind energy. These include, among others, understanding and optimizing the effect on drag reduction of parameters such as riblet configuration, height, or positioning on an airfoil. Because of the wide variety of application methods, airfoil designs, and riblet configurations, there is a dearth of clear and universal conclusions regarding riblet performance, and no equations exist to help select the optimal riblet setup and size.

Goals and Objectives

This work focuses on investigating passive flow control strategies to provide wind turbine manufacturers with a robust technology that will increase turbine energy capture. To achieve this goal, the application of riblet structures on the surface of an airfoil, like those shown in Figure 2.1.1, is systematically investigated. The performance of several riblet configurations is explored for both complete and partial airfoil coverage scenarios.

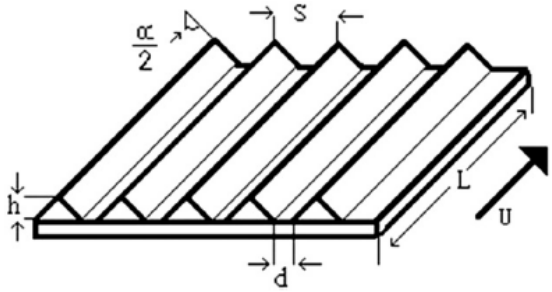

Figure 2.1.1. Example of a riblet configuration with base spacing d. (V-groove is achieved when d= 0).

SOPO Defined Purpose, Approach, and Outcomes:

Purpose: Develop and test passive flow control techniques based on riblets and vortex generators to maximize the recovery of potential energy at a given site by increasing peak efficiency and broadening the operating envelope of the rotor.

Approach: Perform wind tunnel experiments coupled with CFD simulations to determine optimal riblets and vortex generators arrangements. Validate the so-determined optimal solution on the 2.5MW turbine by comparing post- and pre-treatment wind turbine output.

Outcomes: Design guidelines and expected performance benefits for riblets and vortex generators and a CFD-based framework for turbine-specific implementation of passive flow control devices.

Project Team

Roger Arndt is a Professor Emeritus of Civil Engineering with research specializations in fluid mechanics with emphasis on turbulent shear flows and vortex flows; cavitation; aeroacoustics including jet noise and turbomachinery noise; alternative energy with an emphasis on hydropower and wind turbine technology; and aeration technology with a view towards developing cost effective environmental remediation techniques. He served as Director of the St. Anthony Falls Hydraulic Laboratory for 16 years and as program manager of the Fluid Mechanics and Hydraulics Program at the National Science Foundation for 3 years. He is a Life Fellow of ASME, Fellow of the American Physical Society, and Associate Fellow of AIAA.

Fotis Sotiropoulos is James L. Record Professor of Civil Engineering at the University of Minnesota and has served as director of St. Anthony Falls Laboratory since 2006. Fotis Sotiropoulos' research is aimed at developing high-resolution, fluid-structure interaction, computational algorithms for enabling virtual experiments and simulation-based engineering design in real-life environmental, renewable energy, and biological applications. Sotiropoulos earned his Ph.D. in Aerospace Engineering from the University of Cincinnati.

Leonardo P Chamorro is now an Assistant Professor in the Mechanical Science and Engineering Department, University of Illinois at Urbana-Champaign. Previously he was a research associate in experimental fluid mechanics, the coordinator of wind and hydrokinetic energy research efforts, and research manager of the boundary layer wind tunnel at the Saint Anthony Falls Lab, University of Minnesota. His main areas of interest are flow & structure interaction, renewable energy applications related to wind and hydrokinetic energy, atmospheric boundary layer flows including thermal and roughness heterogeneity, and experimental instrumentation development. Dr. Chamorro holds a Bachelor's degree in Civil Engineering (fluid mechanics) from the University of Chile, and an MSc and PhD in Civil Engineering with minor in Aerospace Engineering and Mechanics at the University of Minnesota. He has received a number of awards, including the outstanding postdoctoral scholar award and the doctoral dissertation fellowship from the University of Minnesota and the best paper presentation award at AMS - 18th Symposium on Boundary Layers and Turbulence.

Aaron Boomsma is a Ph.D. candidate at the University of Minnesota. He conducted the numerical studies of riblets along with Fotis Sotiropoulos. His primary research areas of interest are in high-fidelity numerical simulations of turbulent boundary layers under pressure gradients, roughness in turbulent flows, and efficient algorithms for massively parallel supercomputers. Boomsma earned a Bachelor degree in Mechanical Engineering from South Dakota State University and a Master of Science degree in Mechanical Engineering from the University of Minnesota.

G. Memo Izzi (now retired) was Lead Senior R&D Specialist at 3M in the Renewable Energy Division Laboratory. Dr. Izzi received his doctorate in Organic Chemistry from Università degli Studi di Parma in Italy. He served in his role of Lead Senior R&D specialist at 3M for over 12 years after holding other positions at 3M and Imation Corp. His role in Task 2.1 was as primary researcher and project manager for 3M's involvement with the project.

Thomas Herdtle 3M Advanced Research Specialist—Predictive Engineering—Corporate Laboratory.

Thomas Muehle Product Development Engineer – Renewable Energy Division Laboratory.

Zachary Malmberg Contract Engineer Testing Support—Renewable Energy Division Laboratory.

Technical Approach

The first phase of research in this task was to evaluate the performance of different riblet configurations and understand, fundamentally, the complex behavior of turbulent flow near the surface of the riblet films.

Three-dimensional, high-fidelity numerical studies were performed on several riblet geometries to elucidate the mechanisms of drag reduction and to determine the performance of those geometries. Simulations were performed by solving the incompressible Navier-Stokes fluid equations on a curvilinear body-fitted grid. Two types of simulations were performed: 1) Very high-resolution results were obtained using Direct Numerical Simulation (DNS) at low Reynolds numbers with riblet films in a fully-developed turbulent channel-flow to study the mechanisms of drag reduction, and 2) Large Eddy Simulations (LES) were performed to study riblet performance in zero and adverse pressure gradients.

The Navier-Stokes equations were solved using the implicit fractional step method proposed by Ge & Sotiropoulos [1]. In this method, the momentum equations are discretized using the hybrid staggered/non-staggered grid approach [2]. The momentum equations provide an intermediate velocity flux that is not divergence-free. Thus, the Poisson equation is solved for a pressure corrector, which is added to the intermediate velocity. The result is a divergence-free velocity field that satisfies the continuity equation.

The numerical method is central-difference, 2^{nd} order accurate in time and space. The turbulence closure problem was handled using the Dynamic Smagorinsky model to approximate fluid stresses smaller than the grid. No wall-models are utilized, as the wall normal direction fully resolves each turbulent boundary layer.

The DNS cases were simulated in a turbulent channel-flow, which was driven with a fixed flux. Periodic boundary conditions in the streamwise and spanwise directions were used to mimic an infinite plane of riblets. Under such conditions, the pressure gradient is constant and favorable. DNS cases were first validated against a canonical riblet geometry seen in Choi et al. [3]. Figure 2.1.2 shows a cross-sectional view of the riblet domain, along with flow conditions. The top and bottom surfaces were given a no-slip boundary condition.

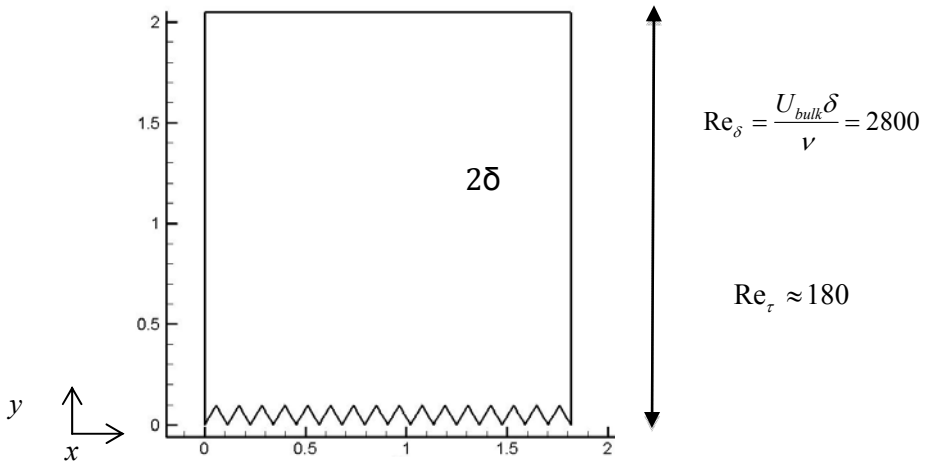

Figure 2.1.2.Validation domain and flow conditions for V-Groove riblets.

Figure 2.1.3 highlights an excellent comparison between the simulations. The horizontal axis shows normalized spanwise location, as one moves from riblet valley to the riblet tip. The vertical axis measures normalized local shear—paramount in accurately determining riblet performance.

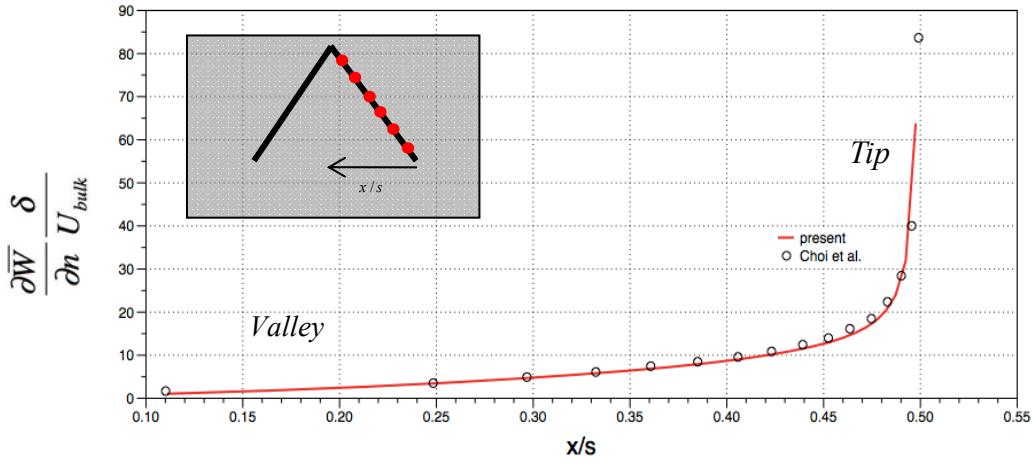

Figure 2.1.3.Comparison in normalized local shear from riblet valley to tip.

The LES cases included Zero Pressure Gradients (ZPG) and Adverse Pressure Gradients (APG). Studying riblet performance in such pressure gradients is extremely important because nearly all literature focuses on riblets in channel flow, which is not at all similar to wind turbine blade flows. Adverse pressure gradients are particularly evident on the suction side of turbine rotors.

Riblets in pressure gradients have hardly been studied computationally due to the requirement of realistic turbulent inflows. This problem was overcome using the rescaling method of Lund, Wu, & Squires [4] to create a spatially developing turbulent boundary layer. Using this method, time-accurate planes of turbulence were saved from a statistically steady boundary layer, and then fed into a testing domain (seen in Figure 2.1.4). Method validation was obtained by

comparing time-averaged statistics with the experimental results of DeGraaf & Eaton [5]. To control the development of the boundary layer, the continuity equation was integrated over the boundaries and a flux for the top of the domain was then calculated from Equation 2.2.1.

$$v(z) = U_\infty \frac{d\delta^*}{dz} + (\delta^* - h)\frac{dU_\infty}{dz}$$

Equation 2.2.1.

Where *v(z)* is the wall-normal Cartesian component of velocity, δ^* is the displacement thickness, and *h* is the height of the domain. When simulating a ZPG, the second term is identically zero. For the LES cases, a mild APG was simulated ($\beta \approx 0.26$) by specifying the freestream velocity as a function of downstream direction.

Figure 2.1.4 shows a typical riblet simulation domain that shows instantaneous contours of streamwise velocity. The riblet surface is shaded.

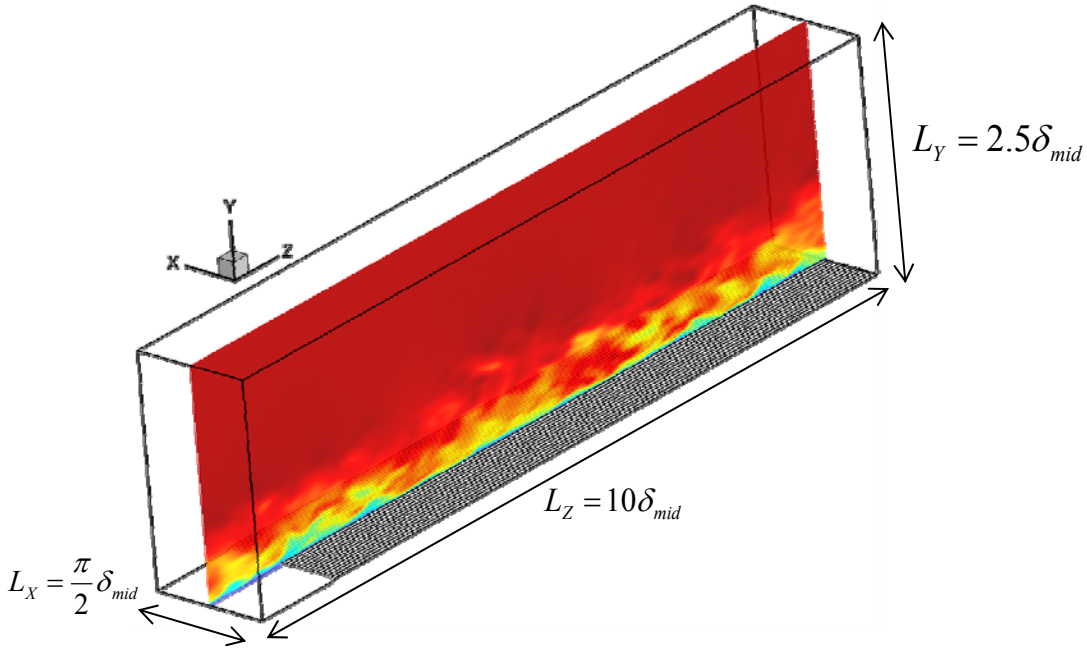

Figure 2.1.4. Representative riblet testing domain, with instantaneous contours of streamwise velocity. δ_mid is the boundary layer height in the center of the domain.

Physical experiments were also conducted to determine riblet performance in the SAFL wind tunnel. This facility has a 1.7m wide × 1.7m high × 16m long test section. There is a contraction with a 6.6:1 area ratio upwind of the test section along with flow conditioning/turbulence control consisting of a coarse wire mesh and honeycomb flow-straightener. Surface characteristics (including thermal heterogeneity patterns) and wind velocity (up to roughly 40 m/s) can be controlled.

Initially, a series of 5 flat plates were constructed and installed in the wind tunnel. Mean shear was measured on 4 different riblet films and compared with a smooth surface under 2 different flow conditions. High resolution measurements of the turbulent flow over a flat plate with a riblet surface were obtained at different locations using an array of 4 hot-wire anemometers.

Based on the results of these initial tests, 3M Company developed new experimental riblet films. These films were manufactured by 3M in November and December 2010. By the time research was ready to move to the next stage, 11 different riblet films had been developed. These films varied in riblet height, peak to peak distance and angle.

The second phase of research involved a two-dimensional airfoil force balance that was designed and fabricated specifically for this study. Special care was taken to ensure that high quality 2D airfoil data would be produced. Test airfoils having a collective span of 1.7 m and a chord of 1 m fill the breadth of the wind tunnel test section. The foils are mounted on a structure that is fixed to a supporting foundation for the wind tunnel, thereby isolating the force balance from tunnel vibration. At an angle of attack of 0^o, the supporting structure holds the airfoil at approximately the center of the tunnel. Three independent airfoil sections were manufactured using a rapid prototyping machine. The airfoil under study is a DU 96-W-180 model, of 18% thickness. The central section, 0.6 m wide, is isolated from the rest of the foil for best testing conditions. Force sensors are mounted in the central section for the measurement of lift and drag forces. The overall experimental set-up is illustrated in detail in Figures 2.1.5 and 2.1.6. As depicted in Figure 2.1.3, the central part of the airfoil (the instrumented section) is structurally isolated from either wall by non-instrumented (dummy) sections. Both the riblets and the instrumentation were located in this central section. This configuration permits an infinite aspect ratio and at the same time eliminates boundary layer effects caused by the test section walls. The specific riblet geometries tested in this study are described in Tables 2.1.1 and 2.1.2. Not all riblets used for complete coverage testing were used for the partial coverage tests because of their clear negative performance on reducing drag. The experimental riblets used in both portions of this study were samples developed by 3M's Renewable Energy Division Laboratory. A diagram illustrating the riblet parameters is provided in Figure 2.1.7. Testing focused on finding the geometry of riblets that performed the best (maximum drag reduction) when mounted on the DU 96-W-180 airfoil. The blade was tested within a constant Reynolds number, based on the chord length, of $Re=2.2\times10^6$ and an angle of attack ranging from 0^o to 10^o.

Table 2.1.1. 3M Experimental riblet configurations tested for complete coverage scenario
3M Experimental riblet configurations tested for complete coverage scenario.

h (mm)	40	40	44	62	80	80	80	100	150	180	225
s (mm)	80	80	44	62	80	80	150	100	150	180	225
d (mm)	40	59	0	0	0	37	70	0	0	0	0
a (d)	53	30	53	53	53	30	53	53	53	53	53

Table 2.1.2. 3M Experimental riblet configurations tested for partial coverage scenario.

h (mm)	40	40	62	80	80	80	100	150
s (mm)	80	80	62	80	80	150	100	150
d (mm)	40	59	0	0	37	70	0	0
a (d)	53	30	53	53	30	53	53	53

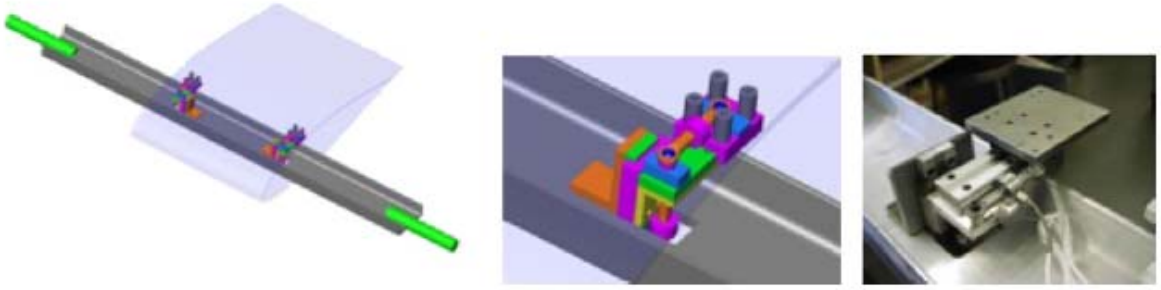

Figure 2.1.5. Internal mounting of force sensors in the instrumented center section (left). Detail of the orthogonal sensor system (right).

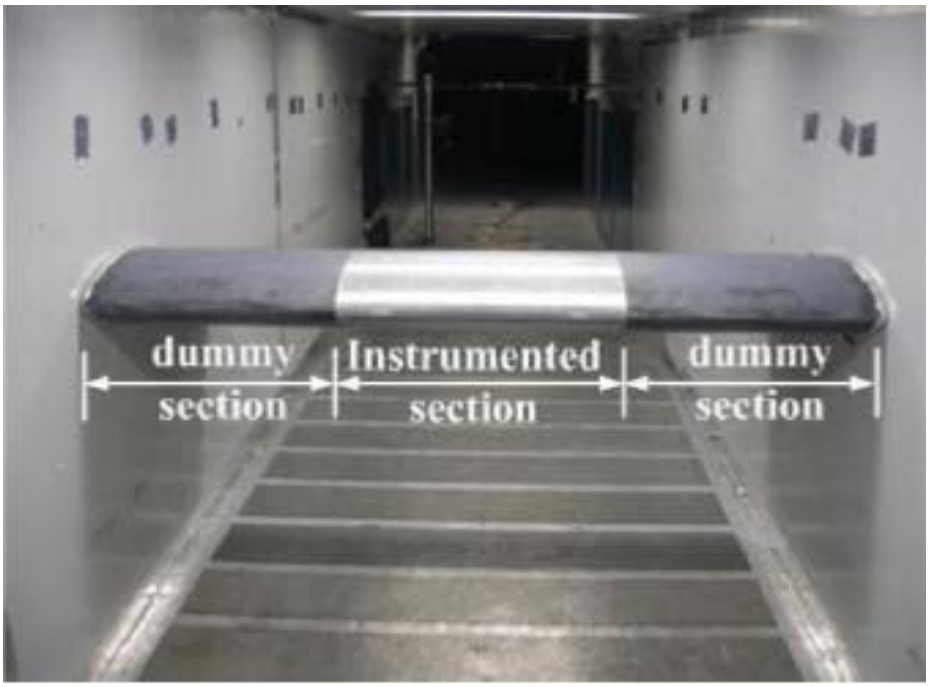

Figure 2.1.6. Full scale wind turbine airfoil in the wind tunnel.

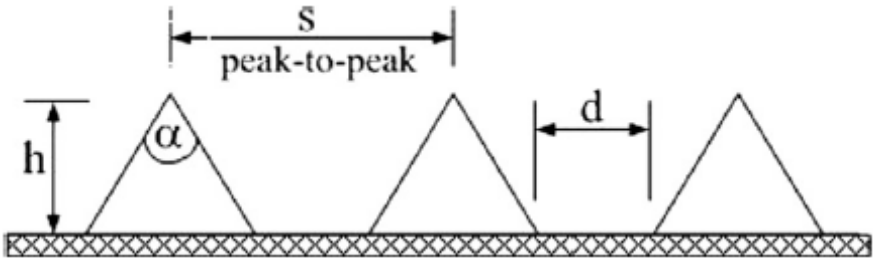

Figure 2.1.7. Geometrical parameters of the riblet films studied.

Results

Drag Reduction Mechanisms

Utilizing DNS, we have seen that the primary method of drag reduction by riblets is the ability of the riblet to prohibit turbulence from impacting skin-friction on much of the riblet surface. Figure 2.1.8 shows instantaneous iso-surfaces of Lambda 2 (a well-known parameter used to visualize turbulence) colored by velocity magnitude.

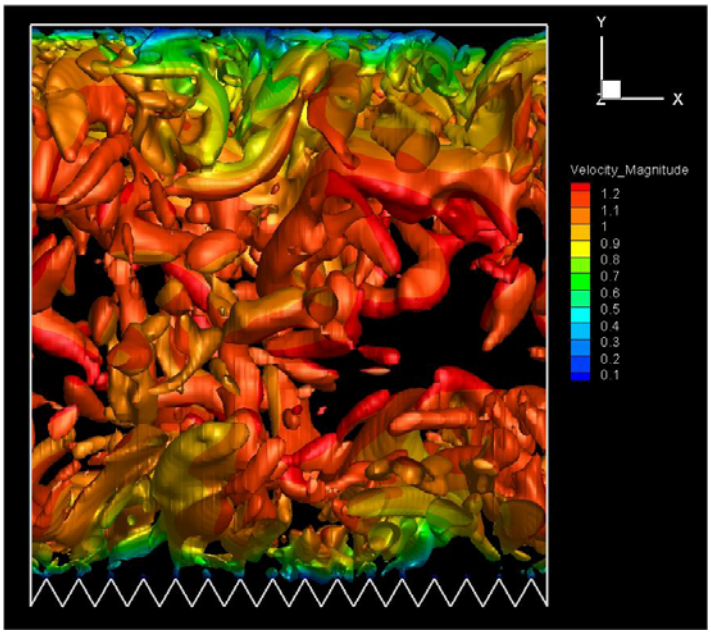

Figure 2.1.8. Instantaneous iso-surfaces of lambda2, colored by velocity magnitude.

As seen, compared to the top flat plate surface, much of the riblet surface area appears secluded from turbulence; the only such structures seen very-near the riblets are streamwise counter-rotating vortices that are visible in time-averaged contour plots, as seen in Figure 2.1.9.

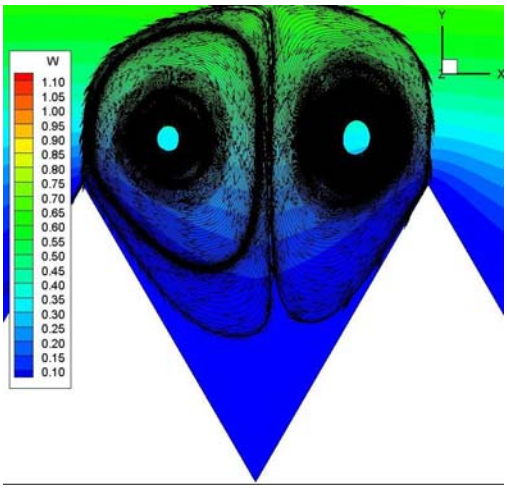

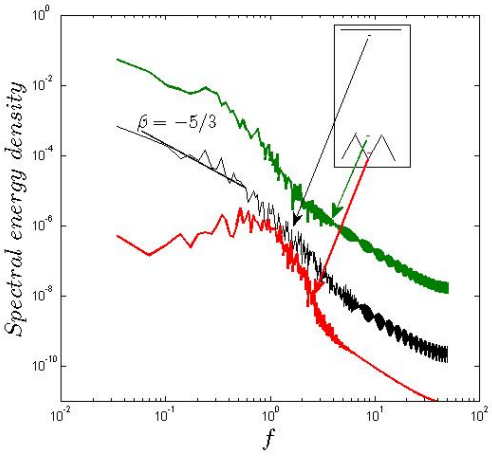

Figure 2.1.9. (Left) Mean contours of streamwise velocity with streamlines.

Figure 2.1.10. (Right) Spectral energy density plots from different wall-normal locations.

Furthermore, Figure 2.1.10 shows spectral energy density at different locations in the channel. The black line is from a point very near the surface of a flat plate turbulent boundary layer, the green line is spectrum at the riblet tip, and the red line is spectrum in the riblet valley. Figure 2.1.10 shows that near the riblet tip, there are large-scale structures that contain energy greater than seen on a flat plate (counter-rotating voices). But inside the riblet valley, there are very few large-scale structures, with very little energy. Stated again, riblets aligned with the streamwise flow prohibit turbulence from interacting with much of the riblet surface area, which in turn, creates a more laminar-like velocity field (seen in Figure 2.1.9) within the riblet. This laminar-like region produces weaker velocity gradients near the riblet valley, and the result is a reduced over all skin-friction.

Comparisons of Riblet Performance.

Using DNS, riblet performance comparisons were made. In particular, three different types of riblets were simulated—those seen in Figure 2.1.11.

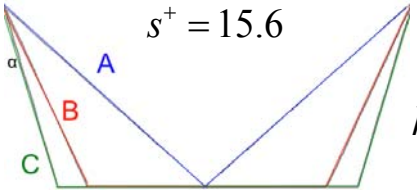

Riblet Type	Drag Reduction
A	-3.70%
B	-5.40%
C	-7.70%

Figure 2.1.11. Three riblet geometries and results. Riblet angles are 45°, 22.5°, and 15°.

Drag reduction performance for each case is also seen in Figure 2.1.11. In these simulations, the spacing between riblets is held constant, but the angle at the tip is decreased. These results echo the experimental results of Bechert et al. [6]. The physical reason for more drag reduction was seen in plots of time averaged streamwise vorticity. Since the spacing is

constant, the relative position, size, and strength of the counter-rotating vortices in the mean are unchanged, and thus less riblet surface area is near these vortices.

Riblet Performance in APG.

We also conducted LES of riblets in ZPG and APG. A mild APG was chosen ($\beta \approx 0.26$) because of some confusion within the current literature. A previous experimental paper claimed that mild APG *reduced* the effectiveness of riblets, while a recent computational paper claimed that mild APG *doubled* the effectiveness. Because of the APG present around turbine rotors, accurate information is *crucial* for riblet placement. The computational grid and geometry can be seen in Figure 2.1.12.

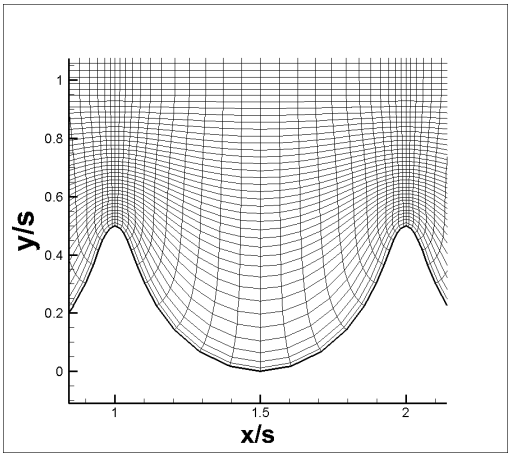

Figure 2.1.12. Riblet geometry and computational grid for LES.

Two cases were chosen: 1) Drag increasing case ($s^+ \approx 28$) and 2) Drag reducing case ($s^+ \approx 18$). Figure 2.1.13 shows that the effectiveness of these riblets is reduced.

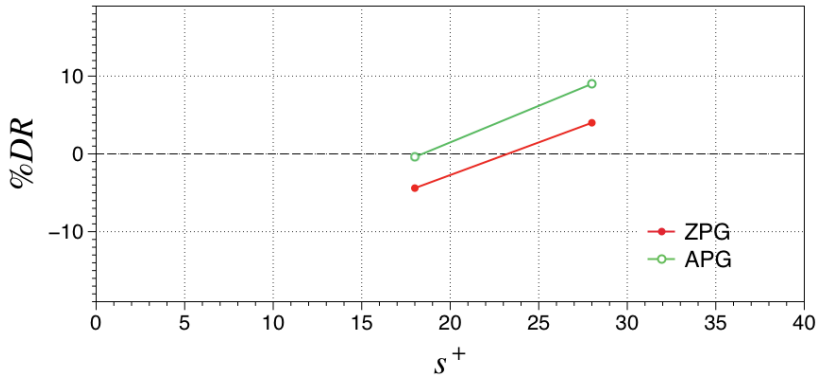

Figure 2.1.13. Drag reduction results for different pressure gradient flows for two riblet geometries.

The high-resolution LES shows, in Figure 2.1.14, that the reason for reduced effectiveness is due to an increase in normalized streamwise vorticity for the APG cases ($s^+ \approx 18$ size shown in figure, similar trend seen for larger size).

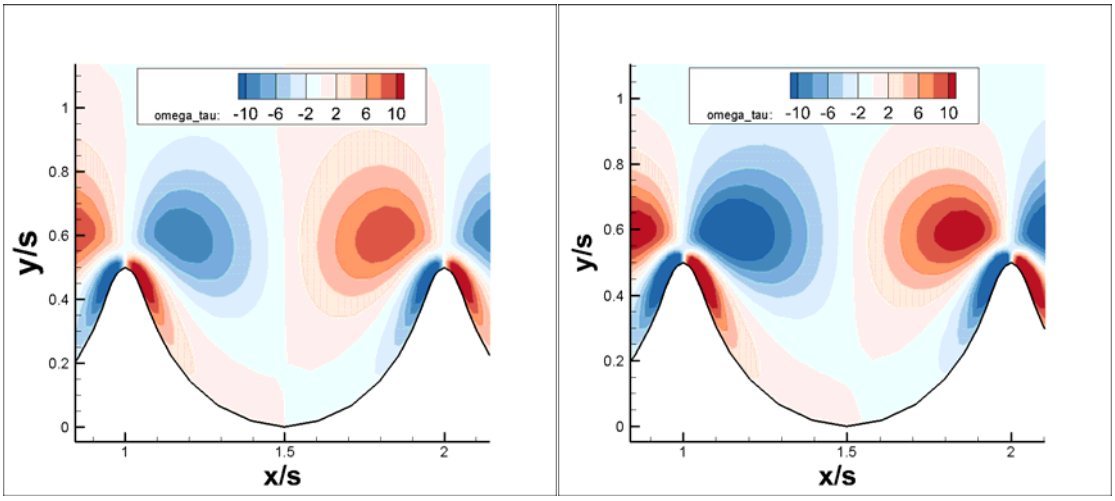

Figure 2.1.14. (Left) Mean contours of streamwise velocity for ZPG. (Right) Same for APG.

This increase in vorticity brings high momentum fluid from the freestream downwards toward the riblet surface area. This, in turn, increases skin-friction all along the riblet surface, as is shown in Figure 2.1.15. The horizontal access is spanwise movement along the riblet from the riblet valley to the tip. The vertical axis plots the difference in local shear (between ZPG and APG) for the $s^+ \approx 18$ case.

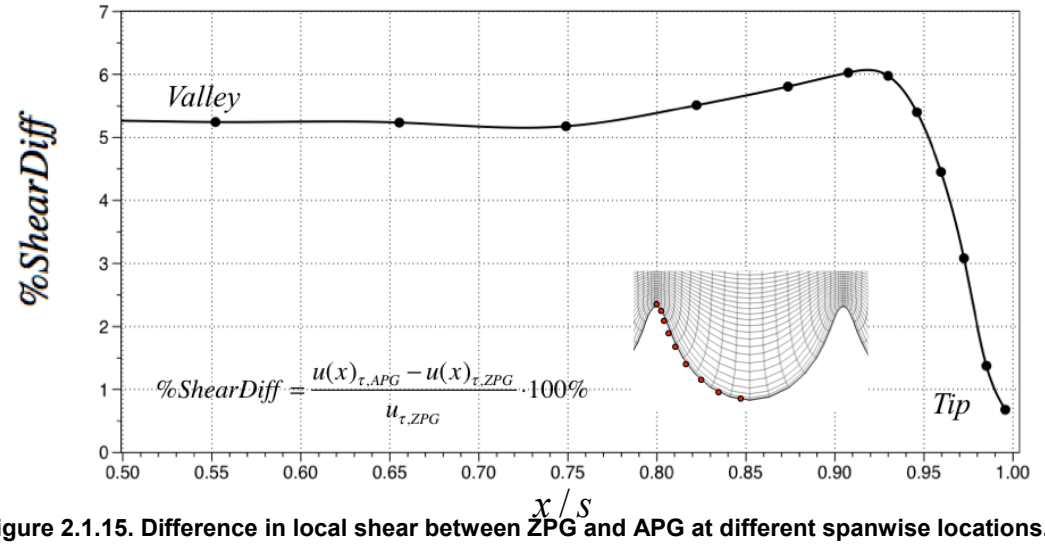

Figure 2.1.15. Difference in local shear between ZPG and APG at different spanwise locations.

Experimental Studies of Riblets on Airfoils

In this section we present a summary of the mean drag coefficients obtained in the airfoil at different angles of attack for the different riblets defined in Table 2.1.1. A comparison of the complete and partial coverage is included to determine the best configuration. The definition for

partial coverage is shown in Figure 2.1.16. An example of the results for a full coverage is illustrated in Figure 2.1.17.

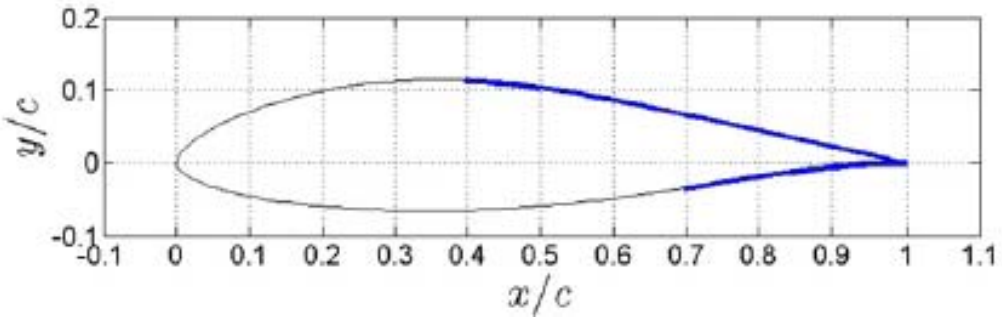

Figure 2.1.16. Schematic of the airfoil DU 96-W-180 with partial riblet film coverage (40% on the upper surface and 70% on the bottom side).

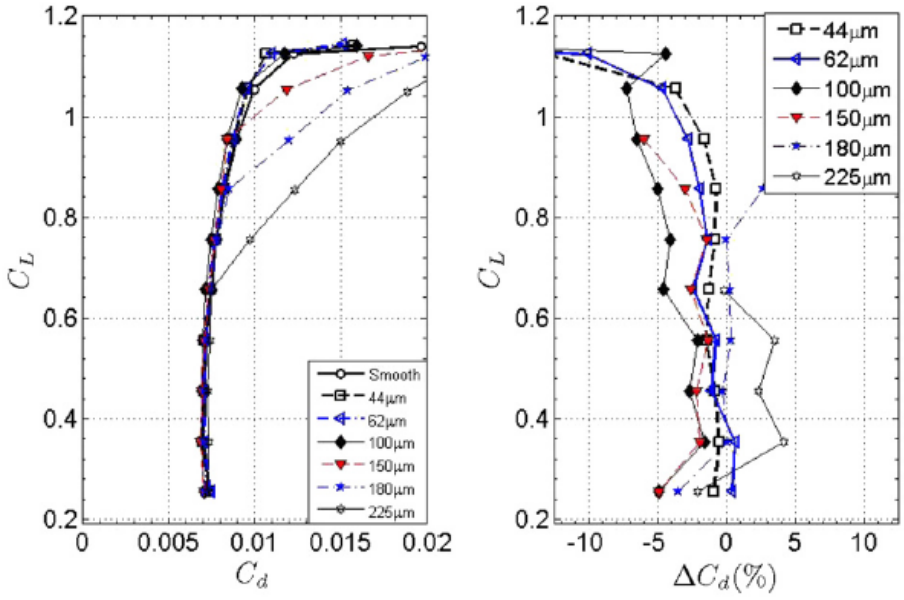

Figure 2.1.17. Left: Drag polar comparison for V-groove riblets (d=0). Right: percentage of drag changes. Negative values imply a net drag reduction.

Figure 2.1.18 and 2.1.19 show the best riblet configurations for achieving maximum drag reduction. Cases with full and partial coverage are included.

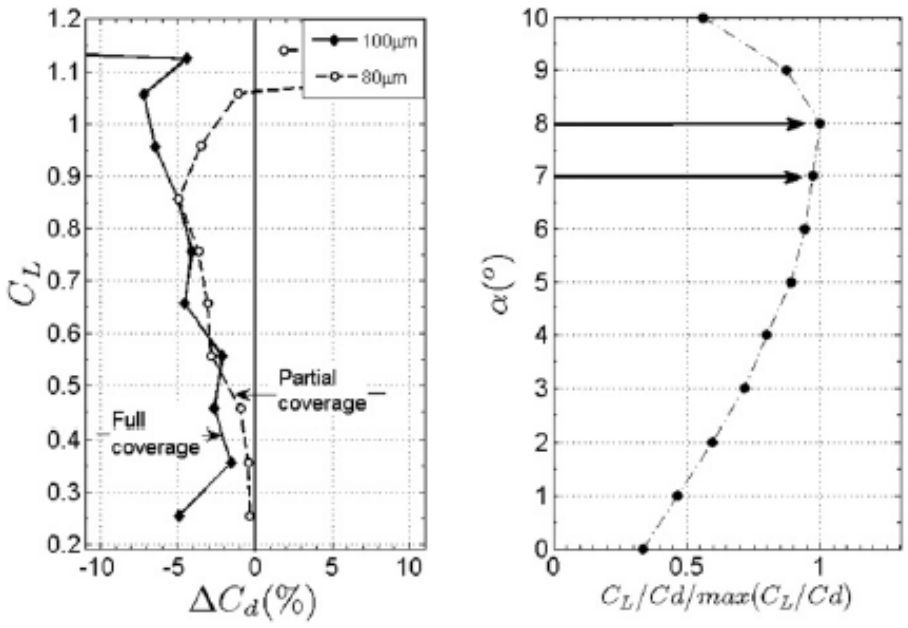

Figure 2.1.18. Optimal riblet configuration for the full and partial coverage cases (left) and normalized drag lift ratio at different angles for the smooth surface (right).

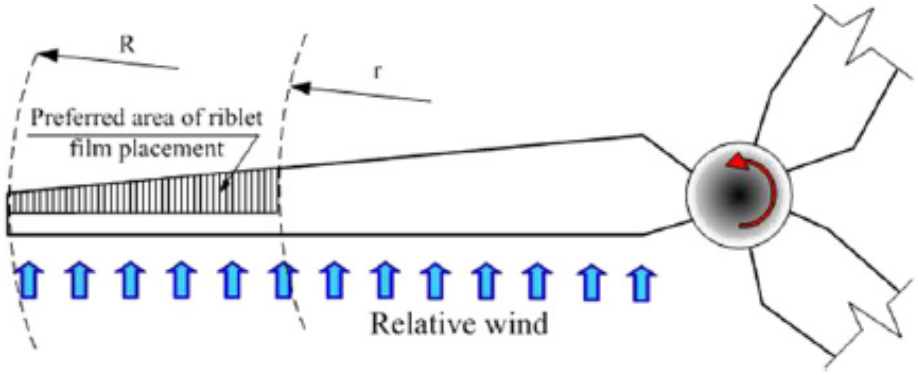

Figure 2.1.19. Schematic of partial riblet coverage in the latter section of a blade.

Based on results from flat plates, the following general formula is proposed to determine the optimum riblet configuration:

$$\frac{l_{\text{opt}}}{c} \approx 15 C_d^{-1/2} Re^{-1}$$

where Re is the Reynolds number based on the chord length *c* and l_{opt} is the square root of the groove cross-section for the optimum riblet.

Publications and Presentations

Arndt, R., Chamorro, L.P., Sotiropoulos, F., "Drag reduction in large wind turbines through riblets: Evaluation of different geometries," 50th AIAA Aerospace Sciences Meeting Including the New Horizons Forum and Aerospace Exposition, paper number AIAA 2012-0232, 2012.

Boomsma, A., and Sotiropoulos, F., "Drag-Reduction Effectiveness of Riblet Films in Adverse Pressure Gradients," 66th Annual Meeting of the APS Division of Fluid Dynamics, Piitsburgh, PA, Nov. 24-26, 2013.

Boomsma, A., and Sotiropoulos, F., "A Computational Parametric Study of Drag Reducing Riblet Geometries," 64th Annual Meeting of the APS Division of Fluid Dynamics, Baltimore, Maryland, Nov. 20-22, 2011.

Boomsma, A., Wen, L., Lauder, G., and Sotiropoulos, F., "Turbulent Flows Over Three-Dimensional Shark Skin," 65th Annual Meeting of the APS Division of Fluid Dynamics, San Diego, CA, Nov. 18-20, 2012.

Chamorro L.P., Arndt R.E.A. and Sotiropoulos F. (2013) Drag reduction in large wind turbines through riblets: Evaluation of riblet geometry and application strategies. *Renewable Energy,* 50, 1095-1105.

References

[1] Ge & Sotiropoulos, "A numerical method for solving the 3D unsteady incompressible Navier-Stokes equations in curvilinear domains with complex immersed boundaries," J. Comp. Phys., 2007, **225**, pp. 1782-1809.

[2] Gilmanov & Sotiropoulos, "A hybrid Cartesian/immersed boundary method for simulating flows with 3D, geometrically complex, moving bodies," J. Comp. Phys., 2005, **207**, pp. 457-492.

[3] Choi, Moin, & Kim, "Direct numerical simulation of turbulent flow over riblets," J. Fluid Mech., 1993, **255**, pp. 503-539.

[4] Lund, Wu, & Squires, "Generation of Turbulent Inflow Data for spatially-Developing Boundary Layer Simulations," J. Comp. Phys., 1998, **140**, pp. 233-258.

[5] DeGraaff & Eaton, "Reynolds-number scaling of the flat-plate turbulent boundary layer," J. Fluid Mech., 2000, **422**, pp. 319-346.

[6] Bechert, Bruse, Have, Van Der Hoeven,& Hoppe, "Experiments on drag-reducing surfaces and their optimization with an adjustable geometry," J. Fluid Mech., 1997, **338**, pp. 59-87.

Task 2.2: Active Flow Control for Improving Aerodynamic Performance and Reducing Noise

Literature Review and Background

The large scale unsteadiness in the atmospheric can have significant adverse effects on wind turbine performance [8] and require frequent maintenance and repair work, causing turbine downtime and incurring costs. These costs are particularly significant in the case of off-shore wind energy. The large-scale structures in incoming flow could cause instant dynamic blade stall due to the sudden change in the direction or magnitude of freestream velocity as well as the freestream turbulence intensity. The boundary layer separation on the blade suction surface induces fluctuations in the overall blade lift, which in turn increase fatigue loading on the blade and cause power output to fluctuate. In addition, extra noise signals are generated.

One possible solution to these problems is to use active flow control technology to increase the operating envelope of the blade and reduce the aerodynamic fatigue loading and aeroacoustic noise.

On the aerodynamic performance side, active flow control on different geometries has been extensively studied over the past three decades. Many past studies focus on separation control over airfoil surfaces, ensuring lift enhancement or drag reduction. Wygnanski [9] gives a comprehensive review of the active separation control for different airfoil configurations. The concept of controlling boundary layer separation by blowing has been investigated heavily for aeronautical applications since as early as 1960s. Leading edge blowing on the suction side of the airfoil provides extra momentum into its boundary layer so that the flow can overcome a higher adverse pressure gradient and thus stay attached to the blade for higher angles of attack. Moreover, it has been shown by Greenblatt et al. [10] that oscillatory blowing at the leading edge can delay boundary layer separation more effectively than steady blowing. This is because the large coherent structures introduced by oscillatory blowing enhance the transport of momentum across the shear layer, energizing the boundary layer in a more effective way. Many successful experiments by Amitay et al. [11] and Pinier et al. [12] have also used zero-net-mass flux devices such as synthetic jets as actuators since the late 90s. The principle of the synthetic jet is similar to that of unsteady blowing. By changing the volume of an enclosed cavity at a certain frequency, the synthetic jet creates a periodic alternating blowing/suction at the orifice and enhances the mixing inside and across the boundary layer. However, for wind turbine applications, active flow control technology using momentum addition is a relatively new concept. In the late 2000s, a few studies of load alleviation for wind turbine blades using active flow control technology have been carried out using different techniques [13], [14]. A comprehensive report by Sandia National Laboratories [15] summarizes the flow control efforts that have been done previously with a focus on load mitigation for wind turbine blades using a variety of actuators.

The aeroacoustic effects of active flow control have been investigated on different, but aeroacoustics has not been considered as thoroughly as aerodynamics. Two major research fields are the jet noise problem and the cavity flow induced noise problem. Low et al. [16] use the synthetic jets as actuator coupled with near field pressure information and a closed-loop

controller to reduce jet noise from a high speed jet. Cattafesta et al. [17] give a thorough review for the reduction of the cavity flow noise using active flow control technology. To the author's best knowledge, there has been no effort of using active flow control to reduce wind turbine blade-induced noise.

Goals and Objectives

This work aimed to investigate the effect of the unsteady blowing actuation on the aerodynamic performance of a two dimensional DU-96-W180 airfoil under steady flow conditions, to develop a closed-loop algorithm to reduce the aerodynamic loading fluctuation under large scale freestream unsteadiness conditions, to study the fundamental physics of the phenomenon, and to assess the effect of the interactions in the freestream unsteadiness on the far-field noise signature.

SOPO-Defined Purpose, Approach, and Outcomes:

Purpose: Develop open and closed-loop active flow control strategies based on unsteady suction and/or blowing to delay flow separation and stall in real time, optimize the overall efficiency, and minimize associated noise.

Approach: Carry out a series of wind tunnel experiments to test various active flow control strategies and identify most promising approaches; Use turbulence measurements upwind and downwind of the 2.5MW rotor, which will be obtained in task 2.5, to assess the state of the actual flow that needs to be controlled and develop low-dimensional models; Couple this information with CFD modeling (to be carried out as part of tasks 2.3 and 2.5) and additional wind tunnel experiments to develop guidelines for implementing active flow control strategies in the field.

Outcomes: Develop methods and guidelines to guide future implementation of active flow control on the 2.5 MW turbine.

Project Team

Mark Glauser is Professor of Mechanical and Aerospace Engineering and Associate Dean for Research and Doctoral Programs, LC Smith College of Engineering and Computer Science, Syracuse University, and Professor of Physics, College of Arts and Sciences, Syracuse University. As Associate Dean for Research and Doctoral Programs within the LC Smith College, Glauser is responsible for overseeing current research activities and coordinating the development of the college's future research portfolio. In his own research portfolio, Glauser, along with his co-workers, post-docs, graduate and undergraduate students, conducts major experimental, computational and theoretical efforts to apply low-dimensional models to turbulent and transitioning flows for understanding and control. Flows studied range from high speed aerospace type applications to those around thermal breathing manikins within the micro-environment. Glauser received his BS (1982) and his Ph.D. (1987) from the Department of Mechanical and Aerospace Engineering, the University at Buffalo SUNY.

Guannan Wang is a Ph.D student in the Mechanical and Aerospace Engineering Department at Syracuse University. He graduated with an M.S degree in 2008 from Syracuse University.

Technical Approach

1. A theoretical BEM based analysis was performed for the potential benefit of the separation control on the power output of a wind turbine.

2. A two-dimensional instrumented DU-96-W180 airfoil model was designed and built for the wind tunnel testing.

3. Direct aerodynamic force measurements and simultaneous surface pressure measurements were done for a set of steady flow condition wind tunnel tests. Baseline data as well as open-loop controlled data were collected evaluated.

4. A proportional closed-loop control algorithm was developed and tested using Labview.

5. Wind tunnel testing with large scale unsteadiness in the freestream produced by a 2D cylinder was performed to evaluate the effectiveness of the controller in terms of aerodynamic fatigue loading reduction.

6. Far-field acoustic signals were acquired and analyzed using a six microphone array located 10 chord length away from the leading edge, with/without cylinder and with/without flow control.

Results

Theoretical Results

The impacts of active flow control on wind turbine power output were analyzed theoretically using a BEM model. The Blade Element Momentum (BEM) method uses a 1D actuator disk model for the wind turbine rotor. By combining the local lift and drag information from either airfoil theory or experimental data and momentum equations, BEM model is able to calculate the power output of a turbine. The result as shown in Figure 2.2.1 indicates some positive effects on the overall power output of the wind turbine using active flow control.

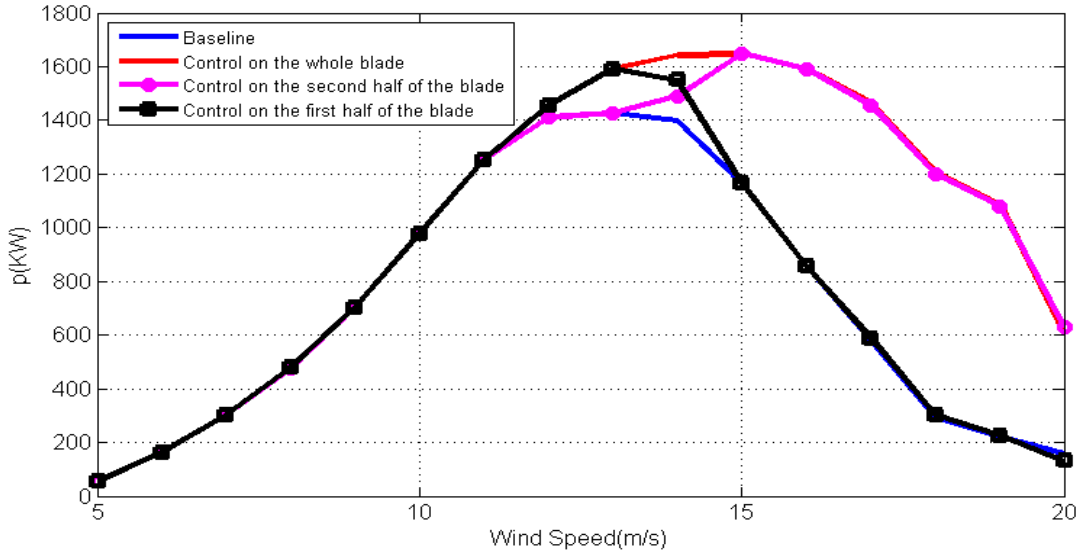

Figure 2.2.1. Power output of the simulated wind turbine with S809 airfoil with and without control.

Experimental Results

The results from the first set of the experiments demonstrated that the leading edge unsteady blowing actuation system was capable of delaying the separation for this specific airfoil under steady flow conditions as shown in Figure 2.2.2. For the cases where large scale unsteadiness dominated the incoming flow, we found that open loop control was not capable of consistently mitigating the fluctuating load. On the other hand, simple proportional closed loop control with the surface pressure information only from one sensor was capable of reducing the overall load (root mean square) RMS consistently by up to 12% at 27 degree angle of attack as shown in the Figure 2.2.3.

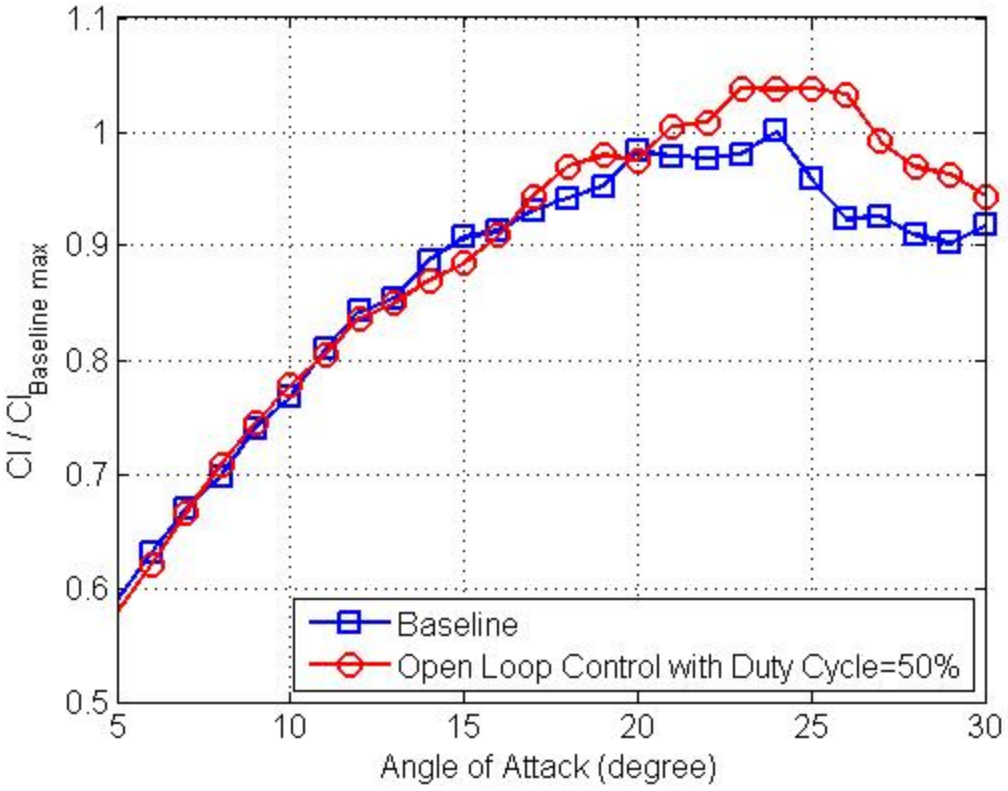

Figure 2.2.2. Open loop control results.

Control Method	F_{rms}	F_{rms} Reduction	Notes
Baseline	0.0181		
Open Loop	0.0165	9%	DC=80%
	0.0161	11%	DC=40%
Closed Loop	0.0165	9%	Use the second sensor
	0.0159	12%	Use the first sensor

Figure 2.2.3. Summary of the closed-loop control results.

The particle image velocimetry (PIV) and simultaneous surface pressure measurements from the second set of the tests gave us a better understanding of the unsteady nature of the flow so we can achieve the goal of building an even more sophisticated controller. Here we focused on the 19 degree angle of attack especially for the unsteady case to see what the effects of the large scale unsteadiness were on the airfoil at the threshold of the separation angle. Figure

2.2.4 shows a contour plot for the streamwise component of the mean velocity for both the steady and unsteady case.

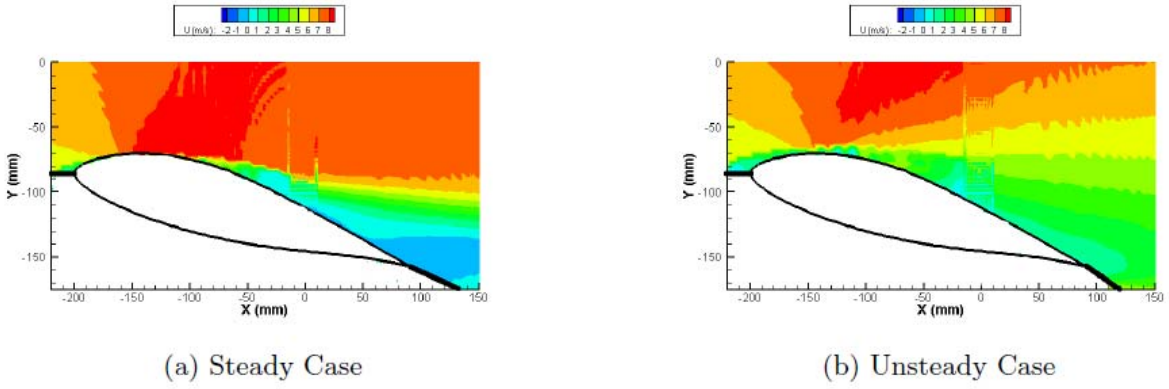

Figure 2.2.4 Streamwise components of the averaged velocity field at 19 degree angle of attack, steady vs. unsteady.

Even with the simple ensemble average, there is a significant difference in velocity field between the steady case and the unsteady case. Comparing with the steady case, the wake region near the trailing edge has expanded further away from the suction surface of the airfoil in the unsteady case, while the magnitude of the U component in the wake region increases significantly.

For the acoustic test, far-field acoustic signals were collected from both steady and unsteady conditions at different angles of attack with and without trip wire. Noise levels increase significantly across a broad band of spectrum from the steady case to the unsteady case. Results from microphone 4 and the tripped airfoil at a 20 degree angle of attack are shown in Figure 2.2.5. Also, peak frequencies associated with the toner noise around 2000 Hz were shifted and had a smaller amplitude in the unsteady case. Similar results were shown for the smooth airfoil. Further research is needed to explain the phenomena physically.

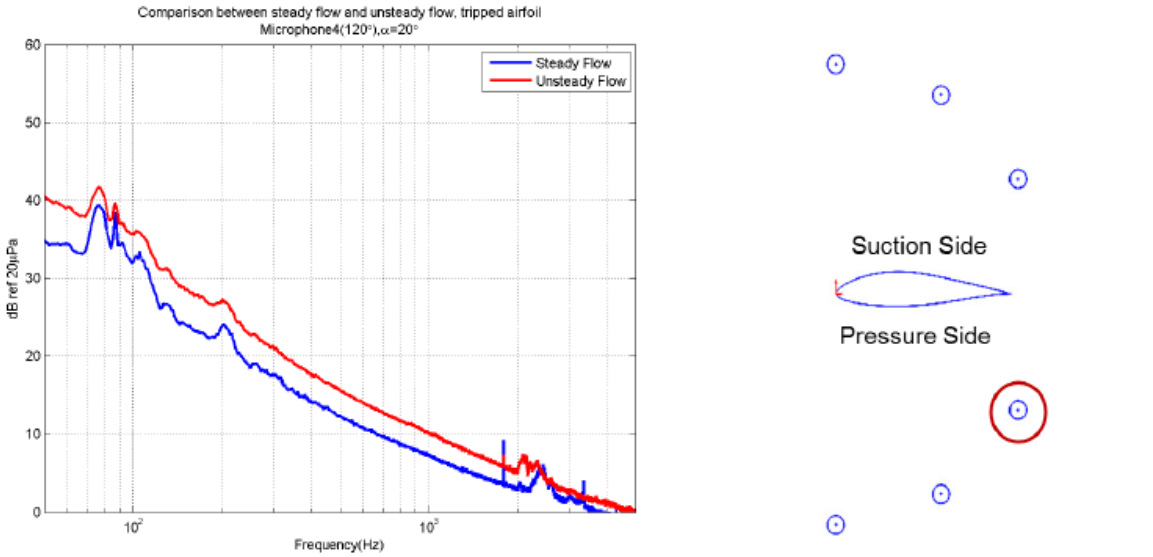

(a) Acoustic signals received by the No.4 microphone at 20 degree angle of attack

(b) Location of the microphone No. 4

Figure 2.2.5. Noise level from the steady and the unsteady cases.

Publications and Presentations

Wang, G., Lewalle, J., Glauser, M., and Walczak, J., Investigation of the Benefits of Unsteady Blowing Actuation on a 2D Wind Turbine Blade, Journal of Turbulence, Volume: 14, Issue: 01, pages 165 - 189.

(Invited) Wang, G., Walczak, J., Elhadidi, B., and Glauser, M., Preliminary Investigation of the Active Flow Control Benefits on wind turbine blades, AIAA Paper 2011-3611, 6th AIAA Theoretical Fluid Mechanics Conference, 27-30 June 2011, Honolulu Hawaii**.**

Wang, G., Glauser, M., Aerodynamic and Aeroacoustic Study of the Interaction between a 2D Wind

Turbine Airfoil and a Cylinder Wake Using PIV and Far-field Microphones, AIAA Paper 2013-0916, 2013 AIAA ASM, Meeting, January 7 - 10, Dallas, TX.

References

[7] Gelman, R. *2011 Renewable Energy Data Book.* s.l. : National Renewable Energy Laboratory, 2012.

[8] *Modeling and measurements of wakes in large wind farms.* Barthelmie, R. J, et al., et al. s.l. : Journal of Physics, 2007, Vol. 75.

[9] *Boundary Layer and Flow Control by Periodic Addition of Momentum.* Wygnanski, I. s.l. : 4th AIAA Shear Flow Conference, 1997. AIAA 97-2117.

[10] *The control of flow separation by periodic addition of momentum.* Greenblatt, D and Wygnanski, I. 7, s.l. : Progress in Aerospace Sciences, 2000, Vol. 36.

[11] *Aerodynamic Flow Control using Synthetic Jet Technology.* Amitay, M, Smith, B.L and Glezer, A. s.l. : 36th AIAA AEROSPACE SCIENCES MEETING AND EXHIBIT, 1998. AIAA 98-0208.

[12] *Proportional Closed-Loop Feedback Control of Flow Separation.* Pinier, J, et al., et al. 1, s.l. : AIAA Journal, 2007, Vol. 45.

[13] *Active Control of Flow Separation and Structural Vibrations of Wind Turbine Blades.* Maldonado, V, et al., et al. 2-3, s.l. : Wind Energy, 2010, Vol. 13.

[14] *Unsteady Separation Control on Wind Turbine Blades Using Fluidic Oscillators.* Cerretelli, C, Wuerz, W and Gharaibah, E. 7, s.l. : AIAA Journal, 2010, Vol. 48.

[15] Johnson, S.J, V.C, Dam and Berg, E.D. *Active Load Control Techniques for Wind Turbines.* s.l. : Sandia National Laboratories, 2008.

[16] *A low-dimensional approach to closed-loop control of a Mach 0.6 jet.* Low, K. R, et al., et al. 4, s.l.: Experiments in Fluids, 2013, Vol. 54.

[17] *Active control of flow-induced cavity oscillations.* Cattafesta, L, et al., et al. s.l.: Progress in Aerospace Sciences, 2008, Vol. 44.

Task 2.3: High-Resolution CFD-FSI code for Aero-elastic Simulations of Turbine Blades

Literature Review and Background

Blades are a critical component of wind turbine design as they require a delicate balance between strength and weight. As opposed to the stationary turbine tower, where strength is essentially the only design concern, the weight of the moving blades significantly affects turbine performance. The tower is sometimes made of a material as heavy as concrete, while the desire to minimize blade weight typically leads to designs involving a combination of materials with complicated characteristics.

Such special blade performance requires a careful design process. A combination of experimental and analytical techniques is used to understand blade behavior and find the optimal shape and distribution of manufacturing materials. Constant exchange of information between these two approaches leads to their mutual improvement and is necessary for progress.

Geometrical and material complexity, and the fact that the blades interact with air (fluid), is the reason that on the analytical side of analysis and design of blades various computational methods are employed almost exclusively. In the large body of relevant, literature, many of the contributions can be grouped into two major categories: contributions based on beam models and those employing shell models.

Models based on beam theory can provide rough “global” information concerning the blade response, which are useful in the preliminary stage of design. The analysis is typically restricted to two-dimensional scenarios and, as such, it is not capable to capture some essential coupling between various three-dimensional modes of blade deformation.

The group based on shell models is on the other end of the spectrum of methods. Other than a fully three-dimensional approach, which is unrealistic and probably unnecessary, it is the most advanced and precise way of dealing with the problem. Shell models are capable of faithfully represent the geometry of the blade, they can account for the composite nature of various materials involved (in the case of more advanced shell models), and they can capture the local deformation and stress fields, which are often a good predictor of failure. There are many publications in which blades are modeled as shells. Recently, even the interaction of the entire turbine and air was analyzed based principally on shell models [45].

Goals and Objectives:

This work aimed to develop a robust, easy to use, and accurate Fluid-Structure Interaction (FSI) code, which can be readily modified in the process of searching for optimal design of the blade (and turbine). To overcome the shortcomings of using either beam or shell theory, the model developed to meet objective 1 will be based on thin-walled beam theory, which will include attributes of both beam and shell theory and also be expanded to include fluid-structure interaction of blades. The developed model would cover variable cross-sections that can change abruptly, allow arbitrary three-dimensional deformations and coupling between various

modes of deformation, and permit material properties to change within a cross-section as well as over the length of the blade.

SOPO Defined Purpose, Approach, and Outcomes:
Purpose: Develop a high-resolution Fluid-Structure Interaction (FSI) CFD code for aeroelastic calculations at field scale.

Approach: Couple high-resolution, rigid-blade CFD code with an advanced Finite Element model of the turbine blade. Validate the CFD-FSI code with both laboratory experiments and measurements from the field-scale facility.

Outcomes: A finite-element FSI structural solver for wind turbine blades. A FSI solver coupling the FE model with the flow solver. The code will be made available to DOE labs and the industry..

Project Team

Henryk K. Stolarski is a professor of Civil Engineering with research specializations in structural and continuum mechanics. His research interests include large deformation inelastic problems, analysis of shell structures, and numerical techniques for nonlinear problems of mechanics. Professor Stolarski holds a MS degree in Structural Mechanics from the Tech. University of Warsaw, (1968), a MS degree in Applied Mathematics from the University of Warsaw (1975), a MS degree in Engineering Mechanics (1977) and a Ph.D. in Engineering Mechanics from the Institute of Fundamental Technological Research, Polish Academy of Sciences (1979). He has been a professor of Civil Engineering at the University of Minnesota for 24 years and is currently a member of the Graduate Studies Committee, Undergraduate Studies Committee and the Faculty Performance Evaluation Committee. Professor Stolarski is a reviewer for several journals, including International Journal for Numerical Methods in Engineering, Computer Methods in Applied Mechanics and Engineering, Computers and Structures, ASCE Journal of Engineering Mechanics, AIAA Journal, Computational Mechanics, ASCE Journal of Structural Engineering, Journal of Aircraft (AIAA), Journal of Applied Mechanics, among others.

Fotis Sotiropoulos is James L. Record Professor of Civil Engineering at the University of Minnesota and has served as director of St. Anthony Falls Laboratory since 2006. Fotis Sotiropoulos' research is aimed at developing high-resolution, fluid-structure interaction, computational algorithms for enabling virtual experiments and simulation-based engineering design in real-life environmental, renewable energy, and biological applications. Sotiropoulos earned his Ph.D. in Aerospace Engineering from the University of Cincinnati.

Ariel Dahl is now a structural engineer at Meyer Borgman Johnson. Previously she was a graduate student at the University of Minnesota, participating in the research for task 2.3. Her master's thesis, "A Computational Model for Thin-Walled Structures with Variable Cross-Sections" was based on research performed as a part of this task.

Antoni Calderer received his bachelor's degree in civil engineering in 2010 at the Technical University of Catalonia in Barcelona. He is currently a PhD student and research assistant in the

University of Minnesota's Saint Anthony Falls Laboratory. His research interests are focused on Computational Fluid Dynamics, covering the fields of turbulence modeling, fluid-structure interaction, two-phase free-surface flows, and wave-structure interaction.

Technical Approach

Discretization and Degrees of Freedom

To discretize the blade, first series of cross-sections along the length of the blade is introduced. They are perpendicular to a straight *reference line,* orthogonal to the root cross section. In general, this reference line does not coincide with an axis of the blade, which is a three-dimensional curve. A number of nodes along the wall within each of these cross-sections are then selected. The data needed to specify the position of those nodes consists of three special coordinates, one of them being the location of the cross-section along the blade. It is noted that the kind of data needed for blade discretization is consistent with the data used in blade manufacturing; it easy to modify this data any time the shape of the blade needs to be changed. Each cross-section has the same number of nodes, so the nodes of neighboring cross-sections can be connected to form a series of quadrilateral elements, or mesh, to be used in the model.

The proposed thin-walled beam model considers two types of degrees of freedom: those associated with the behavior of the entire cross-section (beam degrees of freedom) and nodal degrees of freedom with respect to the individual nodes within the cross-section, which are parallel to the straight reference line (warping, or distortional, degrees of freedom). The three-dimensional motion of each cross-section has five components: two displacements and three rotations. If the long dimension of the blade is directed along the *x*-axis, the displacements of the cross-section are in the *y*- and *z*-direction. The three rotations are around each of the coordinate axes. Displacement in the *x*-direction is captured by distortional degrees of freedom, δ, at each node as seen in Figure 2.3.1.

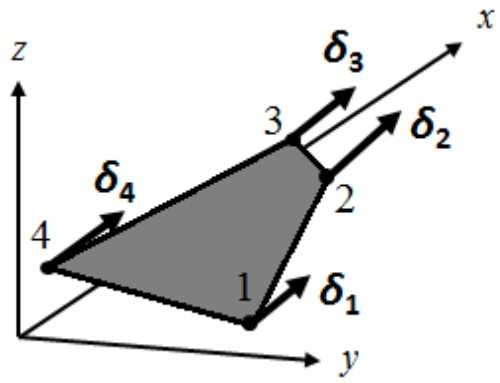

Figure 2.3.1. Membrane Element with Distortional Degrees of Freedom.

The behavior of one element of the mesh is controlled by the movement of the two cross-sections it connects as well as four distortional degrees of freedom, one at each node. When the local numbering of the nodes is assigned as in Figure 2.3.1, and if nodes 1 and 4 within the

cross-section *I* and nodes 2 and 3 are within the neighboring cross-section *J*, the elemental vector of degrees of freedom (which is made up of 14 degrees of freedom) is organized as:

$$\mathbf{d}_{\boldsymbol{e}}^{T} = \left\{ \mathrm{v}_{yJ}, \mathrm{v}_{zJ}, \theta_{xJ}, \theta_{yJ}, \theta_{zJ}, v_{yK}, v_{zK}, \theta_{xK}, \theta_{yK}, \theta_{zK}, \delta_1, \delta_2, \delta_3, \delta_4 \right\}$$

where:
v_{yJ} = displacement of cross-section J in the *y*-direction
v_{zJ} = displacement of cross-section J in the *z*-direction
θ_{xJ} = rotation about the *x*-axis at cross-section J (torsion)
θ_{yJ} = rotation about the *y*-axis at cross-section J (bending in *xz*-plane)
θ_{zJ} = rotation about the *z*-axis at cross-section J (bending in *xy*-plane)
δ_i = displacement of node *i* in *x*-direction (warping)

The total number of beam degrees of freedom (dofs) is five times the number of cross-sections and the total number of distortional degrees of freedom equals the number of nodes in all cross sections. In the global vector of degrees of freedom all beam dofs are placed first, followed by distortional dofs. The advantage of organizing the degrees of freedom in this way is that one can easily eliminate the warping degrees of freedom from the final system of equations.

Internal Segments
Wind turbine blades will often have an internal spar, or multiple spars, as shown in Figure 2.3.2. These spars, or internal walls, may have material properties that greatly differ from that of the exterior wall. If the internal spars are much stiffer than the rest of the structure, the warping of the cross-section will not be smooth and the blade model must accurately capture this behavior.

Figure 2.3.2. Possible Internal Spar Configurations.

The thin-walled beam model developed in the course of this project is capable of accounting for such internal walls, for abruptly changing material properties and for sharp corners in the cross-section, through the use of segments. One logical use of segments is to have one segment be the exterior walls of the blade and another segment as the internal rib. Each segment could then be assigned its own material property. Additionally, the internal rib (spar) may terminate at some location along the blade, which can also be easily accounted for in the model utilizing the concept of segments.

The addition of internal segments does not affect the number of beam degrees of freedom, which are associated with the entire cross-section (as explained previously). The internal segment would simply add a number of nodes to the cross-section, and thus the number of distortional dofs. The wind turbine blade would then have quadrilateral elements on the exterior of the structure, as well as internal elements at the location of the spar. The displacements of each element are still affected by the translational and rotational degrees of freedom of

neighboring cross-sections as well as distortional degrees of freedom at the nodes along the exterior wall and the nodes along the spar.

Problem Equations and System Reduction

With the quadrilateral finite element mesh just described, the subsequent steps of analysis are essentially the same as in any other finite element calculations. Just like in any finite element analysis each element may have different material properties, including anisotropic properties, which in the case of blade is of paramount importance. The difference from the usual finite element analysis is that all elements between cross-section I and J share those cross-sections' beam degrees of freedom, which makes the strain calculations more elaborate, requiring a different assembly process.

In static problems the global equations may be put in the form having the structure shown in Figure 2.3.3. It is assumed there that the dominant loading pattern is associated with the beam degrees of freedom, and that the distortional dofs only modify the stiffness properties of the blade. In the case of blade analysis this appears to be a realistic assumption as the normal pressure on the blade is the principal wind force.

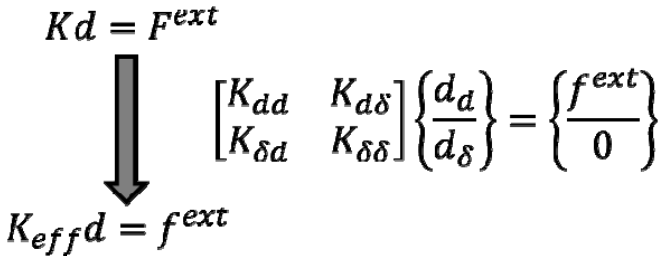

Figure 2.3.3. Static System Reduction.

Under this assumption, the Guyan Reduction, used to eliminate the distortional dofs, does not modify the forcing term (the right hand side) of the equation in Figure 2.3.3, and gives the following form of the effective stiffness matrix, $\mathbf{K}_{\mathbf{eff}}$,

$$\mathbf{K}_{\mathbf{eff}} = \mathbf{K}_{\mathbf{dd}} - \mathbf{K}_{\delta\mathbf{d}}^{\mathrm{T}} \mathbf{K}_{\delta\delta}^{-1} \mathbf{K}_{\delta\mathbf{d}}$$

$\mathbf{K}_{\mathbf{eff}}$ is a square matrix of size $10*\{\text{number of cross-sections}\}$.

The effective stiffness matrix captures the effects of the distortional dofs, so this process significantly reduces the size of the system of equations to be solved and shortens the computation time without compromising accuracy.

Mass and Inertia

The global mass matrix, **M,** may be constructed in the usual way it would have the following form:

$$\mathbf{M} = \begin{matrix} \mathbf{M}_{\mathbf{dd}} & \mathbf{M}_{\mathbf{d}\delta} \\ \mathbf{M}_{\delta\mathbf{d}} & \mathbf{M}_{\delta\delta} \end{matrix}$$

In order to form the reduced system of equation of motion the effects of the warping dofs on the inertia term is neglected (which for the blades appears sufficiently accurate). Thus, the effective mass matrix $\mathbf{M}_{\mathbf{eff}}$, can be taken equal to $\mathbf{M}_{\mathbf{dd}}$., which is a square matrix of size 10*{number of cross-sections}.

Dynamic Equation of Motion

The final system of equations after the system reduction and application of boundary conditions is

$$\mathbf{M}_{\mathbf{eff}}\ddot{\mathbf{d}}(t) + \mathbf{K}_{\mathbf{eff}}\mathbf{d}(t) = \mathbf{f}^{\mathbf{ext}}(t)$$

where d is the global displacement vector and is given by

$$\mathbf{d}^{\mathbf{T}} = \{v_{y1}, v_{z1}, \theta_{x1}, \theta_{y1}, \theta_{z1}, v_{y2}, v_{z2}, \theta_{x2}, \theta_{y2}, \theta_{z2}, \ldots, v_{yn}, v_{zn}, \theta_{xn}, \theta_{yn}, \theta_{zn}\}$$

where v_{y1} is the displacement of cross-section 1 in the *y*-direction, v_{yn} is the displacement of the last cross-section in the *y*-direction, and so on. In the fluid-structure interaction problem, the right-hand-side of the above equation results from the fluid pressure and is not known. It is determined from the coupled solution of the fluid and bade equations.

Results

Bending Test

In the following example, a twisted beam with thin-walled rectangular cross-section was tested in bending through application of a tip point load. The initially undeformed beam was twisted a total of 90 degrees over 140 meters, the total length of the beam. The cross-section was 4 meters by 12 meters with a wall thickness of 0.2 meters. The discretization consisted of 20 nodes at each cross-section, and 15 total cross-sections. The Young's modulus was chosen as 70 GigaPascal, with 100 MegaNewtons applied tip loading in the positive *y*-direction.

The deformed and undeformed shapes are shown in Figure 2.3.4 below. Looking along the *x*-axis (the axis of the beam), Figure2.3.5 gives another view of the deflected shape. Due to the twisted original configuration of the beam, the beam experienced displacement in both *y*- and *z*-directions, seen clearly in Figure 2.3.5, despite being loaded purely in the *y*-direction. This response is important in analysis of blades.

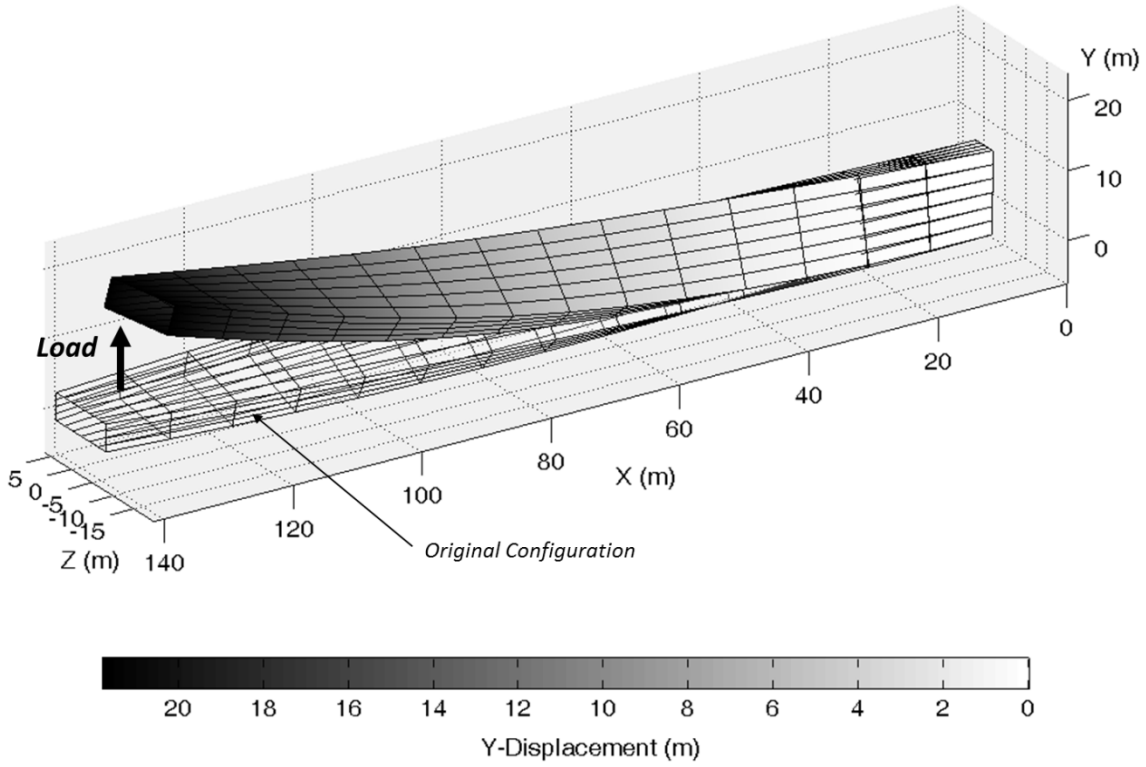

Figure 2.3.4. Bending of Twisted Beam.

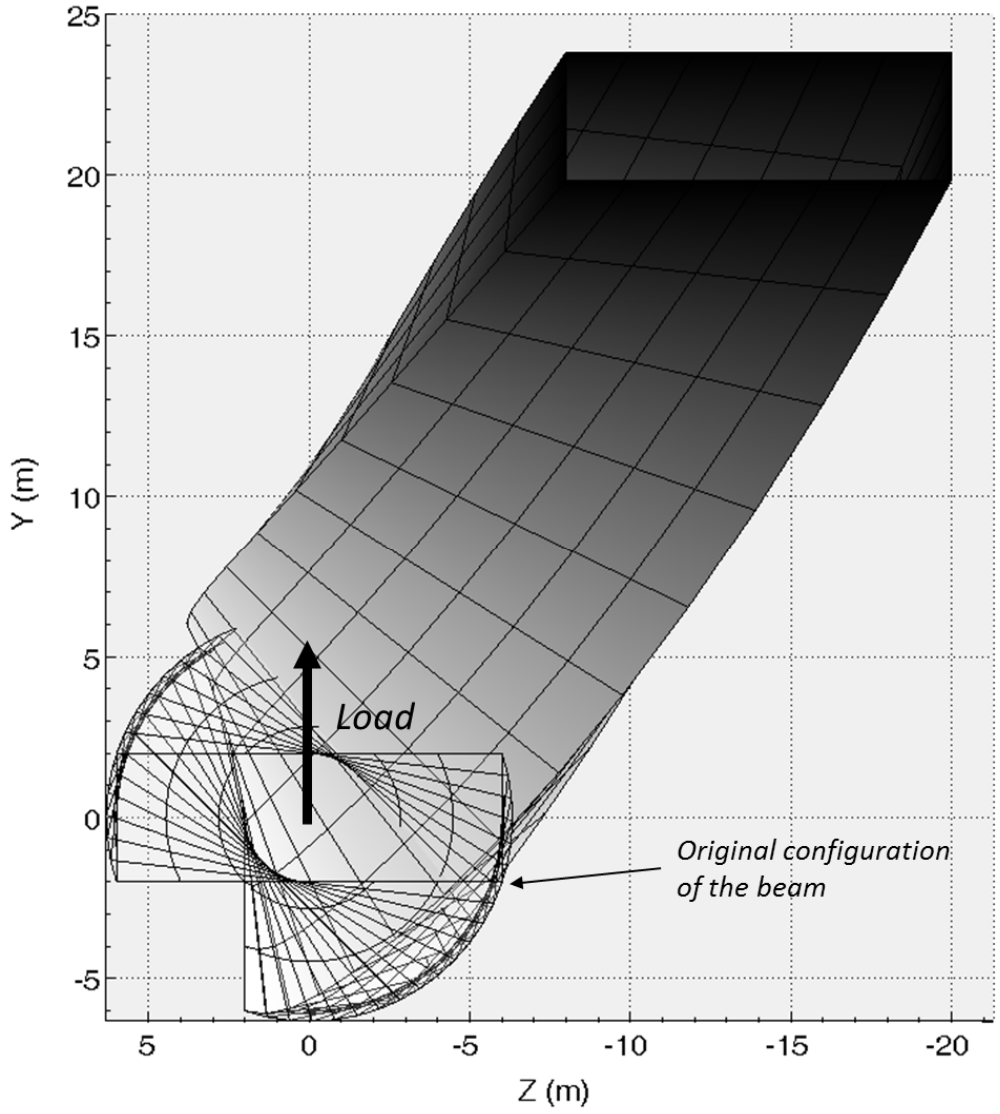

Figure 2.3.5. Original and Deformed Configuration of Twisted Beam.

The analytical solutions, that can be developed based on the a more advanced beam analysis, specifying tip displacements of that beam due to an external force in the *y*-direction, P_y, are given as

$$v_y = \frac{P_y L^3}{6\pi^2 E} \left(\frac{\pi^2 + 6}{I_z} + \frac{\pi^2 \quad 6}{I_y} \right)$$

and

$$v_z = \frac{P_y(\pi^2 \quad 4)L^3}{2\pi^2 E} \quad \frac{1}{I_z} \quad \frac{1}{I_y}$$

where v_y and v_z are the tip displacements in the y- and z-directions respectively. These formulas have been developed for beams with solid (compact) cross-sections and they do not account for warping. The second moments of inertia, Iy and Iz, also appear in these equations along with the beam length, L. A comparison of the analytical versus numerical results for tip displacements is given in Table 2.3.1.

Table 2.3.1. Comparison of Displacements with Py = 1x108 N

	Theoretical	Numerical: Thin-Walled Beam Model	Percent Difference (%)
v_y (m)	21.104	21.798	3.233
v_z (m)	-14.147	-13.980	1.184

The analytical displacements of about 21 and -14 meters in *y*- and *z*-directions, respectively, match well with what is observed visually Figure 2.3.5. In fact, the percent differences between the theoretical and experimental results were as low as 3.233 and 1.184 percent for *y*- and *z*-displacements, respectively. This indicates that the thin-walled beam model is accurately capturing the stiffness of the beam, even with a relatively coarse mesh.

Variable Cross-Section Test

Wind turbine blades are non-prismatic, with cross-sections of varying airfoils along the length to circular cross-sections at the hub. So, for illustration purposes, the following example involves two beams with varying cross-sections. The first test considered a beam that was circular at the fixed end and tapered off to an ovular cross-section at the tip. The second test maintained the same cross-sectional shapes as the first test but also considered a shift in the beam's axis, another trait that is shared by wind turbine blades. Views along the *x*-axis of both beams are shown in Figure 2.3.6 and Figure 2.3.7, with the darker contours indicating the cross-sections nearest the tip.

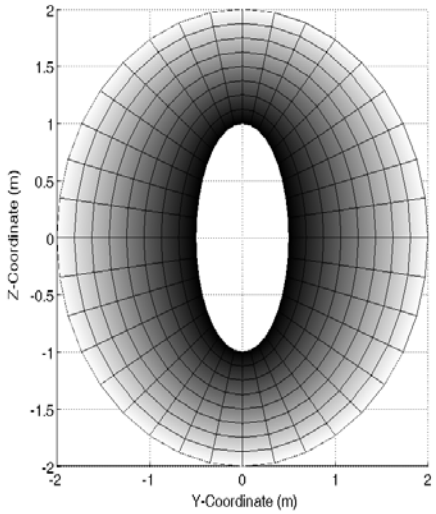

Figure 2.3.6. Variable Cross-Section Beam without Axis Shift.

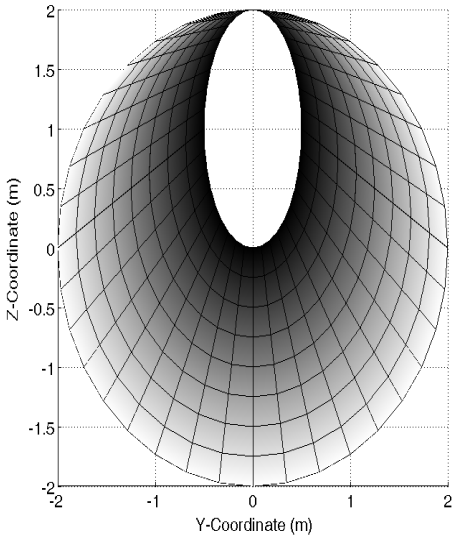

Figure 2.3.7. Variable Cross-Section Beam with Axis Shift.

Similarly to previous examples, the material properties for both beams were taken as 70 GPa for Young's Modulus and Poisson ratio of 0.35. The beam length was 100 meters, with the discretization seen clearly in Figure 2.3.8. Both tests considered loading in the *y*-direction of P_y = 100 MN. The results for both tests for tip displacements and rotations are given in Table 2.3.2. It can be seen that unlike Test 1, in Test 2 with a shifted beam axis, some torsion (0.060 radians) results over the length of the beam. Additionally, the magnitude of the tip displacement is increased from 13.814 to 13.869 meters due to the lower, varying second moment of inertia in Test 2.

Table 2.3.2. Effect of axis shift on torsional rotation		
	Test 1: No Axis Shift	Test 2: Axis Shift
v_y (m)	13.814	13.869
θ_x (rad)	0.000	0.060

Dynamic Tests and Comparisons: Free Vibration

The first few modes of vibration will likely be decisive in full fluid-structure interaction analysis. The frequencies for free vibration of the first four modes are presented in this section for validation of the thin-walled beam model. The natural frequencies are found by finding roots of the following characteristic equation

$$\left| \mathbf{K}_{\mathbf{eff}} - \omega_i^2 \mathbf{M}_{\mathbf{eff}} \right| = 0$$

with ω_i being the natural frequencies. The results for the thin-walled elliptical beam finite element model are given in Figure 2.3.3 for a beam fixed at one end and free at the other (cantilever). The present results are based on discretization consisting of 24 elements within a cross-section and 20 elements along the length of the beam. After reduction the total number of degrees of freedom in the above equation was 100.

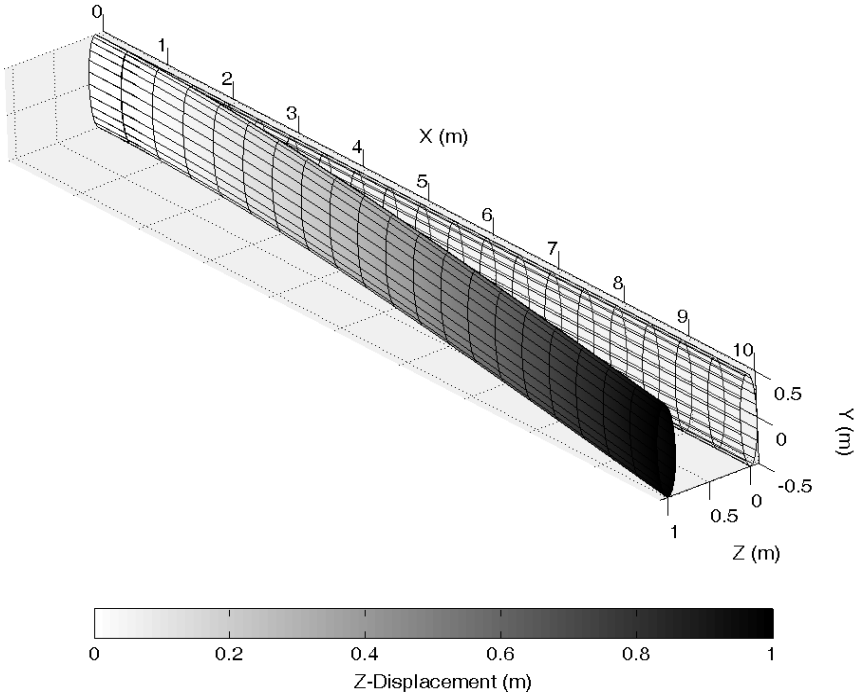

Figure 2.3.8. First Weak-Axis Bending.

The present results are compared in Table 2.3.3, with the natural frequencies found for the same structure using a shell model from a well-known commercial code ABAQUS. The model used 8-node quadratic shell elements with reduced integration and Lanczos method for calculating modes and frequencies of vibration. In the shell model 28 elements around the perimeter of the cross-section were used with 100 elements along the length of the beam resulting I a total of 14,000 dofs. As seen in Table 2.3.3, the frequencies obtained by the present approach are in close agreement with those obtained using a significantly more elaborate model, in spite of the huge disparity between the number of degrees of freedom in these two models. Although not shown, the mode shapes were also in a very good agreement.

Table 2.3.3. Comparison of Natural Frequencies, f (Hz)

	Shell Model	Thin-Walled Beam Model
Mode 1: First Weak-Axis Bending	2.277	2.249
Mode 2: First Strong-Axis Bending	8.476	8.434
Mode 3: Second Weak-Axis Bending	13.799	13.596
Mode 4: First Torsion	36.068	36.192

FSI coupling

The structural model based on the thin-walled structure theory has been fully coupled with the curvilinear immersed boundary method (CURVIB) of Ge and Sotiropoulos [1]. The CURVIB solves the incompressible Navier-Stokes equations in generalized curvilinear coordinates using a second-order central difference scheme in space and second-order fractional step method to advance in time. The motion of geometrically complex moving bodies is tracked using a sharp interface immersed boundary method. The FSI algorithm that couples the fluid with the structural motion is the partitioned approach [18]. In partitioned FSI algorithms the fluid and structural domains are solved independently and coupled by imposing boundary conditions at its interface, i.e. the fluid domain provides the pressure and shear stresses at the surface of the body to the structural model, and the structural model computes the displacements that are incorporated back to the fluid domain.

The interfacing of the present FE model with the CURVIB method required special attention due to the fact that the two approaches use different typology of meshes. While the CURVIB method represents the body with an unstructured triangular mesh, the structural model uses a structured quadrilateral mesh. With the objective of minimizing the error of transmitting the forces and displacements, the two meshes are constructed with coincident grid nodes as illustrated in figure 2.3.9. The idea is that given a quadrilateral element, the triangular elements are then generated by following these two steps: (1) each quadrilateral element is divided in a subset of 4 quadrilaters of equal area, and (2) the newly formed quadrilaters are divided through its diagonal in two triangles of equal area.

On the other hand, the CURVIB method provides the pressure at the centroid of each triangular element of the structural mesh while the FE model reads the pressure at the center of each of the four quadrilaters forming the quadrilateral elements. By construction, the center of the small quadrilaters coincides with the midpoint of the segment delimited by the centroids of two adjacent triangular elements. For example, in figure 2.3.9, the point a1 is the midpoint of the segment delimited by a2' and a1". Therefore, the pressure value at the centers a1, a2, a3, a4 can be easily interpolated.

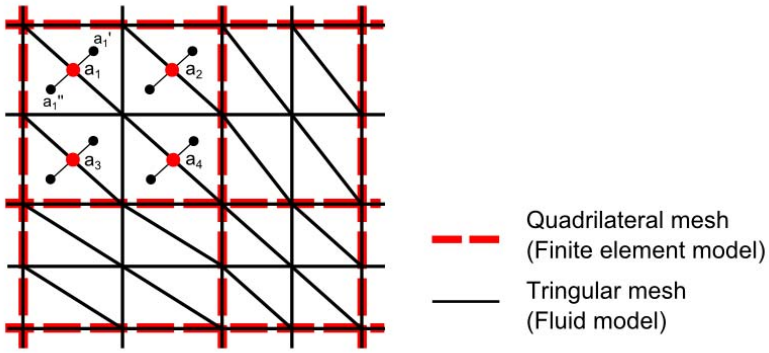

Figure 2.3.9. Schematic description of the structural meshes and the nodes where pressure is computed.

An initial simulation to illustrate the capability of the FE structural model to calculate the response of a real wind turbine, and its compatibility with the CURVIB method is presented. A wind turbine blade with S809 airfoil has been placed in a uniform flow, and the structural response of the blade has been calculated with a prescribed pressure distribution. Figure 2.3.10 show the deformed blade geometry and the structural response.

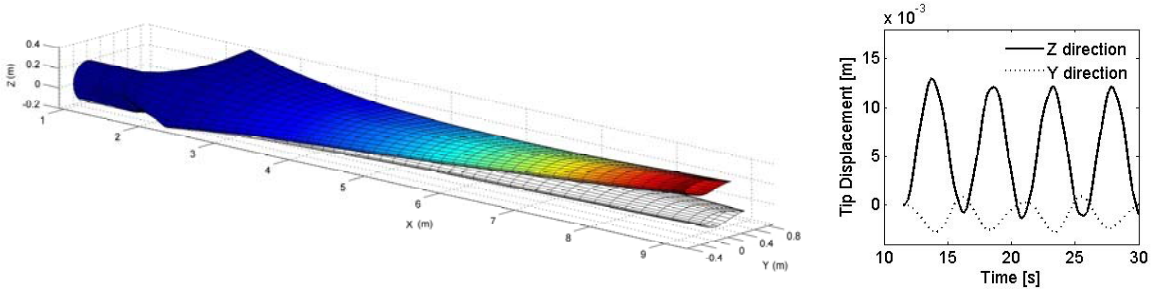

Figure 2.3.10. Deformed wind turbine blade geometry (left), and structural response (right).

To validate the coupling FE-CURVIB algorithm in a fully Fluid-structure interaction form, we have applied it to simulate the benchmark test case of vortex induced vibrations of a cantilever beam, proposed by Wall et. al. [19]. The configuration, illustrated in figure 2.3.11, consists in a thin elastic structure attached to a fixed square cylinder submerged into a uniform flow in which the elastic body results in self-induced oscillations. The inflow velocity is v=31.5cm/s, the

dynamic viscosity of the fluid is $\mu=1.82\text{x}10^{-4}$ g/cm/s, the density $\rho_f=1.18\text{x}10^{-3}$ g/cm^3 and a Reynolds number Re=204. The structure has a modulus of elasticity of $E=2.5\text{x}10^7$Pa, a poison ratio of u=0.35 and density of $\rho_f=0.1$g/cm^3. Vorticity contours and tip displacements are presented in figure 2.3.12. Comparison with the results of Zilian et. al. [20] shows very good agreement.

Further validation of the code with field measurements was not possible during the scope of the project since field data were not available on time and it will be pursued in the near future. Ongoing research projects in SAFL involve the use of the current code to simulate wind and hydrokinetic turbines with elastic blades.

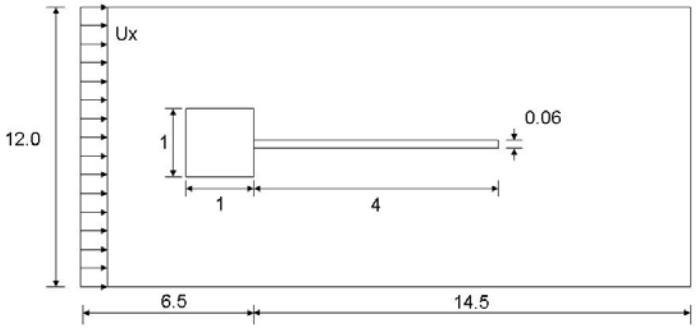

Figure 2.3.11. Vortex-induced vibrations of a cantilever beam: configuration. Units are in cm.

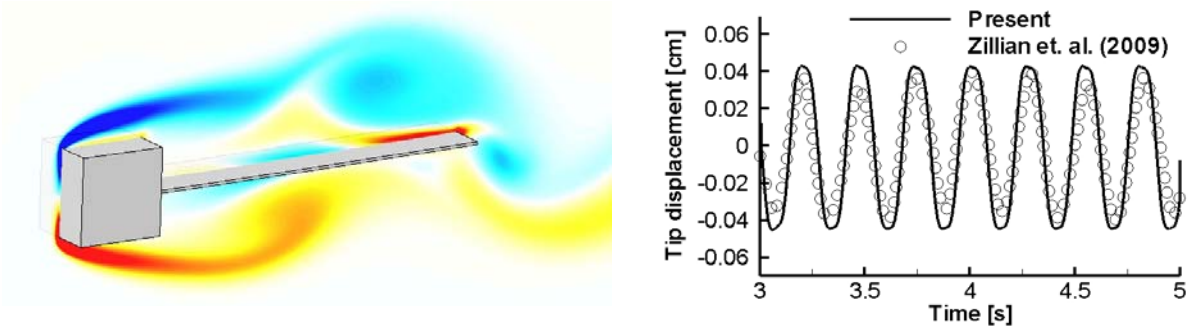

Figure 2.3.12. Vortex-induced vibrations of a cantilever beam: Vorticity contours (left) and tip displacements (right).

Publications and Presentations

Dahl, Ariel. “A Computational Model for Thin-Walled Structures with Variable Cross-Sections.” MS. Thesis, Department of Civil Engineering, University of Minnesota, September 2011.

References:

[45] Hsu, M-C. and Bazilevs, Y., "Fluid structure interaction modeling of wind turbines: simulating the full machine", *Computational Mechanics,* 2012, **50**, 6, 821-833.

[18] Borazjani, Iman, Liang Ge, and Fotis Sotiropoulos, “Curvilinear Immersed Boundary Method for Simulating Fluid Structure Interaction with Complex 3D Rigid Bodies.” *Journal of Computational Physics* 227, no. 16 (August 2008): 7587–7620.

[1] Ge & Sotiropoulos, “A numerical method for solving the 3D unsteady incompressible Navier-Stokes equations in curvilinear domains with complex immersed boundaries,” J. Comp. Phys., 2007, **225**, pp. 1782-1809.

[19] Wall, Wolfgang A. “Fluid-Struktur-Interaktion Mit Stabilisierten Finiten Elementen” (1999).

[20] Zilian, A., D. Dinkler, and A. Vehre. “Projection-based Reduction of Fluid–structure Interaction Systems Using Monolithic Space-time Modes.” *Computer Methods in Applied Mechanics and Engineering* 198, no. 47–48 (October 2009): 3795–3805.

Task 2.5: Multi-Scale Modeling for Wind Farm Siting

Literature Review and Background

Large-eddy simulation (LES) of wind farms with parameterization of wind turbines is emerging as a powerful tool for improving the performance and lowering the maintenance cost of existing wind farms and assessing potential sites for installing wind farms. The spacing of turbines in a wind farm determines the turbine wake interactions as well as interactions with the atmospheric boundary layer, which collectively determine the performance of the wind farm. Complex terrains have significant effects on wind resources and also influence the wake recovery and wake interactions of wind turbines.

Wind turbines in computational models can be modeled in 4 levels of increasing sophistication: 1) actuator disk parameterization; 2) actuator line parameterization; 3) actuator surface parameterization and 4) geometry-resolving approach. The actuator surface model is still not widely used in wind energy applications. The geometry-resolving approach requires large number of grid nodes to resolve the boundary layer around the blade and the details of the complex turbine geometry, and for that it is not feasible for wind farm simulations. The actuator disk and actuator line parameterizations, on the other hand, which avoid resolving the boundary layers around the blades and the details of the turbine geometry, are commonly employed in wind energy applications.

Simulations of wind turbines and wind farms in complex terrains have been carried out by solving the Reynolds-averaged Navier–Stokes (RANS) equations. To the best of our knowledge, however, numerical methodologies for carrying out LES in complex terrain have not been reported.

Goals and Objectives

The goal of this work is to develop a multi-scale computational framework for simulating wind over wind turbines and wind farms. This computational tool will help improve the performance of existing wind farms and assess the wind resources at the potential sites. More specifically, we validate the present computational framework by comparing with wind tunnel measurements. The developed CFD tool is then applied to simulate an operational wind farm in flat terrain and wind at a site with complex terrain.

SOPO Defined Purpose, Approach, and Outcomes:

Purpose: Develop and test novel CFD tools for the prediction of high-resolution wind and turbulence in the atmospheric boundary layer, and their interactions with wind turbines and wind farms. Provide a tool for science-based optimization of wind farm design.

Approach: Multi-scale modeling coupling meso-scale models with atmospheric LES and high-resolved CFD of turbine blades. Integration of wind tunnel experiments with detailed measurements in the field for model validation.

Outcomes: High-resolution Large Eddy Simulation framework for multi-scale simulations and site-specific optimization of wind farms.

Project Team

Fotis Sotiropoulos is James L. Record Professor of Civil Engineering at the University of Minnesota and has served as director of St. Anthony Falls Laboratory since 2006. Fotis Sotiropoulos' research is aimed at developing high-resolution, fluid-structure interaction, computational algorithms for enabling virtual experiments and simulation-based engineering design in real-life environmental, renewable energy, and biological applications. Sotiropoulos earned his Ph.D. in Aerospace Engineering from the University of Cincinnati.

Xiaolei Yang is a Post-Doctoral Associate at the University of Minnesota. Yang joined St. Anthony Falls Laboratory in 2010 as a Post-Doctoral Associate with expertise in computational fluid dynamics. Yang received his Ph.D. in Fluid Mechanics from the Institute of Mechanics, Chinese Academy of Sciences, China in 2010.

Technical Approach

In this project, the Virtual Wind Simulator (VWiS) software was developed for simulating turbulent flow over wind turbines and wind farms. The conceptual features of the VWiS are shown in Figure 2.5.1.

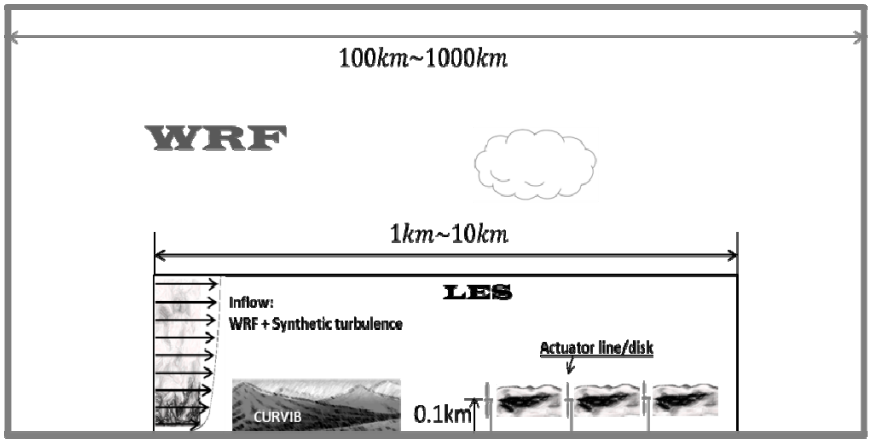

Figure 2.5.1. Schematic of the VWiS (Virtual Wind Simulator). The Weather Research and Forecasting (WRF) model is used to carry out mesoscale simulations of atmospheric wind conditions to provide boundary conditions for a fine mesh Large-Eddy Simulation (LES) model.

With reference to Figure 2.5.1, the major features of the software VWiS are:

1. Mesoscale simulations at hundreds of kilometers are carried out using WRF (Weather research and forecasting model) to obtain boundary conditions for the inner domain where wind-farm-scale simulations will be carried out.
2. Wind farm scale simulations are carried out using LES [21] with input from the WRF mesoscale simulations. The LES resolves unsteady turbulent fluctuations, which are responsible for intermittent fluctuations of power output and dynamic loadings on wind turbines.

3. Arbitrarily complex, site-specific land topography is simulated using the curvilinear immersed boundary method (CURVIB) [1], which can reduce the time for grid generation and take advantage of efficient solver for structured grids.
4. Wind turbines are parameterized using either actuator disk or actuator line theory [21] [22].
5. The VWiS is efficiently parallelized using Message Passing Interface (MPI) and can take full advantage of HPC resources.

The flow solver

For the flow solver of VWiS, the governing equations for the incompressible turbulent flows are the 3D, unsteady, filtered continuity and Navier-Stokes equations in non-orthogonal, generalized, curvilinear coordinate. Second-order central differencing is employed for spatial discretization. A second-order accurate fractional step method is used for advancing the continuity and momentum equations. An algebraic multigrid acceleration along with GMRES solver is used to solve the pressure Poisson equation and matrix-free Newton-Krylov method is used for the filtered momentum equation. The subgrid scale stress tensors for both velocity and temperature fields are modeled by the dynamic eddy-viscosity subgrid scale model. At the bottom boundary, the shear stress boundary condition and no-flux boundary condition are used for the wall-parallel and wall-normal velocity components, respectively. The wall shear stress is calculated from the logarithmic law for rough wall. For a smooth wall, the wall shear stress is calculated from a simplified boundary layer equation. A wall model for the temperature is also employed. Arbitrarily complex geometries are represented by the CURVIB method. In CURVIB method, the grid nodes near the immersed boundaries provide boundary conditions for the flow simulation, where the velocities are interpolated from the surrounding fluid nodes and boundary values.

Inflow generation technique

Inflow conditions are essential for wind farm simulations using LES. As mentioned in last paragraph, two inflow generation techniques are employed in the VWiS. For the first one, the turbulent flow field at the inlet is generated from a separate fully developed turbulent flow. Using this method, the domain size, the mesh and time step usually should be the same as those of the wind farm simulation. If they are different, interpolation over space and time are needed. For the second one, the flow field (the velocity and temperature) at the inlet of wind farm region is interpolated spatially and temporally from the WRF solution. Because of the coarse grid using in WRF (hundreds of meters, which are usually ten or twenty times larger than that used in LES), the turbulence scales explicitly resolved by WRF are much larger that in LES. To reconstruct the small unresolved turbulence scales for inflow velocities of the LES, a synthetic turbulence generation technique developed by [24].

Parameterization of wind turbines

To avoid an excessive computational cost to solve the boundary layer flow around the blade, actuator disk and actuator line models are employed for parameterization of the effects of wind turbine on the flow. For the actuator disk model, the wind turbine rotor is represented by a permeable disk. The forces are uniformly distributed on the disk for actuator disk model, in which the thrust force coefficient is from the one-dimensional momentum theory. For the

actuator line model, the rotor blade is represented by a single line. The drag and lift coefficients are obtained from a look-up table. The mesh for the actuator disk/line model generally does not coincide with the background mesh for the fluid. A regularized delta function is used to transfer the quantities between the two meshes.

Results

Validation of VWiS

The actuator disk/line model was validated by simulating the flow over a single turbine and an aligned wind-turbine array in comparison with wind tunnel experiments. The comparisons for the single turbine are shown in Figure 2.5.2. The comparisons for the turbine array case are shown in Figure 2.5.3. As seen, good agreements with measurements are obtained.

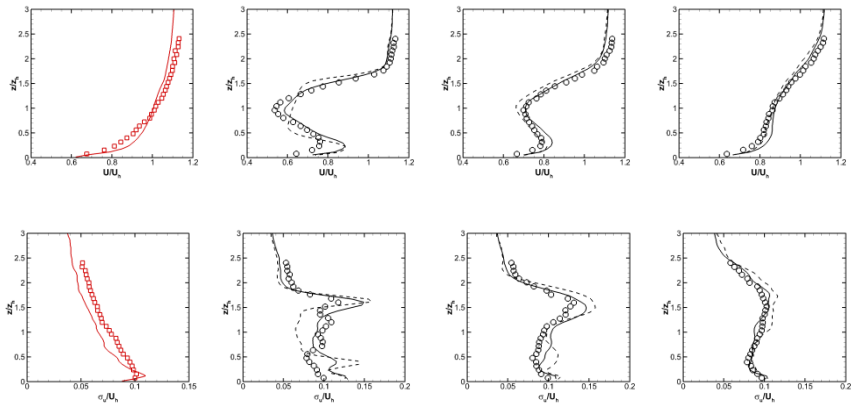

Figure 2.5.2. Comparison of mean velocity profiles (first row) and streamwise turbulence intensities (second row) at different downstream locations. From left to right: Inflow, 2D, 5D and 10D. Symbols: experiment; solid line: actuator line model, dashed line: actuator disk model.

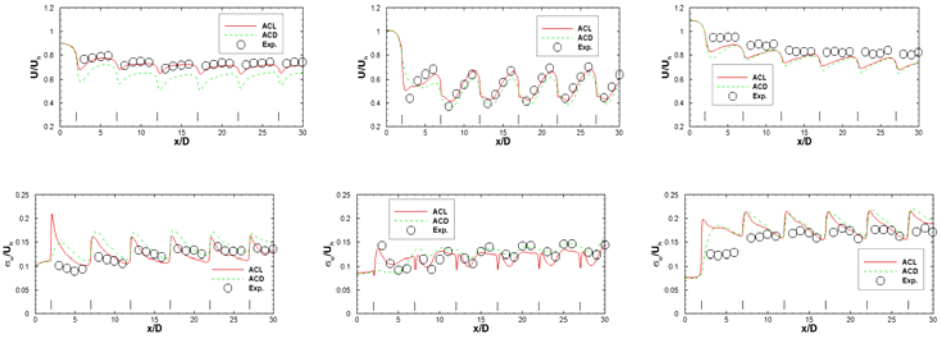

Figure 2.5.3. Comparison of the mean streamwise velocity (top) and streamwise turbulence intensity (bottom) from actuator disk model and actuator line model with wind tunnel measurements at different vertical locations (left: bottom tip; middle: hub height; and bottom: top tip).

Application of *VWiS* to an operational farm in flat terrain

Using the multi-scale modeling for our VWiS, we simulate the Mower County wind farm and performed comparison with field measurements for the period ranging from 6 am to 8 am on July 2, 2010. In Figure 2.5.4, we show the computational domains for this case.

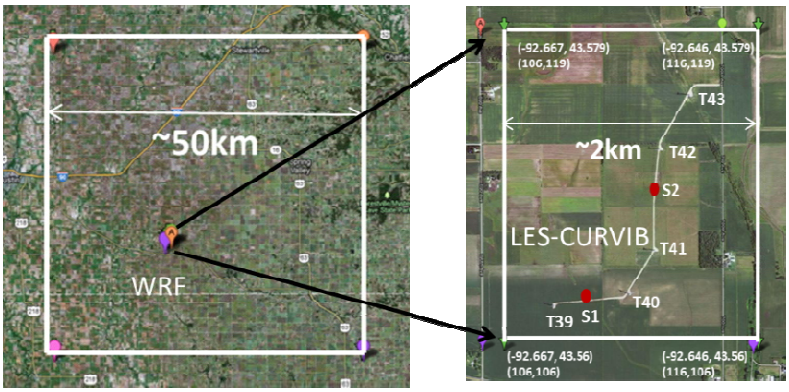

Figure 2.5.4. Computational domains for multi-scale simulation.

Table 2.5.1 shows the comparisons of the power output with the field measurements. It is seen that overall good agreements are obtained for turbines T39, T40, T41 and T43 for both cases, that is, for the simulation with and without synthetic turbulence at the inlet. For the T42 turbine, however, which is in the wake of T41, the simulation with synthetic turbulence significantly improves the predictions of power output compared with the one without inflow synthetic turbulence. These results underscore the ability of the VWiS to simulate with good accuracy the power output of real-life wind farms and underscore the need to account in the simulation for the effects of atmospheric turbulence.

Table 2.5.1. Comparison of the mean power output

	T39 (MW)	T40(MW)	T41(MW)	T42(MW)	T43(MW)
Measurements		2.15	2.14	1.86	1.85
Inflow: without synthetic turbulence	2.38	2.25	2.07	0.79	1.94
Inflow: with synthetic turbulence	2.38	2.13	2.75	1.51	2.14

Application of *VWiS* for assessment of wind resources at a undeveloped site with complex terrain

In this task, we apply the VWiS to assess the wind resources at Prairie Island with the effects of the complex topography. The incoming velocity at one measurement point (M1) at the complex terrains in the upstream of Prairies land is 9.4 m/s. The wind is from southwest, in which direction complex terrains are located. The size of the computational domain, the contours of the land surface elevation and the 8 suppositional wind turbines are shown in Figure 2.5.5.

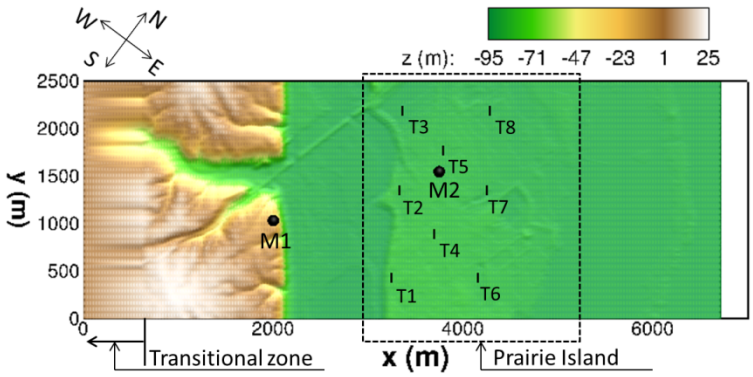

Figure 2.5.5.Topography and 8 suppositional wind turbines (T1-T8) at Prairie Island. The two points (M1 and M2) in the figure show the locations of measurements. The wind is from left to right.

The comparisons of the time-averaged mean streamwise velocity with the field measurements are shown in Figure 2.5.6. As seen, good agreement is obtained for both upstream (M1 in Figure 2.5.5) and downstream locations (M2 in Figure 2.5.5). The time-averaged contours of the streamwise velocity and turbulence kinetic energy at horizontal plane located at hub height are shown in Figure 2.5.6.

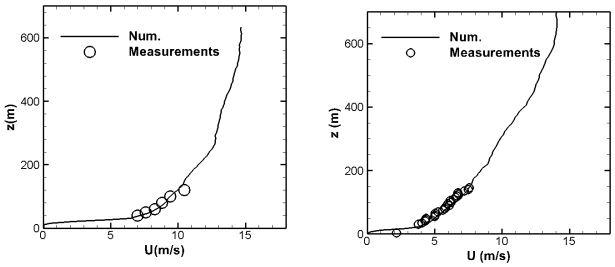

Figure 2.5.6. Comparison of the computed time-averaged streamwise velocity with measurements for Prairie Island case, in which the comparison at M1 (at the upstream complex terrains) and M2 (at the downstream Prairie Island) are shown in the left and right figures,

The time averaged streamwise velocity and turbulence kinetic energy with 8 suppositional wind turbines are shown in Figure 2.5.7.

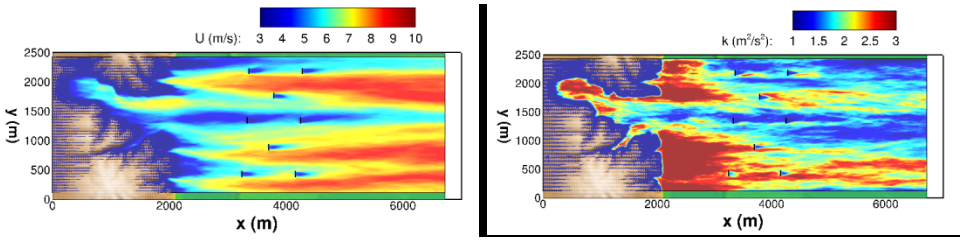

Figure 2.5.7. Time-averaged flow field (mean streamwise velocity (left) and turbulence kinetic energy (right)) at hub height (80 meters from the Prairie Island) for Prairie Island case with 8 suppositional wind turbines.

Publications and Presentations

Chamorro, L.P., Guala, M., Arndt, REA, and Sotiropoulos F. On the evolution of turbulent scales in the wake of a wind turbine model. J. of Turbulence, 13, No.27, 1-13, 2012.

Chamorro, L.P., Arndt, R.E.A. and Sotiropoulos F. Reynolds number dependence of turbulence statistics in the wake of wind turbines. Wind Energy 15(5), 733-742, DOI: 10.1002/we.501, 2012.

Chamorro, L.P., Arndt, R.E.A. and Sotiropoulos F. Turbulence properties within a staggered wind farm. An experimental study. Boundary-Layer Meteorology, 141, 349-367, 2011.Yang X., Kang S. and Sotiropoulos F. Computational study and modeling of turbine spacing effects in infinite aligned wind farms. Phys. Fluids 2012. **24**, 115107.

Chamorro, L., Arndt, R.E.A. and Sotiropoulos, F. Fundamental aspects in the wind farm optimization: Wind tunnel experiments. The Science of Making Torque from Wind, Oct. 9-11, 2012, Oldenburg, Germany.

Chamorro, L., Tobin, N., Arndt, R.E.A., and Sotiropoulos, F., Variable-sized wind turbines are a possibility for wind farm optimization. in press, Wind Energy, 2013.

Chamorro, L., Lee, S., Olsen, D., Milliren, C., Marr, J., Arndt, R.E.A., and Sotiropoulos, F. Turbulence effects on a full-scale 2.5 MW horizontal-axis wind turbine under neutrally stratified conditions. in press, Wind Energy, 2014.

Green, D.J., Chamorro, L.P., Arndt, R.E., Sotiropoulos, F., Sheng, J. Phase-locked PIV measurement in the wake of model wind turbines under various inflow conditions. American Society of Mechanical Engineers, Fluids Engineering Division (Publication) FEDSM, 1 (PARTS A AND B), pp. 1507-1514, 2012

Kang S., Yang X., Sotiropoulos F. On the onset of wake meandering for an axial flow turbine in a turbulent open channel flow. J. Fluid Mech. Under review.

Sotiropoulos F., Yang X., Kang S. On the effects of turbine geometry on the far wake dynamics of an axial flow hydrokinetic turbine. The 66th Annual Meeting of the American Physical Society, 2013, Pittsburgh, Pennsylvania.

Yang X., Sotiropoulos F. 2011. “LES investigation of turbine spacing effects in wind farms”. The 64th Annual Meeting of the American Physical Society, Baltimore, Maryland.

Yang, X.; Sotiropoulos, F. An improved effective roughness height model for optimization of wind farm layout. 65th Annual Fall DFD Meeting, November 18-20, 2012, San Diego, California.

Yang, X.; Sotiropoulos, F. LES investigation of infinite staggered wind-turbine arrays. The Science of Making Torque from Wind, October 9-11, 2012, Oldenburg (Oldb), Germany.

Yang, X.; Kang, S.; Sotiropoulos, F. Toward a simulation-based approach for optimizing MHK turbine arrays in natural waterways. Proceedings of the 1st Marine Energy Technology Symposium METS2013, April 10-11, 2013, Washington, D.C.

Yang, X.; Sotiropoulos, F. On the predictive capabilities of les-actuator disk model in simulating turbulence past wind turbines and farms. The 2013 American Control Conference, June 17 - 19, Washington, DC.

Yang X., Sotiropoulos F., Conzemius R. J., Wachtler J. N., and Strong M. B., Large-eddy simulation of turbulent flow past wind farms in complex terrains: The Virtual Wind Simulator (VWiS). Wind Energy. Under review.

Yang X., Sotiropoulos F. Wake characteristics of a model turbine in the downstream of a 3d hill. In preparation.

References

[1] Ge & Sotiropoulos, “A numerical method for solving the 3D unsteady incompressible Navier-Stokes equations in curvilinear domains with complex immersed boundaries,” J. Comp. Phys., 2007, **225**, pp. 1782-1809.

[21] Yang X., Kang S. and Sotiropoulos F. Computational study and modeling of turbine spacing effects in infinite aligned wind farms. Phys. Fluids 2012. **24**, 115107

[22] Yang, X.; Sotiropoulos, F. On the predictive capabilities of les-actuator disk model in simulating turbulence past wind turbines and farms. The 2013 American Control Conference, June 17 - 19, Washington, DC.

[24] Mann, J., Wind field simulations. Probabilistic Engineering Mechanics, 1998, Vol. 3, No.4, pp 269-282.

Task 2.6: A Novel Power Electronics based Electrical Generation System for Wind Turbines

Literature Review and Background

Wind energy is becoming increasingly relevant as more emphasis is put upon energy resources that are renewable and sustainable. Like most renewable resources however, wind energy needs to be harnessed at points usually far away from the consumption areas and has to be transmitted over long distances. The power generated in windmills is at a low voltage, typically in the range 600-700V. This low voltage is stepped up to a high voltage like 34.5kV [1] by a line frequency transformer for distribution purposes to reduce transmission line losses. In on-shore windmills, the transformer is located at the tower base and the power is carried at low voltage levels from the nacelle to the transformer [2]. This system is shown in Figure 2.6.1. These cables carry a large amount of current, leading to large copper (I^2R) losses.

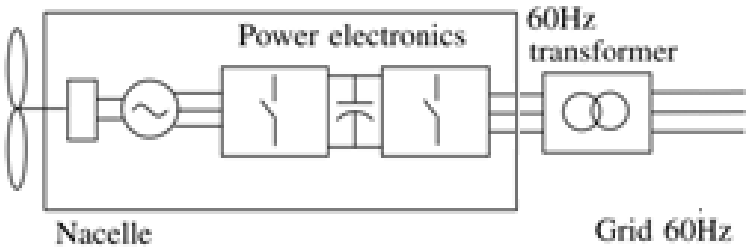

Figure 2.6.1. Schematic of typical wind turbine generator electrical configuration.

Recently, wind turbine manufacturers have started to employ a different configuration, where the transformer is installed inside the nacelle, therefore eliminating the low voltage cables [3]-[5]. However, this leads to an increase in the weight of the nacelle. So, it would be worthwhile to explore power electronic transformers which operate at high frequencies thereby reducing size of the equipment in the nacelle.

In addition to the weight reduction in the nacelle, the long term reliable operation of the generator in wind turbines is important. Pulse Width Modulator (PWM) converters used in electric drives facilitate easy control of the generator, but they also produce high-frequency switching common-mode voltage across the machine. Switching common-mode voltage can cause problems like electromagnetic interference, bearing and shaft currents (which can lead to bearing failure)[6]-[8]. So, PWM converter topologies and control schemes that can eliminate or reduce common-mode voltage should be researched.

Goals and Objectives:

The goal of this project was to develop smaller and lighter power electronics transformer technology that can be used in wind energy applications. Smaller and lighter components can

greatly reduce the fabrication and construction costs of wind turbines, especially when those components are required in the nacelle of the wind turbine.

SOPO Defined Purpose, Approach, and Outcomes:
Purpose: Develop a novel electrical generation system for wind turbines using power electronics.

Approach: To connect the wind generator to the utility grid, the proposed system will replace the conventional 60-Hz transformer and the conventional converter system with a novel power-electronic-transformer technology, which uses a high-frequency transformer that can be smaller and lighter than a conventional 60-Hz transformer by a factor of as much as 100. The lab prototype of such a system will be demonstrated.

Outcomes: Demonstrate that the proposed system results in a nacelle with significantly lighter weight and reduced volume and higher reliability.

Project Team

Ned Mohan joined the University of Minnesota in 1975, where he is Oscar A. Schott Professor of Power Electronic Systems. He received his undergraduate education in India. He joined the University of Wisconsin in 1969 and earned his MS in Nuclear Engineering, and PhD in electrical engineering under the supervision of Professor Harold Peterson. He conducts research in areas of power systems, power quality, control of electronic machines, soft-switching converters and inverters, and electronic converters for interfacing of wind energy, solar energy, and plug-in hybrid vehicles.

Gysler Castelino completed her PhD in Electrical Engineering at the University of Minnesota in 2013. Her research interests are AC-AC and AC-DC power conversion using matrix converters and high frequency transformers.

Rohit Baranwal received his Bachelors of Technology degree in Electrical Engineering from Indian Institute of Technology Roorkee in 2008. Currently, he is pursuing a PhD in Electrical Engineering at the University of Minnesota. His areas of interest are power electronics and its applications in renewable energy sources.

Technical Approach

The proposed topology is illustrated in Figure 2.6.2.

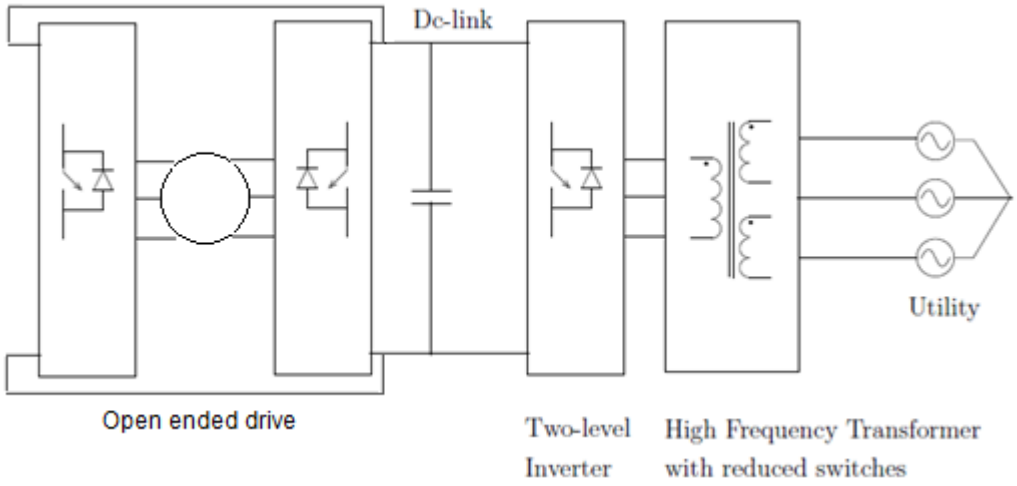

Figure 2.6.2. Proposed electrical topology examined in research study.

The topology consists of two parts, which will be described in the sections below.

Three phase line frequency AC to controlled DC converter with high frequency transformer (HF-transformer)

This converter consists of a high frequency transformer and a two level converter. The diagram of this system is shown in Figure 2.6.3. The high frequency transformer in this circuit has only two power electronic switches to produce a high frequency ac waveform as opposed to the multiple switches required in other designs.

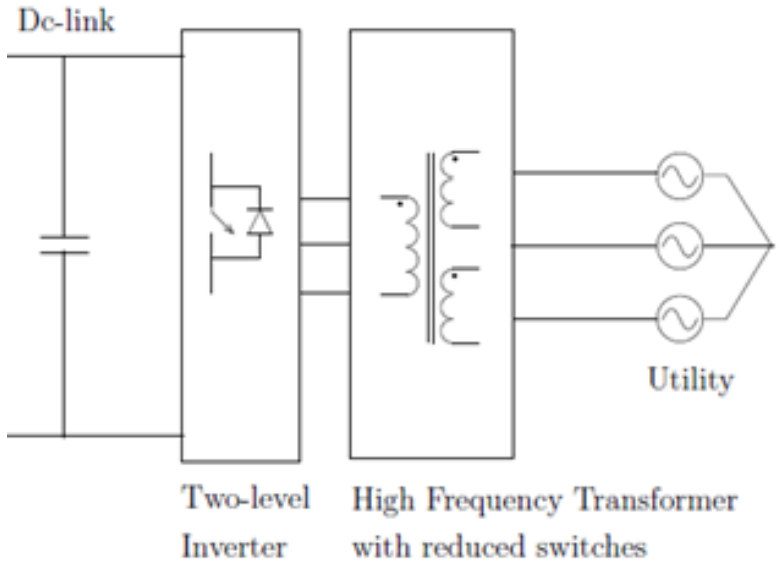

Figure 2.6.3. Schematic of high frequency transformer.

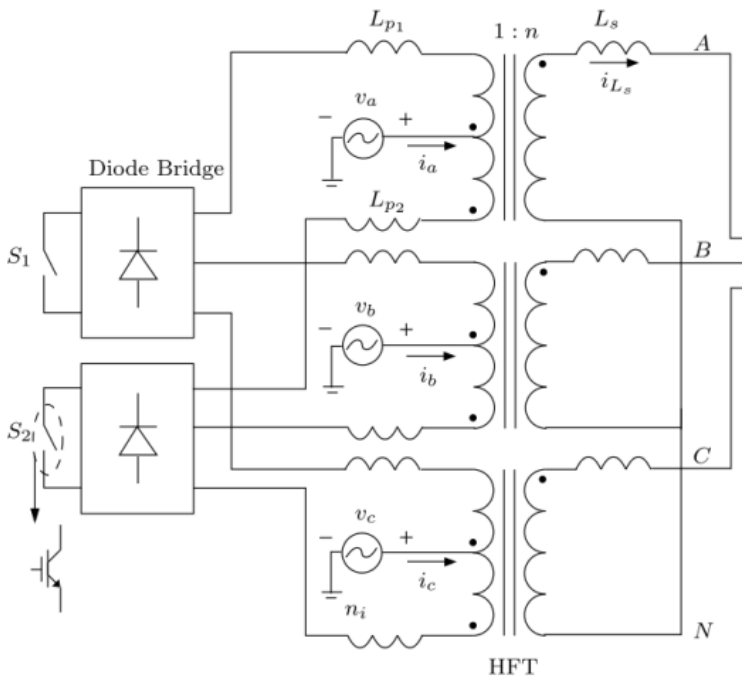

Figure 2.6.4. Detailed schematic of HF-transformer arrangement.

A figure of this transformer arrangement which is a push-pull topology is shown in Figure 2.6.4. It consists of three transformers, each with three windings, two on primary side and one on secondary side. The dot indicates the polarity of voltage induced in each of the windings. The two primary windings connect the AC source to two power electronic switches through diode rectifiers. The switches S_1 and S_2 are switched alternately with a 50% duty ratio i.e. they are ON alternately for half of one switching period. The switching pulses for the switches are illustrated in Figure 2.6.5. When S_1 is ON, current flows through the first primary winding causing the secondary side voltage to be of same polarity as that of the ac source voltage. When S_2 is ON, current flows through the second primary winding causing the secondary side voltage to be of opposite polarity as that of source voltage. This causes the secondary side voltage to have a chopped shape. This is shown in Figure 2.6.6. The voltage v_a is the primary voltage waveform and the voltage v_{AN} is the secondary voltage waveform which is chopped in appearance.

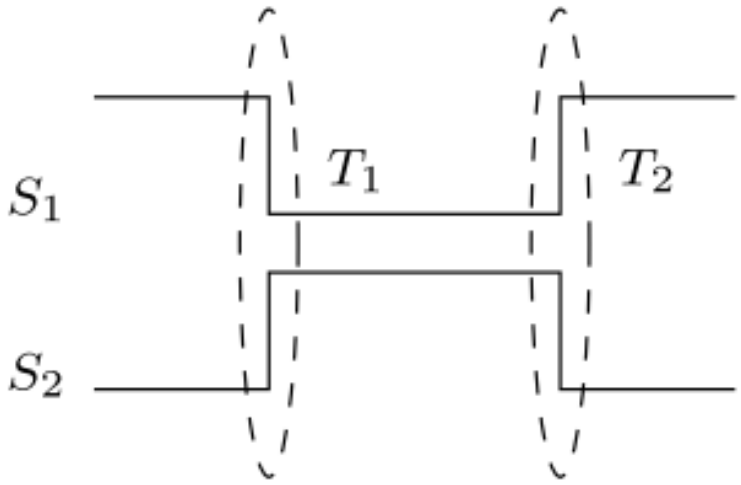

Figure 2.6.5. Diagram of switching pulses of switch S1 and S2. The transitions T1 and T2 are where one switch goes OFF and the other turns ON.

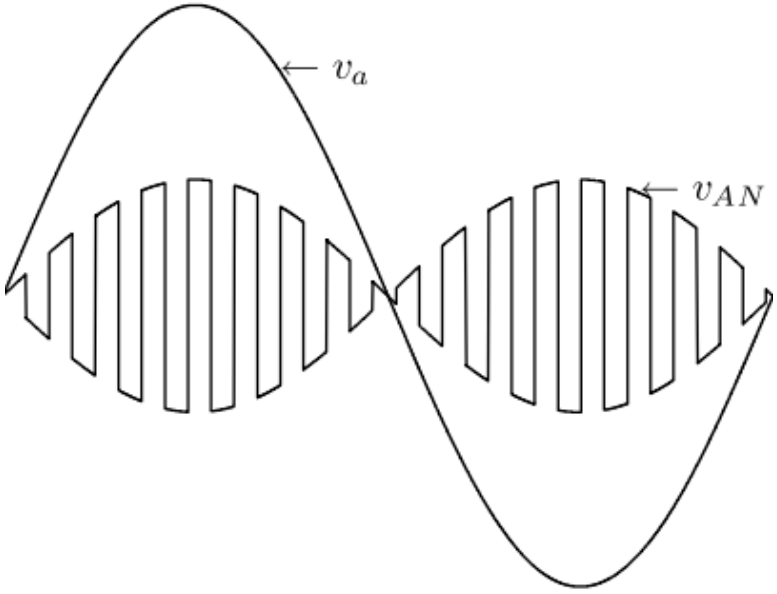

Figure 2.6.6. AC voltage (v_a) on HF-transformer primary side along with chopped ac voltage (v_{AN}) on secondary side.

The high frequency transformer used to step up/down this voltage will require a smaller core area than it would be needed at line frequency [9], which is a big advantage since it can reduce the weight of the transformer.

The power transfer through and from the DC link to the AC source takes place by the dual active bridge principle. The leakage inductance of the transformer is used to transmit the power. Between two AC systems with voltage amplitudes V_1, V_2 and a phase difference of δ between then, power is transferred according to the expression

$$P = \frac{V_1 V_2}{X} \sin \delta$$

where X is the reactance between the two systems. For a unity power factor operation, $V_1 = V_2$. Similarly, in the proposed system, the voltage at the secondary side of the transformer is taken as feedback and the same voltage is generated at the terminals of the two level inverter such that the fundamental component of the generated voltage leads or lags the fundamental of the transformer secondary voltage by some angle for power transfer while maintaining unity power factor.

Dual two-level converter, open-end winding induction machine drive

This is a drive connected at the left side of the DC link. A diagram of the drive is shown in Figure 2.6.7.

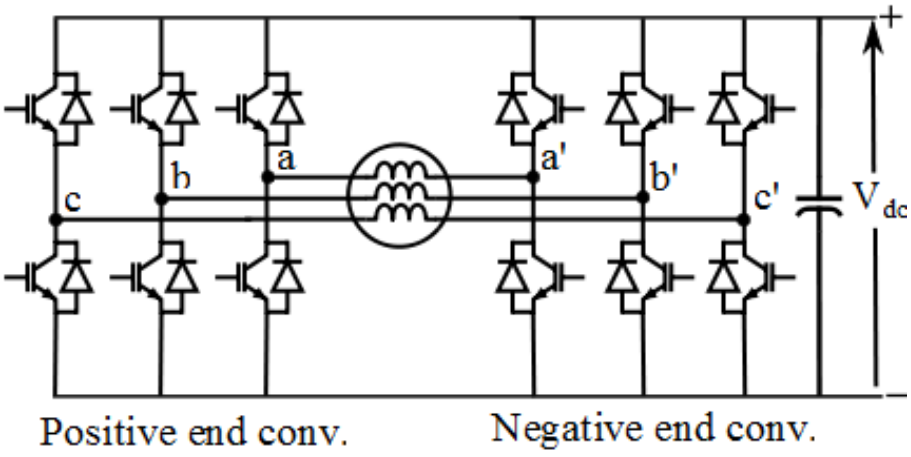

Figure 2.6.7. Circuit diagram of open end winding drive.

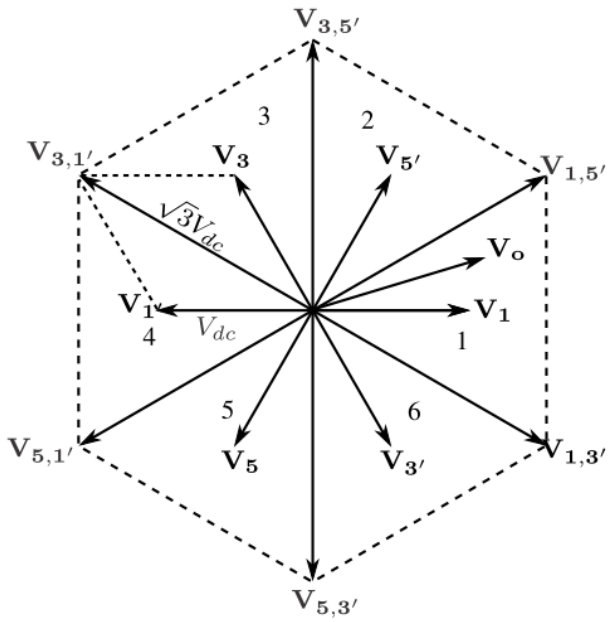

Figure 2.6.8. Space vector diagram for open-end winding drive.

The drive consists of two two-level converters sharing a dc bus and powering the two ends of a three phase load with six terminals. In this case, the load is an open end winding squirrel cage induction machine. The converter is operated using the space vector PWM control. The space vectors used are shown in Figure 2.6.8. The figure shows two sets of vectors, the smaller ones being V_1, V_3, V_5, $V_{1'}$, $V_{3'}$ and $V_{5'}$ while the bigger ones are $V_{1,3'}$, $V_{1,5'}$, $V_{3,5'}$, $V_{3,1'}$, $V_{5,1'}$ and $V_{5,3'}$. The vectors V_1, V_3, V_5 are generated by the positive end converter (as in Figure 2.6.5) and the vectors $V_{1'}$, $V_{3'}$, $V_{5'}$ are generated by the negative end converter. The vectors are generated as illustrated in Table 2.6.1.

Table 2.6.1. Space vectors in open end winding drive and machine terminal connections

Vector	a is connected to	b is connected to	c is connected to
V_1	P	N	N
V_3	N	P	N
V_5	N	N	P
Vector	a' is connected to	b' is connected to	c' is connected to
$V_{1'}$	P	N	N
$V_{3'}$	N	P	N
$V_{5'}$	N	N	P

As written in the table, when the vector V_1 is active, the output terminal *a* is connected to the positive terminal P of dc link and terminals *b* and *c* are connected to the negative terminal N of the dc link. Similarly, the rest of the smaller vectors are generated. So when the vectors V_1 and

$V_{3'}$ are generated simultaneously at the positive end converter and negative end converter respectively, the vector $V_{1,3'}$ is generated. Similarly, the rest of the bigger space vectors are generated. Using these vectors, the maximum phase voltage $V_{aa'}$ that can be generated is equal to the dc link voltage. This is 73.2% more than what can be generated using a single two level converter with conventional space vector PWM.

The common-mode voltages at the positive and negative end machine terminals are defined as:

$$V_{com,positive} = \frac{V_{aN} + V_{bN} + V_{cN}}{3} \qquad V_{com,negative} = \frac{V_{aN} + V_{bN} + V_{cN}}{3}$$

where V_{aN} denotes the voltage between output terminal *a* and the negative terminal N of the dc link. The other voltages in above expressions are defined similarly. Regular space vector PWM will cause the positive end common-mode voltage to fluctuate at high frequencies (the negative end is not present for a single two level inverter). This can cause problems like shaft currents, bearing failure in the motor in the long run. The PWM strategy used in the project maintains the common-mode voltage fixed at both ends and the across common-mode voltage is zero, which is an improvement over conventional space vector PWM. In addition, a carrier based implementation for this algorithm has also been studied which doesn't require any complex trigonometric operations as required by the space vector approach.

Results

The proposed topology is tested using prototype hardware and power transfer is achieved in both directions. The open ended drive with dual two level inverters is built using Microsemi APTGF90TA60PG power electronic switches, driven by Concept gate drivers. The high frequency transformers are custom designed. The inverter at the secondary side of the transformer is built using International Rectifier IRAM136-3063B power module. The induction machine used is Baldor ZDM3581T (1HP, 1765 rpm, 230/460V). The hardware results obtained will now be presented.

Motoring mode (Power transfer from AC source to motor)

The system was run with following settings:

Induction machine speed	450 rpm
DC link voltage	100 V
DC link current	0.55 A
AC source voltage(rms phase)	14 V

The AC source voltage and filtered ac source current along with dc link voltage and dc link current are shown in Figure 2.6.9. The ac current (green waveform) is in phase with the voltage (blue waveform), which means that the system operates at unity power factor. The DC bus voltage (yellow) is at 100V and the DC link current (pink) has an average value of 0.55A. Figure 2.6.10 shows the dc link voltage and dc link current (top two waveforms) and the motor currents for two phases, which are sinusoidal.

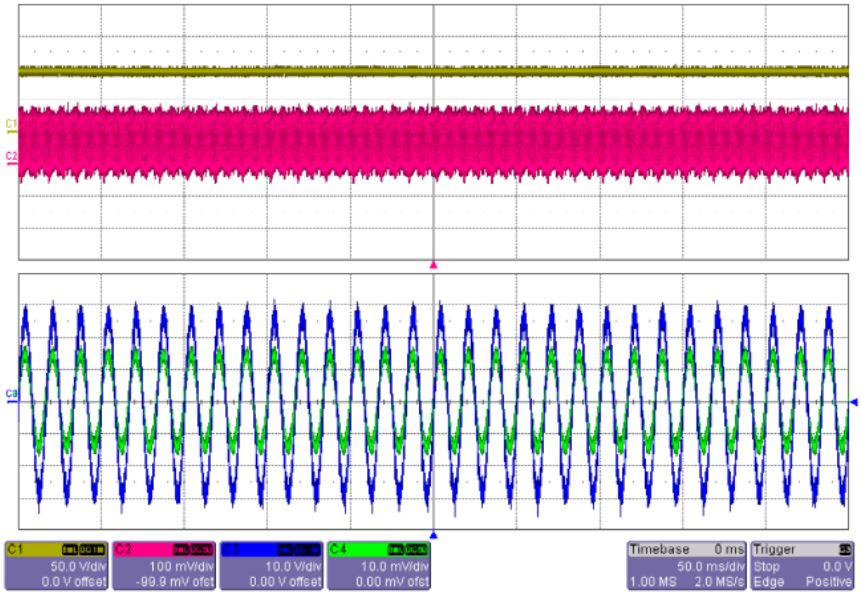

Figure 2.6.9. (Motoring mode) DC link voltage and current (channel 1 and 2 respectively), ac source voltage and current (channel 3 and 4 respectively).

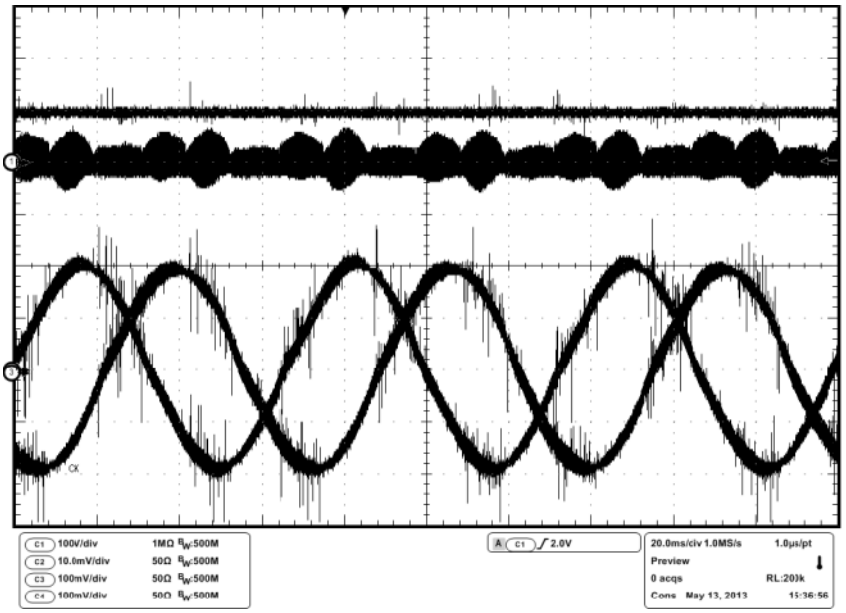

Figure 2.6.10. (Motoring mode) Induction machine phase a and b currents (channels 3 and 4) and dc link voltage and current (channel 1 and 2 respectively).

Generating mode (Power transfer from motor to ac source)
The operating settings are:

Induction machine speed	800 rpm
DC link voltage	105 V
DC link current	1.5 A
AC source voltage(rms phase)	14 V

The AC source voltage and filtered AC source current along with DC link voltage and DC link current are shown in Figure 2.6.11. The AC current (green waveform) is out of phase with the voltage (blue waveform), which means that the power flow is towards the AC side. The DC link current is negative in this case, as seen by the pink waveform. Figure 2.6.12 shows the dc link voltage and DC link current (top two waveforms) and the motor currents for two phases, which are again sinusoidal.

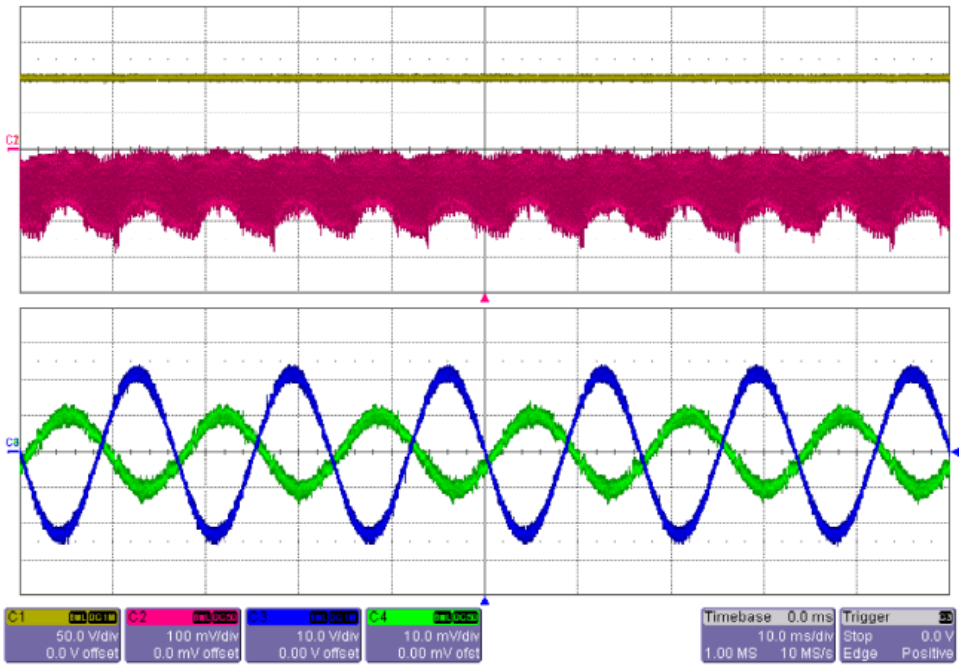

Figure 2.6.11. (Generating mode) DC link voltage and current (channel 1 and 2 respectively), ac source voltage and current (channel 3 and 4 respectively).

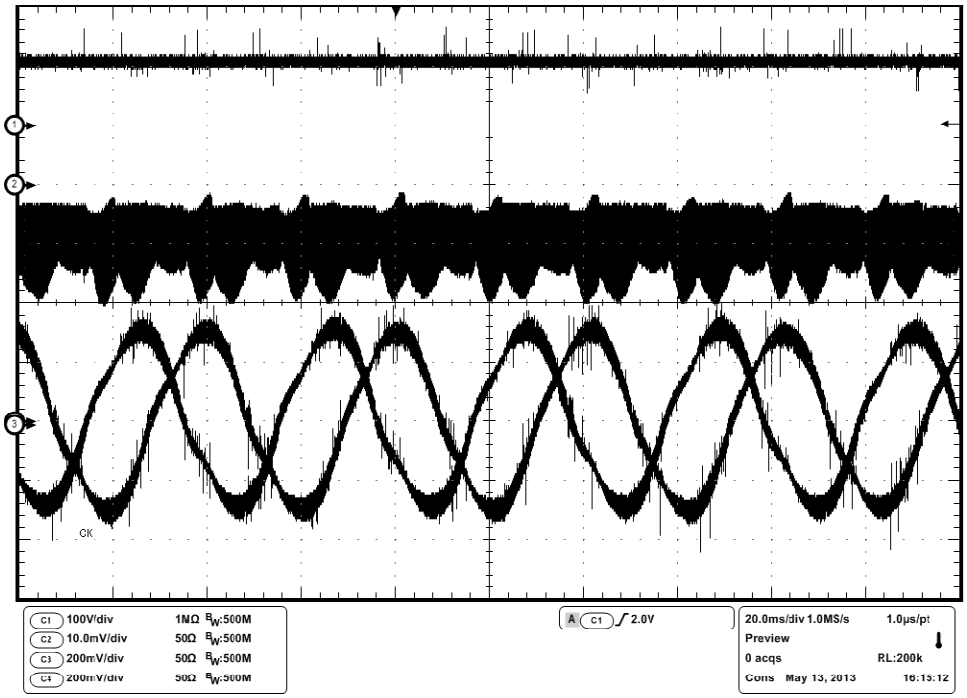

Figure 2.6.12. (Generating mode) Induction machine phase a and b currents (channels 3 and 4) and dc link voltage and current (channel 1 and 2 respectively).

Common-mode voltage elimination

Figures 2.6.13 and 2.6.14 show the pole voltages and their sum at the positive end and negative end for the open ended drive. The sums are at a constant level, implying that the common-mode voltages are held fixed on both ends and the common-mode voltage across the machine is zero.

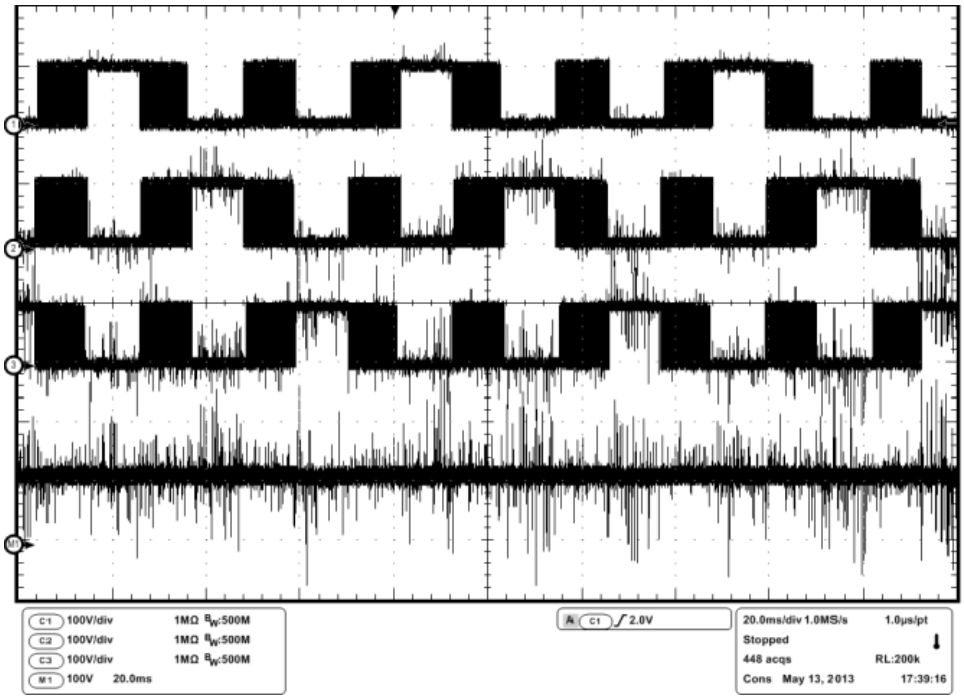

Figure 2.6.13. Positive end pole voltages (channels 1, 2, 3) of induction machine and their sum.

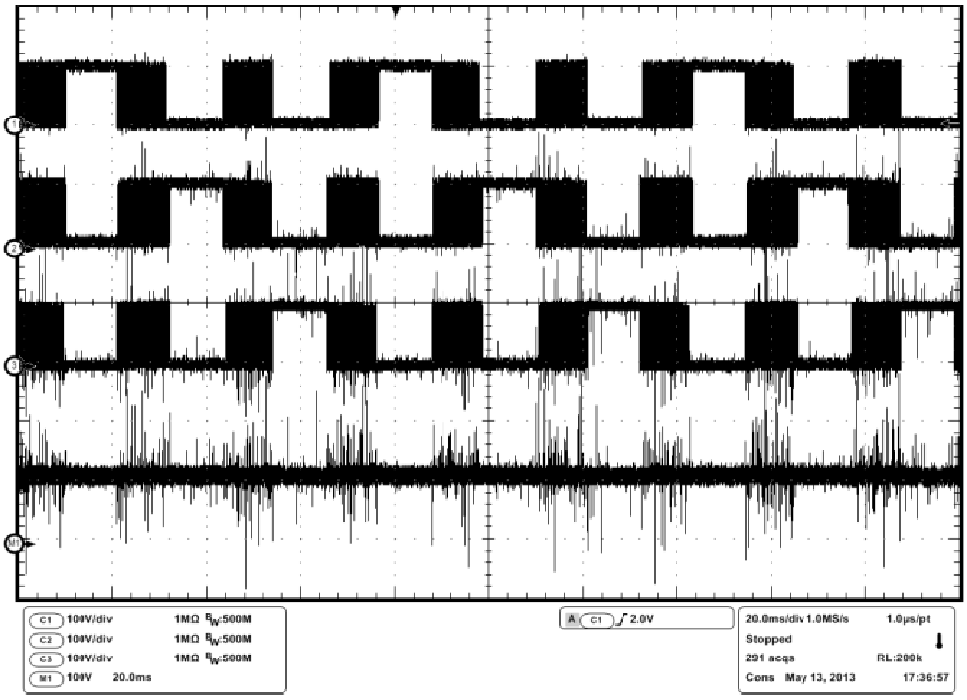

Figure 2.6.14. Negative end pole voltages (channels 1, 2, 3) of induction machine and their sum.

Publications and Presentations

Castelino, G.; Basu, Kaushik; Weise, N.; Mohan, Ned, "A bi-directional, isolated, single-stage, DAB-based AC-DC converter with open-loop power factor correction and other advanced features," *Industrial Technology (ICIT), 2012 IEEE International Conference on* , vol., no., pp.938,943, 19-21 March 2012

Gysler Castelino, Kaushik Basu, and Ned Mohan. A novel three-phase bidirectional, isolated, single-stage, dab-based ac-dc converter with open-loop power factor correction. In Power Electronics, Drives and Energy Systems (PEDES), 2012 IEEE International Conference on, pages 1–6, 2012

Baranwal, R.; Basu, K.; Mohan, N., "Dual two level inverter carrier SVPWM with zero common mode voltage," *Power Electronics, Drives and Energy Systems (PEDES), 2012 IEEE International Conference on Power Electronics, Drives and Energy Systems (PEDES)* , vol., no., pp.1,6, 16-19 Dec. 2012 doi: 10.1109/PEDES.2012.6484305

Patents

1. US8169179 B2: Open-ended control circuit for electrical apparatus
2. US 8,446,743: Soft Switching Power Electronic Transformer

References

[26] T. Ackerman, T., *Wind power in power systems*. John Wiley and Sons, 2005.

[27] Blaabjerg, F., Chen, Z., and Kjaer, S., “Power electronics as efficient interface in dispersed power generation systems,” IEEE Transactions on Power Electronics, 2004, vol. 19, no. 5, pp. 1184–1194.

[28] [Online]. Available: http://www.vestas.com/

[29] [Online]. Available: http://www.gepower.com/

[30] [Online]. Available: http://www.gamesacorp.com/en

[31] Erdman, J.M., Kerkman, R.J., Schlelgel, D.W., and Skibinski, G.L. “Effect of PWM inverters on AC motor bearing currents and shaft voltages,” IEEE Trans. Ind. Applicat., 1996, vol. 32, pp. 250–259, Mar./Apr.

[32] Chen, S., Lipo, T.A., and Fitzgerald, D., “Source of induction motor bearing currents caused by PWM inverters,” IEEE Trans. Energy Conv., 1996, vol. 11, pp. 25–32,

[33] Wang, F., “Motor shaft voltages and bearing currents and their reduction in multilevel medium-voltage PWM voltage-source-inverter drive applications,” IEEE Trans. Ind. Applicat., 2000, vol. 36, pp. 1336–1341.

[34] Mohan Ned, “Power Electronics: A First Course”, Wiley, 2011

Task 2.7: Radar Interactions with Wind Turbines

Literature Review and Background

Wind turbines of conventional shape (consisting of a tower, nacelle on top of the tower and rotating blades extending outward from the nacelle) negatively affect radar operations. The negative impact is due to both the obstruction caused by the massive turbine structure as well as the blade rotation caused by the wind. While the obstruction creates a strong radar echo at zero Doppler frequency, blade rotations contribute to a set of fluctuating echoes with a wide range of Doppler frequencies caused by a continuum of radial velocities proportional to the distances from the nacelle of effective scattering centers along the length of the blades. Because most radar systems detect the mean echo power from a target and estimate its radial velocity component, erroneous conclusions may be drawn from the mean Doppler values obtained from the contaminated data. In addition, short dwell times of scanning radars on a given resolution cell do not provide sufficient observation time to afford spectral selectivity of a broadband interference from a turbine on a narrowband desired target such as an aircraft or a weather phenomenon. This lack of selectivity renders classical moving target indicator (MTI) processors ineffective or causes them to detect false targets. With the proliferation of wind farms since the early 2000s, the problem of radar interference began to attract attention from organizations that deploy and use radars for civilian (air traffic control, weather) and defense (navigation and surveillance) purposes. An example of the seriousness of such concerns can be found in [35].

The wind turbine radar interference problem has necessitated regulations that restrict the siting of turbines within lines of sights of certain radars [36], slowing the expansion of wind energy. Therefore, there has been interest in finding alternative turbine designs with stealth characteristics [37], as well as addition of ancillary systems to provide better or complementary radar coverage around the turbines [38]. If successful, these approaches are applicable to new installations, but they are costly. There has been considerable interest in developing flexible, low-cost, signal processing algorithms to mitigate the wind turbine clutter that are applicable to existing radar and turbine technologies. Most of signal processing approaches in the open literature for detecting and mitigating wind farm clutter have been limited to weather Doppler radar systems. Examples of these approaches that predate the work presented in this project include the summary provided in [39].

Goals and Objectives:

The goal of this work is to minimize or eliminate the negative impacts of wind farm interference on weather Doppler, surveillance, and navigation radars by understanding the nature of radar clutter. This includes clutter caused by a single wind turbine and from a collection of turbines in a wind farm for different classes of radar systems. The information gathered will inform the development of algorithms for the mitigation of the interference. The University of Minnesota team will work with Lockheed Martin Corporation with the goal of developing a new clutter detector based on azimuth-Doppler cross-spectral processing and machine learning, and a mitigation method based on space-time-frequency excision of contaminated bands.

SOPO Defined Purpose, Approach, and Outcomes:

Purpose: Minimize or eradicate the negative impacts wind farms have on FAA and weather radars.

Approach: Understand the nature of clutter and develop active and/or passive mitigation techniques, including development of new generation of high spectral resolution radar signal processors to provide discrimination against this emerging source of clutter. Study mitigation techniques at a field scale radar facility. Extend results of mitigation techniques to address the needs of the National Oceanic and Atmospheric Administration.

Outcomes: Development and field demonstration of new clutter mitigation techniques and signal processing algorithms for FAA and weather radars.

Project Team

Mostafa Kaveh is Professor of Electrical and Computer Engineering, and Associate Dean for Research and Planning, College of Science and Engineering, University of Minnesota. Professor Kaveh has been a faculty member at the University of Minnesota since 1975. He is the Past-President of the IEEE Signal Processing Society, and has consulted on signal processing for high-resolution microwave direction finding methods for the MIT Lincoln Laboratory. He has received a number of scientific and professional awards, including elections as a Fellow of the IEEE, and a Fellow of the AAAS.

Jimeng Zheng received his PhD in electrical engineering at the University of Minnesota in 2012. He is currently a staff member at Qualcomm in San Diego, CA. Jimeng was a part-time research assistant on this project.

Bryan Perfetti received his MS in electrical engineering at the University of Minnesota in 2012. He is currently a staff member at HGST in San Jose, CA. Bryan was a part-time research assistant on this project.

Ross Crandall received his BS in electrical engineering at the University of Minnesota in 2013. He carried out his Senior Honors project on the development of machine learning algorithms for wind turbine detection from scanning Doppler weather radar data. He plans to pursue a medical degree.

Robert Monson**,** PhD, was the lead co-principle investigator from Lockheed Martin. He is now a manager at Carestream Health.

Svetlana Bachmann, PhD, was the Lockheed Martin scientist on the project.

Technical Approach

Methods were developed for mitigating clutter contamination in weather Doppler radar caused by wind turbines. The core of the approach consists of the automatic detection of interference and creation of clutter maps, and methodologies for the mitigation of the contaminated signal. The detection method not only identifies the range cell with contaminations from the wind turbine(s) but also identifies the Doppler spectrum coefficients responsible for the contaminated return. Preliminary results have also indicated a potential approach for the classification of the

severity of the interference, so that if below a certain threshold, mitigation, other than standard stationary clutter filtering is deemed unnecessary. This is important to leave as much of the weather generated signal and its spectrum untouched for weather parameter estimation.

The approach to the development of the detection and mitigation algorithms was built on extensive spectral analysis on measured radar returns from turbines and weather phenomena. The samples of the radar echo signal were analyzed in various combinations and decomposed by short-time spectral estimators. Certain combinations of samples exposed the attributes and behaviors needed for the identification of contaminants. In particular, cross-spectral analysis of successive azimuth frames showed attributes in the evolutionary azimuth-Doppler spectra, which were deemed useful for the identification of the clutter returns. The mitigation of clutter, when necessary, was carried out by notching the contaminated Doppler spectrum coefficients, and performing newly-developed interpolations in 3D data (azimuth-range-Doppler).

The methodology that was developed demonstrated very promising results that were competitive with those reported in the open literature. The benchmark comparison for this study was the current state-of-the-art method, referred to as the LM Trade Secret (see [39]). A direct comparison was not possible with this method, due to the novel data ingestions necessary for spectral processing in the current approach. The LM Trade Secret methodology was eventually modified to accommodate a comparison with inconclusive results. The following provides a brief illustration of the key aspects of the data arrangement for scanning pulsed Doppler radars that forms the basis for the new spectral-domain detection and classification algorithms.

A mechanically scanning radar system set at a given elevation transmits a pulse-train at a particular azimuth with range gates periodically sampling the range (half the round trip time of echoes) of the returned signals. This concept is illustrated in top portion of Figure 2.7.1, which depicts five radar beams at five adjacent azimuth locations. In reality, because the weather radar system is rotating while transmitting/receiving, the radar transmits pulses toward increments in azimuth with considerable overlap due to the antenna beamwidth. The series of beams between the previous and current azimuth locations are illustrated in the bottom portion of Figure 2.7.1. This phenomenon implies that each data sample in the backscattered stream following the transmitted pulse is returning to the radar from a slightly lagging azimuth location. This observation leads to the concept of azimuth-Doppler processing in this project in contrast with the standard range-Doppler processing [40], [41]. The data structure will be presented in the next section.

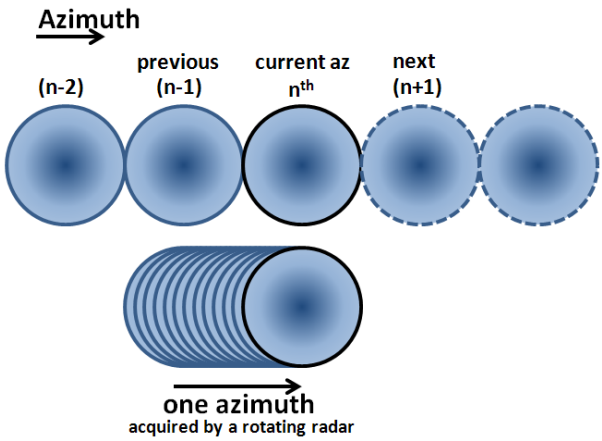

Figure 2.7.1. Due to radar rotation, radar data samples in one beam are not acquired from a discrete azimuth location, but rather at the lagging increments of azimuth.

Figure 2.7.2 shows an example of azimuth-Doppler spectrum at a particular range bin from a WSR-40 radar whose scanned view included a wind farm. The strong returns at zero velocity (DC Doppler) due to the turbine towers along with the very wide Doppler (velocity)–spreads for the returns from the turbines are quite visible. The clutter detection approach that was pursued exploit this combination of azimuth spectra to differentiate turbine returns from other targets, such as weather and stationary ground clutter both of which have relatively narrowband Doppler spectra. A test has been developed to identify clutter based on these features as well as the strength of the returns. An additional test using machine learning algorithms based on spectral features has also been explored to not only detect the presence of turbine clutter, but classify its level of severity to inform whether spectral excision and interpolations are needed to mitigate the influence of the clutter on weather information.

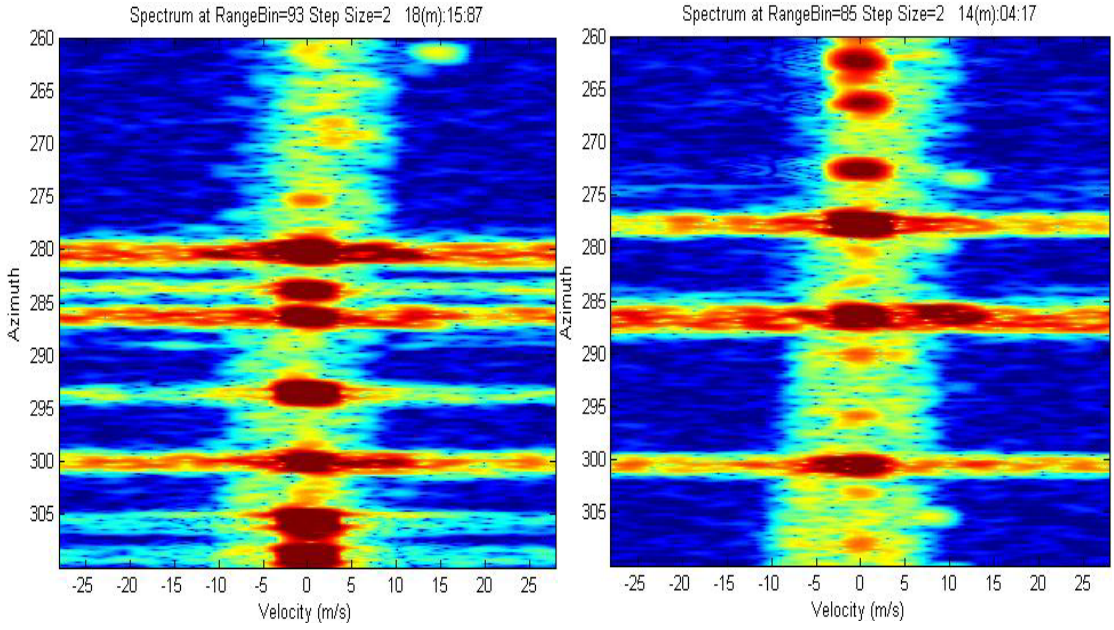

Figure 2.7.2. Azimuth-velocity (Doppler) spectra for two range bins of scanning radar with a field of view that includes a wind farm.

Given the dearth of available radar data, the research approach has also devised a method based on measure data that generates a statistical sample of signals with turbine return features. These synthesized data sets can be used to statistically validate performances of algorithms, and/or serve as training data for machine learning methods [42].

Results

As conceptually illustrated in Figure 1, the algorithms developed in this research are based on the Azimuth-Doppler Spectrum (ADS), which is generated as follows: Suppose, at range gate R, the received complex in-phase/quadrature (I/Q) signal x(t) is from the azimuth angle θ_t with t =0, ..., T , which is assumed to scan through the surveillance area with constant step size. Further, assume that any successive 2WH + 1 samples are within one beamwidth. Thus, centered at azimuth angle θ_t, all the samples between x (t−WH) and x (t+WH) are from the corresponding resolution cell, and form a vector, $x(\theta_t)$, of length 2 WH+1 that forms the basis for spectral processing for this particular range and azimuth. Let $X(\theta_t)$ and $B(\theta_t)$ denote the discrete Fourier transforms (DFTs) of $x(\theta_t)$ and its Blackman -tapered version respectively. Sequences of these DFTs over the azimuth scan times and for the set of range gates under consideration are used in the following to form a detector of turbine clutter, and for nulling of clutter spectra and their interpolation based on surrounding clean range azimuth Doppler spectra. The following summarizes the elements of the new detector and the interpolators that were developed and show some representative results. Technical details are provided in references [43] and [44].

The Phase Difference Detector (PDD)

A typical scanning Doppler weather radar provides a short data record – typically 40-80 samples—for spectral processing per azimuth increment. Such a short record does not allow for high spectral resolution characterization, for example, needed for the estimation of the spectral width of the phenomena under observation. We have demonstrated that the phase of the cross-spectrum of two successive data records, that is, angle[$X(\theta_t)X^*(\theta_{t+1})$], where * indicates complex conjugation, and the product of the DFT vectors are element-wise, is approximately linear within the bandwidth of the signal and deviates randomly and significantly from linearity outside of the band with high selectivity. The PDD was designed to utilize this property. The bandwidths of measured signals are estimated for each azimuth and range by the PDD, and if larger than a threshold, and confirmed by a signal power threshold to indicate significant clutter, the cell is declared to be contaminated. Figure 2.7.3 shows an example of the detected contamination by PDD for measurements from a wind farm by the KDDC Doppler radar in Dodge City, Kansas.

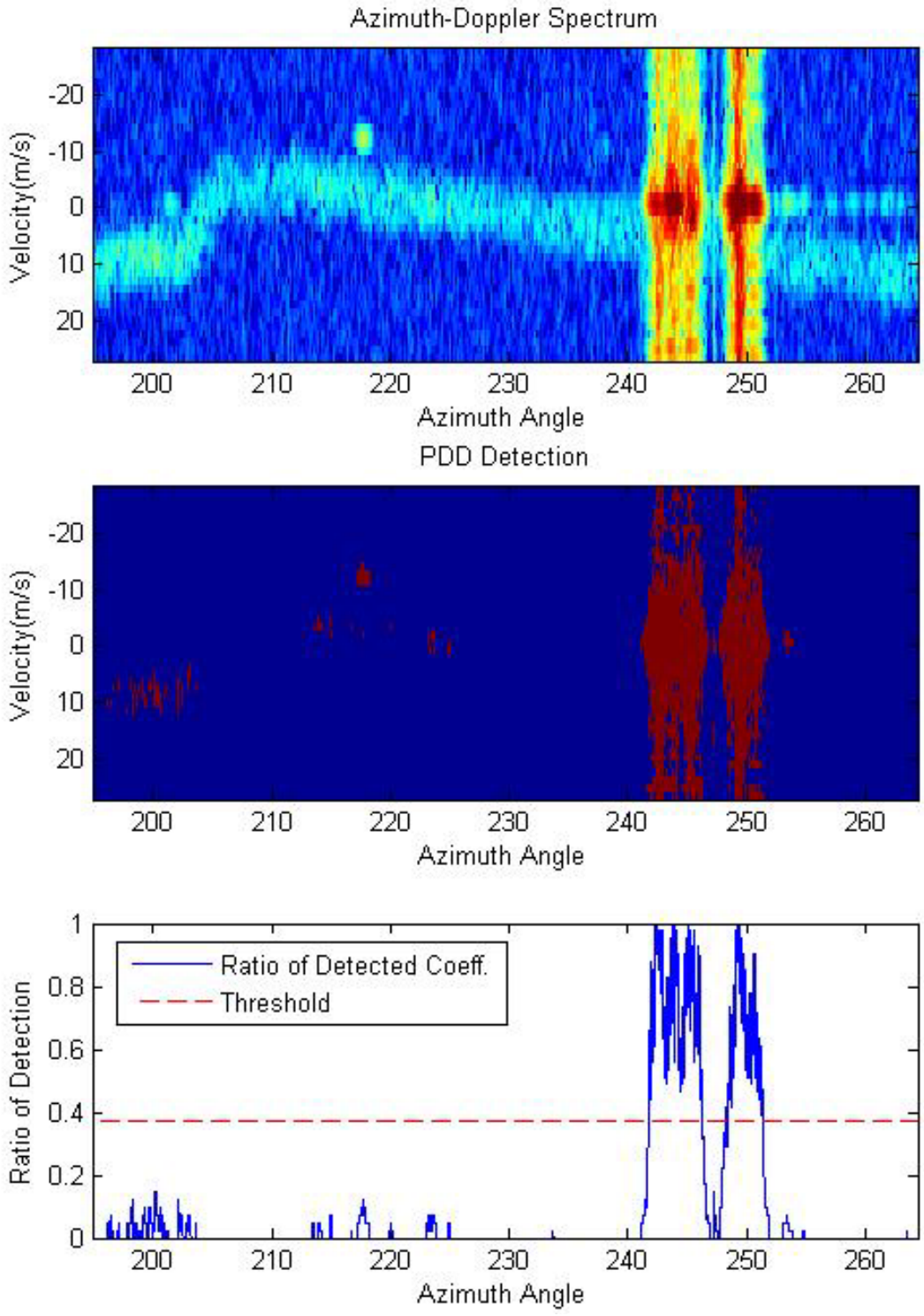

Figure 2.7.3. Azimuth-Doppler spectra and PDD output.

Mitigation

The Doppler coefficients that are deemed corrupted by turbine returns are zeroed, and using an appropriate interpolation method are reconstructed from adjacent uncorrupted cells. Two interpolation methods were developed and compared with previously-proposed ones. The first uses a bilinear interpolation approach, while the second, which has proven more robust and computationally efficient is designated the Sliding Window Average (SWA) method. The mechanism for the SWA is illustrated in Figure 4.

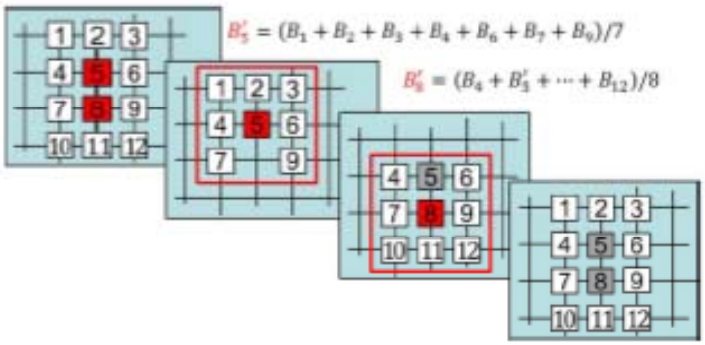

Figure 2.7.4. Illustration of the SWA interpolation. Red cells indicate zeroed coefficients, and grey cells indicate the interpolated coefficients.

The PDD detector was applied to Doppler weather returns from wind farms in clear air using the NEXRAD WSR88-D radar data from a wind farm near Dodge City Kansas, and to synthesized contaminated weather returns in the presence of the same wind farm clutter. Good results in clutter map identification were obtained as shown in the Figure 2.7.5. The right-hand figure shows the identified clutter map derived from the I/Q data which generated the contaminated range-azimuth radar reflectivity image in the presence of weather shown on the left.

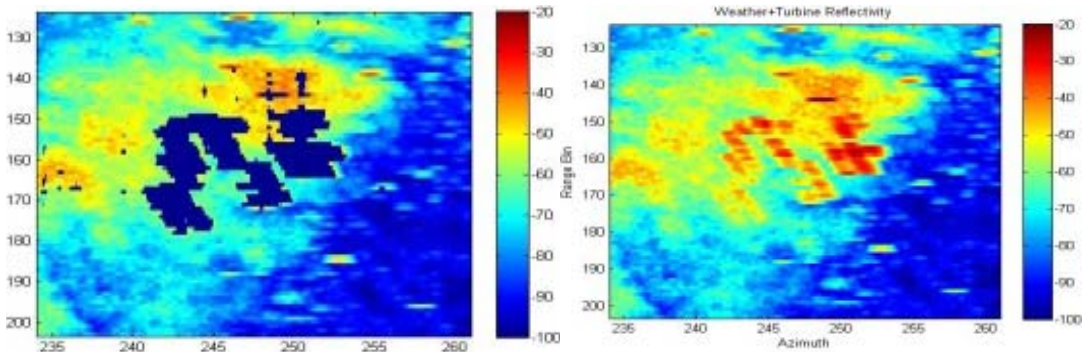

Figure 2.7.5. Left figure is the reflectivity displays of radar returns from wind farm superimposed with returns from weather data. The right figure shows the identified clutter map by the PDD.

Following the nulling of contaminated spectral coefficients within the range-azimuth-Doppler clutter map, the SWA interpolation was employed resulting in the mitigated reflectivity display in Figure 2.7.6. The left figure represents the weather range-azimuth reflectivity image without turbine clutter, while the right-hand figure shows the mitigation of the clutter from that shown in Figure 5 by clutter spectral nulling followed by interpolation using the sliding moving average interpolator.

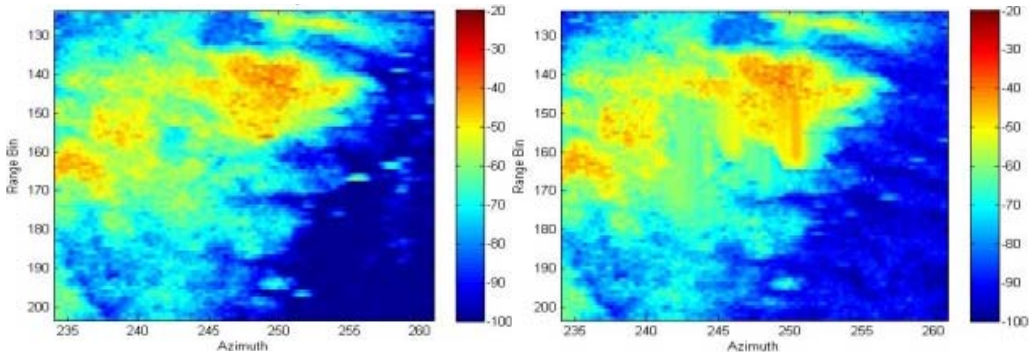

Figure 2.7.6. Uncorrupted (left), and mitigated from Figure 5 reflectivity maps (right).

Finally, the effect of the detection/mitigation methods that were developed on the estimation of average radial velocities can be seen in the results of Figure 2.7.7, in which experimental weather returns were contaminated synthetically with returns from turbines.

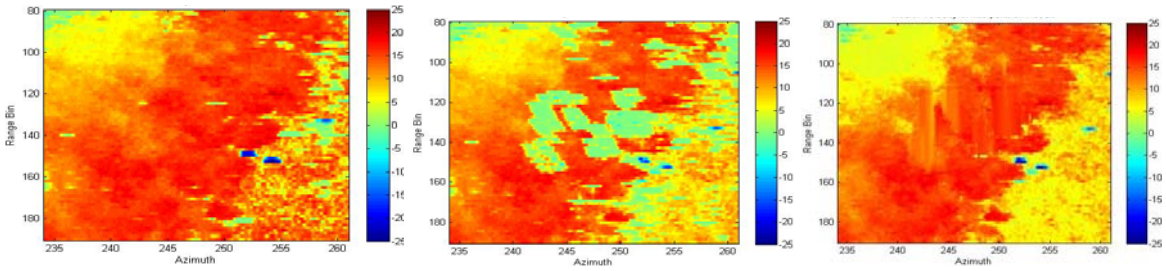

Figure 2.7.7. True weather radial velocities (left), contaminated data (center), mitigated data (right).

Data Synthesis and Simulation

Lack of available extensive experimental data from Doppler weather radar returns from wind turbines motivated the development of statistically relevant simulated signals built on limited experimental data. To accomplish this task, histograms of Doppler coefficients within bands covering stationary, mid and upper band Doppler bands in clear and contaminated range-azimuth cells were first obtained from the available data. Using re-sampling from these histograms “typical” random signal samples were generated with similar spectral content as the real measurements on which they were based. Figure 2.7.8 shows examples of original and re-

sampled histograms of three frequency bands, the baseline experimental specturm, and a sample smoothed spectrum from the new synthetic/simulated data.

Fig. 3a: Power in Outer 35% of Spectrum (Blackman Window)

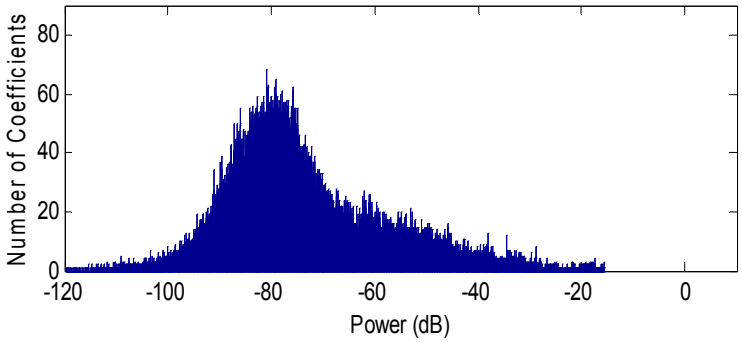

Fig. 3b: Bootstrapped Outer 35% Power (Blackman Window)

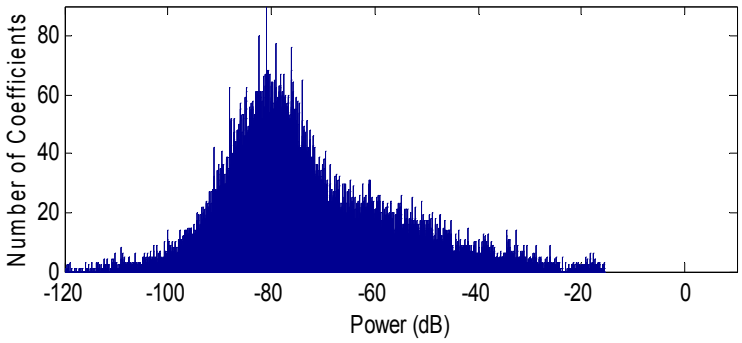

Fig. 2a: Power in Center 5% of Spectrum (Rectangular Window)

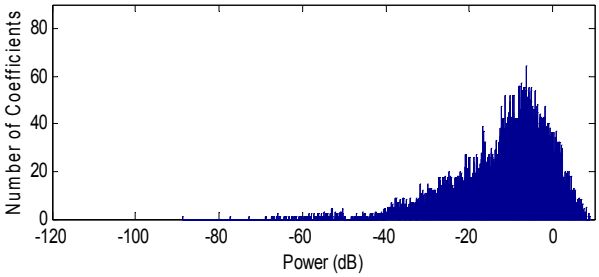

Fig. 4a: Power in Middle 60% of Spectrum (Blackman Window)

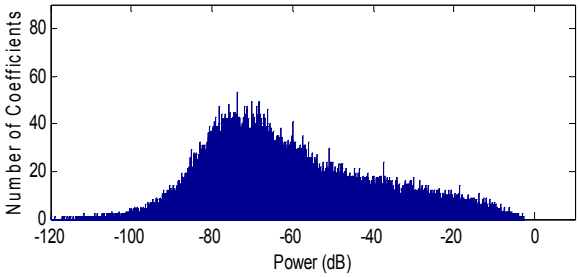

Fig. 2b: Bootstrapped Center 5% Power (Rectangular Window)

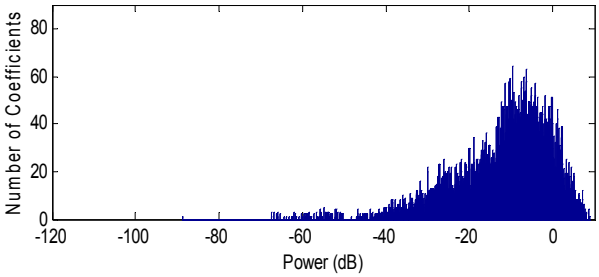

Fig. 4b: Bootstrapped Middle 60% Power (Blackman Window)

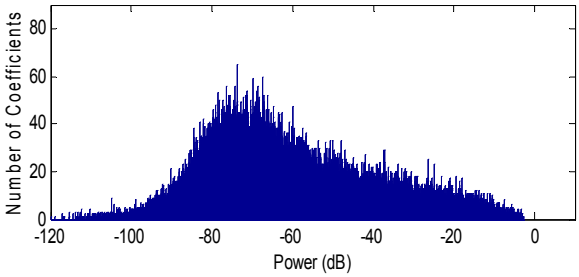

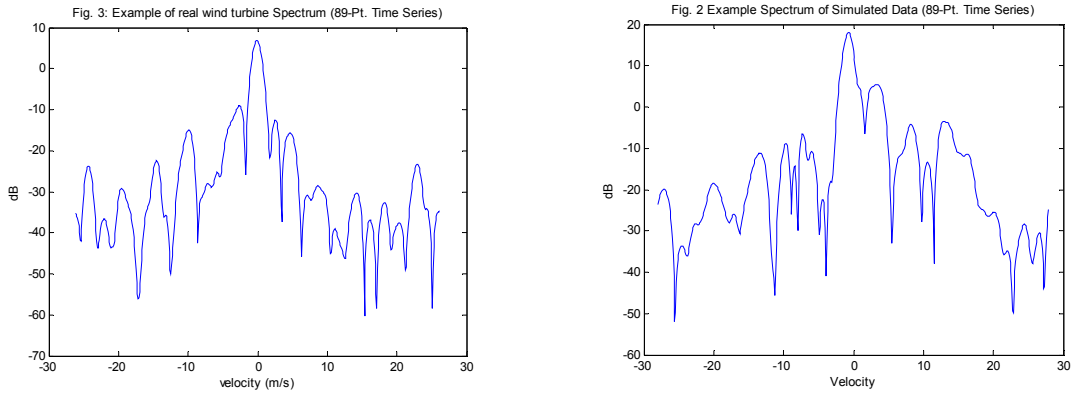

Figure 2.7.8. Histograms (top two rows), and sample Doppler spectra from experimental and synthesized data (bottom figures). The top histograms of three spectral band powers from experimental data, and the bottom histograms are from re-sampled and synthesized data.

The synthesized data proved valuable for evaluating the receiver operating characteristics (ROC) of the PDD [44 10], and for training and evaluating machine learning algorithms for clutter detection and classification.

Publications and Presentations

Jimeng Zheng, B. Perfetti, M. Kaveh, S. Bachmann, and R. Monson, "Azimuth-frequency analysis for wind farm clutter identification and mitigation in Doppler weather radars," Proceedings of the 35th Conference on Radar Meteorology, September 26-30, 2011, Pittsburgh, PA.

Svetlana Bachman, R. Monson, B. Perfetti, J. Zheng and M. Kaveh, "Understanding radar echoes from wind turbines and how to mitigate the impact on radar," Proceedings of the 92nd American Meteorological Society Annual Meeting, January 22-26, 2012, New Orleans, LA.

B. Perfetti, J. Zheng, and M. Kaveh, "Signal processing for wind turbine interference mitigation in Doppler weather radars: data synthesis, clutter detector performance and spectral interpolation in range-azimuth-Doppler, "Proceedings of the IET Radar 2012, October 22-25, 2012, Glasgow, Scotland.

References

[35] Office of the Director of Defense Research, Undersecretary for Space Engineering, and Sensor Systems, Report to the Congressional Defense Committees on the Effect of Windmill Farms on Military Readiness. August 2006.

[36] R.J.Vogt, J.R. Reed,T. Crum, J.T. Snow, R.Palmer, and B. Isom, "Impacts of windfarms on WSR-88d operations and policy considerations," Proceedings of the 23rd Int. Conf. on IIPS for Meteorology, Oceanography, and Hydrology, San Antonio, TX, 2007.

[37] G. Oswald and C.Webster, “Holographic radar mitigation of windfarms.,” Cambridge Consultants presentation to NWCC, October 2009.

[38] A. Cameron. ”Stealth blades get turbines under the radar,” *Renewable Energy World Special Supplement: Wind Technology Magazine*, November 2011.

[39] S. Bachmann, Y. Al-Rashid, B. Isom and B. Palmer, "Radar and Windfarms – mitigating negative effects through signal processing," *6th European Conference on Radar in Meteorology and Hydrology*, Sibiu, Romania, 6-10 September 2010.

[40 6] F. Nai, R. Palmer, and S. Torres, “Wind turbine clutter mitigation using range-doppler domain signal processing method,” in *Preprints, 27th Conf. on Interactive Inform. and Proc. Sys. (IIPS)*, Seattle,WA, 2011.

[41] F. Nai, S.M.Torres, and R.D.Palmer, “Mitigation of wind-turbine clutter using range-doppler spectral analysis,” In *35th Conf. on Radar Meteorology*, Pittsburgh, PA, 2011.

[42] Ross Crandall, “Detecting wind turbine interference with radar using machine learning,” Senior Honors Report, Department of Electrical and Computer Engineering, University of Minnesota, May 2013.

[43] Jimeng Zheng, B. Perfetti, M. Kaveh, S. Bachmann, and R. Monson, “Azimuth-frequency analysis for wind farm clutter identification and mitigation in Doppler weather radars,” Proceedings of the 35th Conference on Radar Meteorology, September 26-30, 2011, Pittsburgh, PA.

[44 10] B. Perfetti, J. Zheng, and M. Kaveh, “Signal processing for wind turbine interference mitigation in Doppler weather radars: data synthesis, clutter detector performance and spectral interpolation in range-azimuth-Doppler, “Proceedings of the IET Radar 2012, October 22-25, 2012, Glasgow, Scotland.

Program Area 3: Curriculum Development.

3.1 Wind Energy Essentials Course

A graduate-level course, *Wind Energy Essentials*, was developed at the University of Minnesota and offered to graduate and senior-level undergraduate engineering students from all disciplines during the Fall semesters of 2010, 2011, and 2012. The seminar style consisted of 13 2-hour lectures presented by industry representatives and University faculty from several different departments. Students were able to register to attend in person or online via the College of Science and Engineering "UNITE" distance-learning interface. The course was jointly managed by Fotis Sotiropoulos, in the Civil Engineering department, and Ned Mohan in the Electrical and Computer Engineering Department. The lectures covered the following topics:

Table 3.1.1. Summary of course syllabus for Wind Engineering Essentials

Topic	Presenter
New Challenges in a High Penetration of Wind Power	Ed Muljadi – National Wind Technology Center, NREL
Introduction to the present day wind energy scenario	Steven W. Saylors, – Vestas (remote via video)
Gears and Transmission	Kim Stelson – Mechanical Engineering
Blade Aerodynamics and Acoustics	Fotis Sotiropoulos and Roger Arndt – Civil Engineering
Foundation Design	Chris Kopchynski and Jennifer Entwistle – Barr Engineering
Controls	Mihailo Jovanovic – Electrical and Computer Engineering and Gary Balas – Aerospace Engineering and Mechanics
Electric Generation and Power Electronics	Ned Mohan – Electrical and Computer Engineering
Materials and Structural Reliability	Sue Mantell – Mechanical Engineering and Henryk Stolarski – Civil Engineering
Wind Assessment and Wind Forecasting	Mark Ahlstrom – WindLogics Inc.
Grid Integration	Matt Schuerger – Energy Systems Consulting Services
Socio-economic aspects of Wind Farm Development	Jack Levi – National Wind LCC
Wind Farm Development	Kate O'Hair – enXco
Environmental Consideration: Radar Interference	Mos Kaveh – Electrical and Computer Engineering

The course also included a tour of the Eolos research and field station. St. Anthony Falls Laboratory engineering staff give a presentation about the maintenance and operation of the turbine and custom data acquisition systems installed at the facility. Students on the tour were

able to enter the base of the turbine tower to see the Generator Control Units, the climbing systems and the tower and foundation structures.

Enrollment in the Wind Energy Essentials course is shown below:

Year	In-person	UNITE	Total
2010	46	5	51
2011	61	13	74
2012	58	23	81
2013	61	6	67
Total	226	47	**273**

In addition to the 206 students who registered in the College of Science and Engineering, a total of 80 students took the course as an online module administered by the College of Continuing Education, earning Continuing Education Credits (CEU). In this format, the presentations from the first semester of the course offering were available as online videos to all registered students at any time until June 30, 2012.

The Wind Energy Essential class will continue to be offered to College of Science and Engineering students in the Fall semester of 2013. The course materials have been adapted for use in curriculum of the Consortium of Universities for Sustainable Power (CUSP). Wind Energy Essentials is one of six courses available for members of CUSP to download free of charge. The course materials include an electronic textbook, discussion problems, hardware and software labs, and homework problems.

3.1 Additional Education and Outreach Efforts

Beyond the course curriculum developed, the Eolos consortium has been involved with other community engagement activities, such as the University of Minnesota Math and Science Family Fun Fair, aimed at elementary- and middle-school aged children, in Fall 2012. The consortium also formed a formal partnership with the Mesabi Range Community and Technical College (MRC). MRC has its own Vestas V27 wind turbine. Data from Mesabi's SoDAR acoustic wind measurement instruments were compared with data from the U of M's met tower, exposing students from both schools to cutting-edge technologies for wind measurement and data collection.

Professor Seiler of the University of Minnesota Aerospace Engineering and Mechanics Department worked with MRC to retrofit their Vestas turbine with a National Instruments cRIO device as its controller. This open-source controller will allow researchers to prototype new control strategies on a mid-size wind turbine. As part of this effort, several graduate students gained hands-on experience writing control laws while students at Mesabi Range College had the opportunity to wire the wind turbine and the new sensor and controller systems. The programming at MRC is funded by a variety of sources including equipment donations from Clipper Wind, software donations from OSIsoft, and grants from Iron Range Resources and the Minnesota Center for Engineering and Manufacturing Excellence.

Project References

[1] Ge & Sotiropoulos, “A numerical method for solving the 3D unsteady incompressible Navier-Stokes equations in curvilinear domains with complex immersed boundaries,” J. Comp. Phys., 2007, **225**, pp. 1782-1809.

[2] Gilmanov & Sotiropoulos, “A hybrid Cartesian/immersed boundary method for simulating flows with 3D, geometrically complex, moving bodies,” J. Comp. Phys., 2005, **207**, pp. 457-492.

[3] Choi, Moin, & Kim, “Direct numerical simulation of turbulent flow over riblets,” J. Fluid Mech., 1993, **255**, pp. 503-539.

[4] Lund, Wu, & Squires, “Generation of Turbulent Inflow Data for spatially-Developing Boundary Layer Simulations,” J. Comp. Phys., 1998, **140**, pp. 233-258.

[5] DeGraaff & Eaton, “Reynolds-number scaling of the flat-plate turbulent boundary layer,” J. Fluid Mech., 2000, **422**, pp. 319-346.

[6] Bechert, Bruse, Have, Van Der Hoeven,& Hoppe, “Experiments on drag-reducing surfaces and their optimization with an adjustable geometry,” J. Fluid Mech., 1997, **338**, pp. 59-87.

[7] Gelman, R. *2011 Renewable Energy Data Book.* s.l. : National Renewable Energy Laboratory, 2012.

[8] *Modeling and measurements of wakes in large wind farms.* Barthelmie, R. J, et al., et al. s.l. : Journal of Physics, 2007, Vol. 75.

[9] *Boundary Layer and Flow Control by Periodic Addition of Momentum.* Wygnanski, I. s.l. : 4th AIAA Shear Flow Conference, 1997. AIAA 97-2117.

[10] *The control of flow separation by periodic addition of momentum.* Greenblatt, D and Wygnanski, I. 7, s.l. : Progress in Aerospace Sciences, 2000, Vol. 36.

[11] *Aerodynamic Flow Control using Synthetic Jet Technology.* Amitay, M, Smith, B.L and Glezer, A. s.l. : 36th AIAA AEROSPACE SCIENCES MEETING AND EXHIBIT, 1998. AIAA 98-0208.

[12] *Proportional Closed-Loop Feedback Control of Flow Separation.* Pinier, J, et al., et al. 1, s.l. : AIAA Journal, 2007, Vol. 45.

[13] *Active Control of Flow Separation and Structural Vibrations of Wind Turbine Blades.* Maldonado, V, et al., et al. 2-3, s.l. : Wind Energy, 2010, Vol. 13.

[14] *Unsteady Separation Control on Wind Turbine Blades Using Fluidic Oscillators.* Cerretelli, C, Wuerz, W and Gharaibah, E. 7, s.l. : AIAA Journal, 2010, Vol. 48.

[15] Johnson, S.J, V.C, Dam and Berg, E.D. *Active Load Control Techniques for Wind Turbines.* s.l. : Sandia National Laboratories, 2008.

[16] *A low-dimensional approach to closed-loop control of a Mach 0.6 jet.* Low, K. R, et al., et al. 4, s.l.: Experiments in Fluids, 2013, Vol. 54.

[17] *Active control of flow-induced cavity oscillations.* Cattafesta, L, et al., et al. s.l.: Progress in Aerospace Sciences, 2008, Vol. 44.

[18] Borazjani, Iman, Liang Ge, and Fotis Sotiropoulos, "Curvilinear Immersed Boundary Method for Simulating Fluid Structure Interaction with Complex 3D Rigid Bodies." *Journal of Computational Physics* 227, no. 16 (August 2008): 7587–7620.

[19] Wall, Wolfgang A. "Fluid-Struktur-Interaktion Mit Stabilisierten Finiten Elementen" (1999).

[20] Zilian, A., D. Dinkler, and A. Vehre. "Projection-based Reduction of Fluid–structure Interaction Systems Using Monolithic Space-time Modes." *Computer Methods in Applied Mechanics and Engineering* 198, no. 47–48 (October 2009): 3795–3805.

[21] Yang X., Kang S. and Sotiropoulos F. Computational study and modeling of turbine spacing effects in infinite aligned wind farms. Phys. Fluids 2012. **24**, 115107

[22] Yang, X.; Sotiropoulos, F. On the predictive capabilities of les-actuator disk model in simulating turbulence past wind turbines and farms. The 2013 American Control Conference, June 17 - 19, Washington, DC.

[24] Mann, J., Wind field simulations. Probabilistic Engineering Mechanics, 1998, Vol. 3, No.4, pp 269-282.

[26] T. Ackerman, T., *Wind power in power systems*. John Wiley and Sons, 2005.

[27] Blaabjerg, F., Chen, Z., and Kjaer, S., "Power electronics as efficient interface in dispersed power generation systems," IEEE Transactions on Power Electronics, 2004, vol. 19, no. 5, pp. 1184–1194.

[28] [Online]. Available: http://www.vestas.com/

[29] [Online]. Available: http://www.gepower.com/

[30] [Online]. Available: http://www.gamesacorp.com/en

[31] Erdman, J.M., Kerkman, R.J., Schlelgel, D.W., and Skibinski, G.L. "Effect of PWM inverters on AC motor bearing currents and shaft voltages," IEEE Trans. Ind. Applicat., 1996, vol. 32, pp. 250–259, Mar./Apr.

[32] Chen, S., Lipo, T.A., and Fitzgerald, D., "Source of induction motor bearing currents caused by PWM inverters," IEEE Trans. Energy Conv., 1996, vol. 11, pp. 25–32,

[33] Wang, F., "Motor shaft voltages and bearing currents and their reduction in multilevel medium-voltage PWM voltage-source-inverter drive applications," IEEE Trans. Ind. Applicat., 2000, vol. 36, pp. 1336–1341.

[34] Mohan Ned, “Power Electronics: A First Course”, Wiley, 2011.

[35] Office of the Director of Defense Research, Undersecretary for Space Engineering, and Sensor Systems, Report to the Congressional Defense Committees on the Effect of Windmill Farms on Military Readiness. August 2006.

[36] R.J.Vogt, J.R. Reed,T. Crum, J.T. Snow, R.Palmer, and B. Isom, “Impacts of windfarms on WSR-88d operations and policy considerations,” Proceedings of the 23rd Int. Conf. on IIPS for Meteorology, Oceanography, and Hydrology, San Antonio, TX, 2007.

[37] G. Oswald and C.Webster, “Holographic radar mitigation of windfarms.,” Cambridge Consultants presentation to NWCC, October 2009.

[38] A. Cameron. ”Stealth blades get turbines under the radar,” *Renewable Energy World Special Supplement: Wind Technology Magazine*, November 2011.

[39] S. Bachmann, Y. Al-Rashid, B. Isom and B. Palmer, "Radar and Windfarms – mitigating negative effects through signal processing," *6th European Conference on Radar in Meteorology and Hydrology*, Sibiu, Romania, 6-10 September 2010.

[40 6] F. Nai, R. Palmer, and S. Torres, “Wind turbine clutter mitigation using range-doppler domain signal processing method,” in *Preprints, 27th Conf. on Interactive Inform. and Proc. Sys. (IIPS)*, Seattle,WA, 2011.

[41] F. Nai, S.M.Torres, and R.D.Palmer, “Mitigation of wind-turbine clutter using range-doppler spectral analysis,” In *35th Conf. on Radar Meteorology*, Pittsburgh, PA, 2011.

[42] Ross Crandall, “Detecting wind turbine interference with radar using machine learning,” Senior Honors Report, Department of Electrical and Computer Engineering, University of Minnesota, May 2013.

[43] Jimeng Zheng, B. Perfetti, M. Kaveh, S. Bachmann, and R. Monson, “Azimuth-frequency analysis for wind farm clutter identification and mitigation in Doppler weather radars,” Proceedings of the 35th Conference on Radar Meteorology, September 26-30, 2011, Pittsburgh, PA.

[44 10] B. Perfetti, J. Zheng, and M. Kaveh, “Signal processing for wind turbine interference mitigation in Doppler weather radars: data synthesis, clutter detector performance and spectral interpolation in range-azimuth-Doppler, “Proceedings of the IET Radar 2012, October 22-25, 2012, Glasgow, Scotland.

[45] Hsu, M-C. and Bazilevs, Y., "Fluid structure interaction modeling of wind turbines: simulating the full machine", *Computational Mechanics,* 2012, **50**, 6, 821-833.

Appendix

1. Appendix A: Statement of Project Objectives
2. Appendix B: Finding of No Significant Impacts
3. Appendix C: Survey Drawings
4. Appendix D: Site Civil Drawings

STATEMENT OF PROJECT OBJECTIVES

University of Minnesota

An Industry/Academe Consortium for Achieving 20% wind by 2030 through Cutting-Edge Research and Workforce Training

A. PROJECT OBJECTIVES

This project will develop an industry/academe consortium led by the University of Minnesota – Twin Cities (UMN), seeking to accelerate the path toward meeting DOE's 20% wind by 2030 goal through cutting-edge, industry-driven research, field-scale demonstration of new technologies, and workforce training. The objectives of the project are to:

- Develop the optimum mix of full-scale and laboratory-scale wind energy research facilities that will allow the cost effective development and then real-world testing and demonstration of a wide range of wind turbine technologies and the related collection of field-scale data sets for validating computational models.
- Utilize these facilities to develop a research agenda driven by industry need for more efficient and more reliable wind turbines; and
- Develop new curricula and educational initiatives for training the next generation of wind industry engineering leaders.

B. PROJECT SCOPE

The consortium will contribute toward meeting DOE's 20% wind by 2030 goals by developing new research facilities, using these facilities to conduct cutting-edge research in collaboration with industry and developing new curricula for educating the next generation of wind energy industry leaders.

Research facilities

The research facilities funded by this DOE grant will allow the University of Minnesota and its industrial partners to complete a wide range of research and development projects throughout the next decade and beyond. This grant will fund the following facilities:

- A new 2.3MW wind turbine research facility will be developed and instrumented with state-of-the-art sensors and measurement devices at the UMN Outreach Research and Education (UMore) Park in Rosemount, MN.
- New laboratory-scale facilities will be developed and used to study novel electric generator systems.
- A cyber-collaboration facility will be developed to enable sharing of data collected at the field and laboratory sites and visualizing experimental and computational results.

Research agenda

The proposed research facilities for this project will enable a wide variety of research over the next decade and beyond. The initial research to be carried out as part of this specific DOE grant includes the following projects:

Project 1: Increasing wind turbine output using vortex generators and riblets
Project 2: Active flow control for improving aerodynamic performance and reducing noise
Project 3: High-resolution CFD-FSI modeling for aeroelastic simulations of turbine rotors
Project 4: Increasing wind turbine output by mitigating blade icing and fouling
Project 5: Multi-scale modeling for wind farm siting
Project 6: Novel power electronics for improved wind turbine electrical systems
Project 7: Radar interactions with wind turbines

Educational agenda

The consortium will undertake an ambitious new renewable-energy educational program targeting university engineering students at the undergraduate or graduate levels. The exact focus of the consortium

program will be determined in consultation with the two other DOE Wind Research Centers (IIT and U of Maine). Our educational approach will be based on developing web-based course modules and programs specifically focused on wind energy technologies.

C. TASKS TO BE PERFORMED

The scope of the project is organized over three Program Areas: 1) Research facility development including both non-construction and construction tasks; 2) Research program involving consortium members; and 3) Curriculum development.

Program Area 1: Development of the field scale research facility

Phase 1: Pre-construction tasks

The UMN has determined that the most cost effective and efficient approach to development of the research facility at UMORE Park will be to retain a single design-build team through a UMN led public procurement process to complete (1) pre-construction (NEPA) evaluation, (2) preliminary design and cost estimation and (3) construction. Following contractor selection (Task 1.1), the contract, with UMN oversight, will complete NEPA and Section 106 approvals (Task 1.2) and facility pre-design (Task 1.3). NEPA review and engineering pre-design will be carried out concurrently. No construction tasks will be performed until a Finding of No Significant Impact (FONSI) has been determined for the project. However, as described below in Project Area 2 (Research) and Project Area 3 (Curriculum Development), some research projects and the curriculum development are independent, discrete projects that are able to proceed without the turbine construction project, and therefore can begin prior to the DOE FONSI determination.

Task 1.1 Procurement of Design-Build Services

Purpose: This task will involve the establishment of a single Design/Build (DB) team to work with the Consortium in carrying out all pre-construction (Phase 1) and construction tasks (Phase 2).

Approach: The UMN will procure a DB team through its standard public procurement process. The DB team will provide all pre-construction and construction services of the project. The UMN's Capital Planning and Project Management Department (CPPM) will lead the procurement process and will use a performance information procurement system (PIPS), which openly solicits proposals and identifies and pre-approves contractors based on past performance. The PIPS program requires submitting designers and contractors to evaluate the risks, and associated costs, and to propose a schedule, all means and methods for construction, and to specify a full contractual team of subcontractors and vendors. The best value for the University is selected from the submitted proposals based on cost (within budget), past performance as identified by a previous customer survey, risk management, safety record, and assigned project personnel experience.

Because this project is supported through the American Recovery and Reinvestment Act, UMN seeks to develop all Program Areas as quickly as possible. A single DB procurement provides the best value in terms of efficiency in NEPA evaluation, design, construction, and quality assurance. The structure of the contract will be such that pre-construction tasks are distinguished from construction tasks and only pre-construction tasks will be conducted prior to issuance of a FONSI.

Outcomes: A DB team will be selected through public competition.

Task 1.2 NEPA and Section 106 Assessments

Purpose: This task will involve conducting an Environmental Assessment and Historic Resources Review for the UMORE park to satisfy NEPA requirements on behalf of the Department of Energy.

Approach: A Memorandum of Understanding will be developed between DOE, UMN, and the DB team to perform the assessments required under the National Environmental Policy Act and Section 106 of the National Historic Preservation Act. The DB team will conduct this study.

Outcomes: The report will be posted in the public domain for comment. The goal is a FONSI and State Historic Preservation Office (SHPO) approval of Section 106 studies.

Task 1.3 Preliminary Design

Purpose: This task will involve the schematic design for all aspects of the turbine installation. The sub-tasks will be carried out by the DB team.

Approach: Preliminary design will occur over eight sub-task areas:

Subtask 1.3.1 Surveying
Subtask 1.3.2 Geotechnical Study Engineering
Subtask 1.3.3 Electrical Engineering and Design
Subtask 1.3.4 Foundation Engineering and Design
Subtask 1.3.5 Site Civil and Assessment
Subtask 1.3.6 Abatement Engineering (if required)
Subtask 1.3.7 Wind Resources Assessment
Subtask 1.3.8 Construction Review (by general contractor of DB team)

Outcomes: Preliminary development documents for the construction project.

Phase 2: Construction tasks

The following tasks will be initiated only after FONSI certification is received for the proposed turbine installation and site and DOE has released funds to proceed with final design and construction.

Task 1.4 Turbine Acquisition

Purpose: This task will involve the purchase of a 2.3 MW wind turbine for the UMORE site and development of terms and conditions of this purchase.

Approach: The UMN team will work with vendor to develop legal terms and conditions for the acquisition of the turbine. The agreement will include purchase of the turbine, turbine supply agreement, warranty, delivery to the installation site, and turbine commissioning.

Outcomes: Terms and condition for sale of wind turbine to the UMN including the Turbine Supply Agreement and warranty.

Task 1.5 Power Utility Interconnection Agreement

Purpose: This task will involve the development of interconnection agreement and power purchase agreement (PPA) with the local power utility.

Approach: UMN will work with the local power utility to develop a formal agreement for interconnection of the research turbine the power grid and for the operation of the turbine and any terms and condition for the purchase of power.

Outcomes: An interconnection agreement and PPA between UMN and the local power utility.

Task 1.6 Construction Cost Estimation and Subcontractor Team Development

Purpose: This task will involve the development of the full construction team, final project schedule, and final cost estimate for construction project.

Approach: Through the DB contract, the general contractor will conduct a public procurement process to assemble a subcontractor team that will carry out the construction of the turbine installation. Through this process, the UMN will be provided with a final cost estimate and schedule for the project and will be provided assurances on the quality of the construction team. This process follows the well-established procedures for Design/Build and will be overseen by UMN CPPM.

Outcomes: Establishment of construction team (general contractor + subcontractors), guaranteed maximum price for construction, and construction schedule.

Task 1.7: Final Design

Purpose: This task will involve development of final construction documents.

Approach: Using any additional information obtained since the completion of pre-construction phase and the issuance of the FONSI, the DB team will complete construction documents. The deliverable from this task will be final construction documents and final construction schedule. Final design will occur over the following eight subtask areas.

Subtask 1.6.1 Surveying (As-built)

Subtask 1.6.2 Geotechnical Study Engineering
Subtask 1.6.3 Electrical Engineering and Design
Subtask 1.6.4 Foundation Engineering and Design
Subtask 1.6.5 Site Civil and Assessment
Subtask 1.6.6 Abatement Engineering (if required)
Subtask 1.6.7 Wind Resources Assessment (Met tower siting and Installation)
Subtask 1.6.8 Construction Review (by general contractor of DB team)

Outcomes: The final construction documents and project schedule will be produced.

Task 1.8: Construction

Purpose: This task will involve all construction activities associated with site civil, foundation, electrical, erection, and commissioning of the research wind turbine.

Approach: The general contractor will coordinate the efforts of subcontractor team to execute the plans detailed in the construction documents. The UMN Capital Planning and Project Management team will monitor project schedule and budget throughout the duration of the task and will handle any change orders encountered during the process.

Outcomes: Installation, commissioning, and operation of 2.3MW wind turbine.

Task 1.9: Construction Project Closeout

Purpose: This task will involve the formal close-out of the project to verify the scope of activities were satisfied and all operational and maintenance information is transferred to the owner.

Approach: The UMN Energy Management team will perform commissioning with the engineer of record to confirm completion, fully operational with compliance to the original design intent and final contract scope compliance. The project will be transferred to the owner.

Outcomes: The project will be transferred to the University of Minnesota as owner.

Program Area 2: Research Program

The research projects funded by this specific grant are listed below as Task 2.1 through 2.7. Each of these projects includes laboratory, numerical, or field work that are discrete, independently valuable research projects. The research efforts do not depend on the larger action (facility construction) for their justification and have no impacts related to the proposed UMore Park facility. Therefore, these studies can begin prior to the completion of NEPA review for the proposed UMore Park wind turbine. Once the turbine is operational, the laboratory- and computational-based research will be field verified and expanded at the UMore Park site or at other DOE-funded utility-scale wind turbine research facilities.

Task 2.1: Increasing wind turbine output using vortex generators and riblets

Purpose: Develop and test passive flow control techniques based on riblets and vortex generators to maximize the recovery of potential energy at a given site by increasing peak efficiency and broadening the operating envelope of the rotor.

Approach: Perform wind tunnel experiments coupled with CFD simulations to determine optimal riblets and vortex generators arrangements. Validate the so-determined optimal solution on the 2.3MW turbine by comparing post- and pre-treatment wind turbine output.

Outcomes: Design guidelines and expected performance benefits for riblets and vortex generators and a CFD-based framework for turbine-specific implementation of passive flow control devices.

Task 2.2: Active flow control for improving aerodynamic performance and reducing noise

Purpose: Develop open and closed-loop active flow control strategies based on unsteady suction and/or blowing to: delay flow separation and stall in real time; and optimize the overall efficiency and minimize associated noise.

Approach: Carry out a series of wind tunnel experiments to test various active flow control strategies and identify most promising approaches; Use turbulence measurements upwind and downwind of the 2.3MW rotor, which will be obtained in task 2.5, to assess the state of the actual flow that needs to be

controlled and develop low-dimensional models; Couple this information with CFD modeling (to be carried out as part of tasks 2.3 and 2.5) and additional wind tunnel experiments to develop guidelines for implementing active flow control strategies in the field.

Outcomes: Develop methods and guidelines to guide future implementation of active flow control on the 2.3 MW turbine.

Task 2.3: High-resolution CFD-FSI code for aeroelastic simulations of turbine blades

Purpose: Develop a high-resolution Fluid-Structure Interaction (FSI) CFD code for aeroelastic calculations at field scale.

Approach: Couple high-resolution, rigid-blade CFD code with an advanced Finite Element model of the turbine blade. Validate the CFD-FSI code with both laboratory experiments and measurements from the field-scale facility.

Outcomes: A high-resolution computer code capable of aeroelastic FSI computations at field-scale that can be used as a tool for wind-turbine blade design. The code will be made available to DOE labs and the industry.

Task 2.4: Increasing wind turbine output by mitigating blade icing and fouling

Purpose: Maximize the recovery of potential energy at a given site by reducing turbine down time and mitigate the reduction in capacity factors caused by ice accumulation on blades. Increase wind plant safety by mitigating ice throws.

Approach: Develop a test system to measure ice-adhesion shear force and evaluate various ice-phobic blade coatings/films via wind tunnel experiments in the SAFL atmospheric wind tunnel.

Outcomes: Develop methods and guidelines for implementing de-icing coating and films at field scale.

Task 2.5: Multi-scale modeling for wind farm siting

Purpose: Develop and test novel CFD tools for the prediction of high-resolution wind and turbulence in the atmospheric boundary layer, and their interactions with wind turbines and wind farms. Provide a tool for science-based optimization of wind farm design.

Approach: Multi-scale modeling coupling meso-scale models with atmospheric LES and high-resolved CFD of turbine blades. Integration of wind tunnel experiments with detailed measurements in the field for model validation.

Outcomes: High-resolution Large Eddy Simulation framework for multi-scale simulations and site-specific optimization of wind farms.

Task 2.6: A Novel Power Electronics based Electrical Generation System for Wind Turbines

Purpose: Develop a novel electrical generation system for wind turbines using power electronics.

Approach: To connect the wind generator to the utility grid, the proposed system will replace the conventional 60-Hz transformer and the conventional converter system with a novel power-electronic-transformer technology, which uses a high-frequency transformer that can be smaller and lighter than a conventional 60-Hz transformer by a factor of 100 or higher. The lab prototype of such a system will be demonstrated at a 5-kVA power level.

Outcomes: Demonstrate that the proposed system results in a nacelle with significantly lighter weight and reduced volume, higher reliability and efficiency. Develop a final report that outlines the results of the sub-scale power electronics package and explains how it can be scaled to a utility scale turbine and the overall benefits.

Task 2.7: Radar interactions with wind turbines

Purpose: Minimize or eradicate the negative impacts wind farms have on FAA and weather radars.

Approach: Understand the nature of clutter and develop active and/or passive mitigation techniques, including development of new generation of high spectral resolution radar signal processors to provide discrimination against this emerging source of clutter. Study mitigation techniques at a field scale radar

facility. Extend results of mitigation techniques to address the needs of the National Oceanic and Atmospheric Administration.

Outcomes: Development and field demonstration of new clutter mitigation techniques and signal processing algorithms for FAA and weather radars.

Program Area 3: Curriculum Development

As with the research described in Program Area 2, much of the proposed curriculum development is discrete and independent from the UMore Park turbine construction itself. The curriculum development would be a Categorical Exclusion under applicable DOE NEPA regulations, and its development does not depend on construction of the UMore Park facility for its justification. The curriculum could be developed and used in concert with other research turbine facilities if necessary. Since curriculum development is a discrete project that is independent from turbine construction, it can begin prior to the completion of NEPA review. However, once the turbine is operational, the curriculum will be facilitated greatly by turbine construction and the installation of related monitoring equipment.

Task 3.1 Curriculum Development

Purpose: Develop educational programs aimed at preparing the workforce on the national scale to meet the challenges in harnessing wind energy, smart delivery that includes new transmission, storage and smart-grid technologies, and efficient end-use.

Approach: Develop a wide range of course modules spanning the entire range of topics that are relevant to the wind industry, including: aerodynamics of wind turbines; wind farm siting; structural dynamics of turbine rotors, towers and foundations; mechanical transmission systems; electric generator systems; transmission lines; diagnostics and preventive maintenance of wind turbines, grid integration and distributed storage, environmental aspects of wind power, etc. Students will have the opportunity to participate in field demonstration project at the consortium field site and intern at our affiliated companies.

Outcomes: A flexible and multi-purpose internet-based, undergraduate or graduate level curriculum on wind energy that can be used to train engineering students both at the UMN and across the nation.

Department of Energy
Golden Field Office
1617 Cole Boulevard
Golden, Colorado 80401-3393

DOE/EA-1791

FINDING OF NO SIGNIFICANT IMPACT

UNIVERSITY OF MINNESOTA

WIND ENERGY RESEARCH CONSORTIUM PROJECT

AGENCY: U.S. Department of Energy, Golden Field Office

ACTION: Finding of No Significant Impact (FONSI)

SUMMARY: The U. S. Department of Energy (DOE) is proposing to authorize the expenditure of Federal funding by the University of Minnesota to design, permit, and construct a wind turbine research facility[1]. This funding has been appropriated under the *American Recovery and Reinvestment Act of 2009.* The University would use the funding to install a wind turbine research facility at its University of Minnesota Outreach Research and Education (UMore) Park in Rosemount, Minnesota. The proposed research facility would consist of a 2.5-megawatt-capacity Clipper Liberty C-100 wind turbine with a total height of 426.5 feet, a meteorological tower of similar height, a 34.5-kilovolt interconnection low-voltage transmission line, a data transfer line, and two short access roads. A portion of the DOE-awarded funding would also be used for turbine and technical research activities.

DOE has completed all discussion, analysis, and findings related to the potential impacts of the proposed project, including the applicant-committed measures, and completed the *Final Environmental Assessment for the University of Minnesota Wind Energy Research Consortium Project* (DOE/EA-1791; Final EA). The Final EA is hereby incorporated by reference.

DOE prepared this FONSI in accordance with the *National Environmental Policy Act* (42 U.S.C. 4321 *et seq.*; NEPA), the Council on Environmental Quality NEPA regulations (40 CFR Parts 1500 to 1508), and DOE's NEPA implementing procedures (10 CFR Part 1021).

ENVIRONMENTAL IMPACTS: The Final EA examined the potential environmental impacts of DOE's Proposed Action to authorize the University of Minnesota to expend Recovery Act funding for a wind turbine research facility and also examined a No-Action Alternative. Under the No-Action Alternative, DOE would not authorize the University of Minnesota to spend

1. Prior to the issuance of this FONSI, DOE has authorized the University to use a percentage of the Federal funding for preliminary activities, which include preparing this EA, conducting analysis, and consulting with regulatory agencies. Such activities are associated with the Proposed Action and do not significantly impact the environment or represent an irreversible or irretrievable commitment by DOE in advance of its conclusion of the potential environmental impacts from the proposed project.

Federal funds on the proposed project and DOE assumed, for purposes of the EA, that the research facility would not be constructed or operated without this financial assistance.

The wind turbine, meteorological tower, transmission line, and other required infrastructure would be located entirely on property owned by the University of Minnesota. Although energy production is not the primary goal of the project, the wind turbine would be connected to the electrical transmission grid. The wind turbine and other infrastructure are expected to have a useful life of 15 years. Construction of all project components would disturb approximately 1 acre; 0.4 acre would be temporary (i.e., during construction) and 0.6 acre would be permanent (i.e., during the 15-year operational life).

Emissions of air pollutants during construction of the wind turbine and other project components would be minimal and temporary, and there would be no emissions during project operations. No surface waterbodies, wetlands, or floodplains would be disturbed, and groundwater, which is much deeper than the proposed foundation depths, would not be affected. No recreational resources are located on the project site. The project would not result in a detectable increase in traffic or require a change in traffic circulation. The turbine and meteorological tower would not present an obstruction to air navigation and would not interfere with long-range radar operations. Additionally, the proposed project would have no impact on any public utility services or communication corridors, and no evidence of contaminants were found in the project site during extensive soil surveys. Therefore, DOE concludes that the project would have no impacts, or minimal impacts, on air quality, water resources, recreational resources, transportation, utilities, and hazardous materials.

Soils at the project site are not very erosive and there would be little erosion or sediment runoff during construction. The project would not adversely affect the availability of prime farmland soils or production of agricultural products in the region. The project would have no impact on primary geologic resources including economically viable deposits of sand and gravel. DOE concludes that the impacts to geology and soils from both construction and operation activities associated with the proposed project would be minor.

The closest potentially affected receptors are residences located about 3,200 to 3,600 feet from the turbine site. At those residences, flickering shadows cast by the turbine would be diffuse and at least partially blocked by surrounding trees. Sound levels from the turbine would be below background levels at the residences, and would comply with the State standard for residential buildings. DOE, therefore, concludes that the project would result in minor adverse effects from shadow flicker and noise.

The turbine is designed to automatically shut down when ice is detected on the blades, and there are no occupied structures within the area onto which ice on the blades might fall. Thus, the risk of harm from ice throw would be negligible.

The project site is primarily cultivated. Conflicts between the project and ongoing land uses are not anticipated. The University, in cooperation with the City of Rosemont, would evaluate all

proposed future land uses to ensure that those proposals are safe and compatible with operation of the turbine. This may result in some proposed uses, such as residential development, being delayed or prohibited from the immediate vicinity of the wind turbine.

The addition of the turbine and meteorological tower would not create a substantial change in the viewshed because there are numerous tall, modern structures in the surrounding area, including water towers, antennae, power lines, and the towers and stacks at a nearby refinery.

The wind turbine and meteorological tower would be located outside of migratory flyways, breeding areas, and designated natural resource areas. The project site does not have high-quality habitat for wildlife, and the project would not result in habitat fragmentation. Trees would be removed from an approximately 25-acre area around the wind turbine to reduce interference with operation of the wind turbine and meteorological tower. Trees in the area occur at low density in narrow strips and small stands, and their removal would have a negligible adverse effect on birds and other wildlife. Some birds and bats probably would collide with and be injured or killed by the meteorological tower and operating turbine. DOE anticipates that the number of birds and bats killed would be similar to or less than the number of mortalities at other wind turbines in the Midwest. Contingent on the availability of funding, the University plans to develop and implement a post-construction bird and bat fatality monitoring plan under the guidance of the U.S. Fish and Wildlife Service and Minnesota Department of Natural Resources.

The proposed project would not affect any species listed as threatened or endangered under the *Endangered Species Act*. One State-threatened bird species, the loggerhead shrike, might occur within or near the project area. That area and immediate vicinity have limited suitable habitat for shrikes, and no shrikes or evidence of their prey or nests were detected during a survey of the project site in 2010. DOE thus concludes that the proposed project would have a negligible impact on this species.

There are no archaeological sites or historic properties listed, or eligible for listing, on the *National Register of Historic Places* within the project area. One historical property, the Edmund H. Knodt Farm, is 0.65 mile from the turbine site and is eligible for listing on the National Register. The wind turbine would be a visible and prominent feature when viewed from the farm and would be out of scale with the surrounding landscape. Because the turbine could alter the setting and feeling of the landscape, the proposed project has the potential to cause an indirect adverse visual effect to the farmstead. To comply with Section 106 of the *National Historic Preservation Act*, DOE consulted with the Minnesota State Historic Preservation Officer and developed a Memorandum of Agreement that identified measures to mitigate this potential adverse effect.

There would be no unusual or potentially unacceptable hazards or risks to construction workers, who would be trained to operate under a site-specific safety program and procedures. During operation, access to the turbine would be limited to maintenance workers and University staff and researchers; therefore, no public health and safety issues are anticipated.

The proposed project could have a minor, short-term economic benefit during construction and might have longer-term impacts on growth and development linked to the expansion of renewable energy research opportunities. DOE concludes that no significant adverse impacts would occur to any members of the communities in or near the project area; therefore, there would be no adverse and disproportional impacts on minority or low-income populations.

DOE evaluated the cumulative impacts of the proposed project and other past, present, and reasonably foreseeable projects in the area, including UMore Park's plans for future development, area mining and gravel projects, and transportation improvement projects. DOE concluded that the proposed project, in conjunction with other activities considered, would have negligible cumulative impacts on all resources considered within the Final EA.

PUBLIC PARTICIPATION IN THE EA PROCESS: DOE sent scoping letters on June 3, 2010, to Federal, State, and local agencies; Tribal governments; businesses; organizations; special interest groups; and interested individuals, providing 15 days to comment on the scope of the EA. DOE published the Scoping Notice on the DOE Golden Field Office Public Reading Room Website and in five local newspapers. In response to the Scoping Notice, DOE received comment letters from six agencies. All comments received, and DOE's responses as appropriate, are included in the Final EA.

DOE issued the Draft EA for comment on January 28, 2011, and posted it on the DOE Golden Field Office Public Reading Room Website. DOE sent postcards announcing the availability of the Draft EA to identified stakeholders and published a Notice of Availability on the Website. The comment period ended on February 15, 2011. The City of Rosemont requested clarification about how the project would be developed and decommissioned, and how it might affect future use of surrounding areas. The U.S. Fish and Wildlife Service suggested that the University monitor the impacts of the wind turbine and meteorological tower on birds and bats and requested that trees not be removed when birds are nesting. The EA was modified to address these comments. DOE also received letters from the Minnesota Pollution Control Agency and Dakota County stating that those organizations had no comments on the EA.

DETERMINATION: Based on the information presented in the Final EA (DOE/EA-1791), DOE has determined that its Proposed Action, funding the design, permitting, and construction of the University of Minnesota wind turbine research facility, does not constitute a major Federal action significantly affecting the quality of the human environment within the context of NEPA. Therefore, the preparation of an environmental impact statement is not required, and DOE is issuing this FONSI.

The University of Minnesota's commitment to obtain and comply with all appropriate Federal, State, and local permits required for construction and operation of the wind turbine research facility, and to minimize potential impacts through the implementation of best management practices and their Applicant Committed Actions detailed in the Final EA, shall be incorporated and enforceable through DOE's financial assistance agreement. The Final EA is available at the

DOE Golden Field Office Reading Room Website
http://www.eere.energy.gov/golden/Reading_Room.aspx , and the DOE NEPA Website, http://nepa.energy.gov.

For questions about this FONSI, contact:

Laura Margason
NEPA Document Manager
U.S. Department of Energy
DOE Golden Field Office
1617 Cole Boulevard
Golden, Colorado 80401
Laura.Margason@go.doe.gov

For further information about the DOE NEPA process, contact:

Office of NEPA Policy and Compliance
U.S. Department of Energy
1000 Independence Avenue, SW
Washington, DC 20585
202-685-4600 or 1-800-472-2756

Issued in Golden, Colorado this 9th day of March, 2011

Carol J. Battershell
Golden Field Office Manager

Appendix C: Site Survey

SITE SURVEY
~ FOR ~
# UNIVERSITY OF MINNESOTA
~ OF ~
# WIND ENERGY RESEARCH CONSORTIUM PROJECT

LEGEND

- ⚥ = HYDRANT
- Ⓜ = MANHOLE
- Ⓔ = ELECTRIC MANHOLE
- Ⓣ = TELEPHONE MANHOLE
- Ⓢ = SANITARY SEWER MANHOLE
- Ⓓ = STORM SEWER MANHOLE
- ▣ = CATCH BASIN
- ▫ = ELECTRIC BOX
- ☼ = LIGHT
- ⊕ = SIGNAL POLE
- —W— = DENOTES WATER LINE
- —S— = DENOTES SANITARY SEWER LINE
- —ST— = DENOTES STORM SEWER LINE
- —UP— = DENOTES UTILITY POLE
- ⊗ = DENOTES LATH SET BY OTHERS
- —P-BUR— = DENOTES UNDERGROUND ELECTRIC LINE
- —P-OH— = DENOTES OVERHEAD ELECTRIC LINE
- —G— = DENOTES UNDERGROUND GAS LINE
- —T-BUR— = DENOTES UNDERGROUND PHONE LINE
- T = DENOTES TELEPHONE PEDESTAL
- E = DENOTES ELECTRIC TRANSFORMER
- TV = DENOTES CABLE TV BOX
- = DENOTES UTILITY POLE GUY WIRE
- = DENOTES GATE VALVE
- ---863--- = DENOTED EXISTING CONTOUR
- x 863.15 = DENOTED EXISTING SPOT ELEVATIONS
- ● = DENOTED MONUMENT FOUND
- ◎ = DENOTED MONUMENT SET
- △ = DENOTED CONTROL MONUMENT
- ◉ = DENOTED CAST IRON MONUMNET

SITE CONTROL

Dakota County Coordinate System
Horizontal NAD-83 (1986 adjustment)
Vertical NAVD 88

NAME	NORTHING	EASTING	ELEVATION	DESCRIPTION
No. 4	194870.73	568010.96	947.80	Northwest Corner Section 36 Township 115 Range 19
No. 5	197500.36	568035.06	916.60	West Quarter Corner Section 25 Township 115 Range 19
No. 10	193971.60	569684.41	927.79	"HAA" Control Point
No. 11	193307.17	569553.03	928.39	"HAA" Control Point
No. 12	193186.93	570062.21	927.25	"HAA" Control Point

NOTES

1. The underground utilities shown have been located from field survey information and exhibiting drawings. The surveyor makes no guarantees that the underground utilities shown comprise all such utilities in the area, either in service or abandoned. The surveyor further does not warrant that the underground utilities shown are in the exact location indicated although he does certify that they are located as accurately as possible from information available. The surveyor has not physically located the underground utilities. Prior to any excavation, contact Gopher State One Call for an on-site location (612-454-0002). The subsurface utility information on this survey is utility quality level D. This quality level was determined according to the guidelines of CI/ASCE 38-2, entitled "Standard Guidelines for the Collection and Depiction of Existing Subsurface Utility Data.

2. Gopher State One-call Ticket Number 100339768

District Code	Company Name	Marking Concerns	Damage/Repair	Customer Service
CRSMNT01	CITY OF ROSEMOUNT	(651)423-4411	(651)423-4491	(651)423-4411
FRTIER02	FRONTIER COMMUNICATIONS	(763)682-3514	(612)510-7969	(763)682-3514
MERC38	MINNESOTA ENERGY RESOURCES	(800)889-9508	(612)889-4970	(800)889-9508
METWAS01	METRO WASTE COMMISSION	(651)602-4511	(651)602-4511	(651)602-4511
QLNMN14	QWEST	(866)861-7678	(800)573-1311	(866)861-7678
XCIEL03	XCEL ENERGY	(651)229-2427	(651)229-2427	(651)229-2427
ZAYO01	ZAYO BANDWIDTH	(515)225-2520	(888)634-7701	(515)225-2520

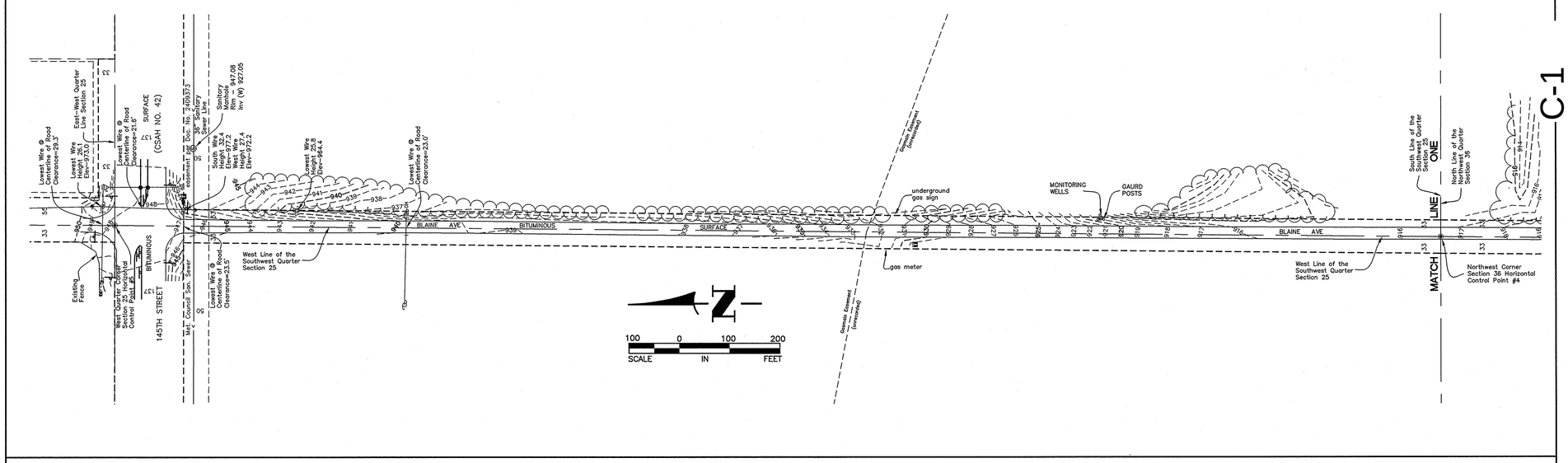

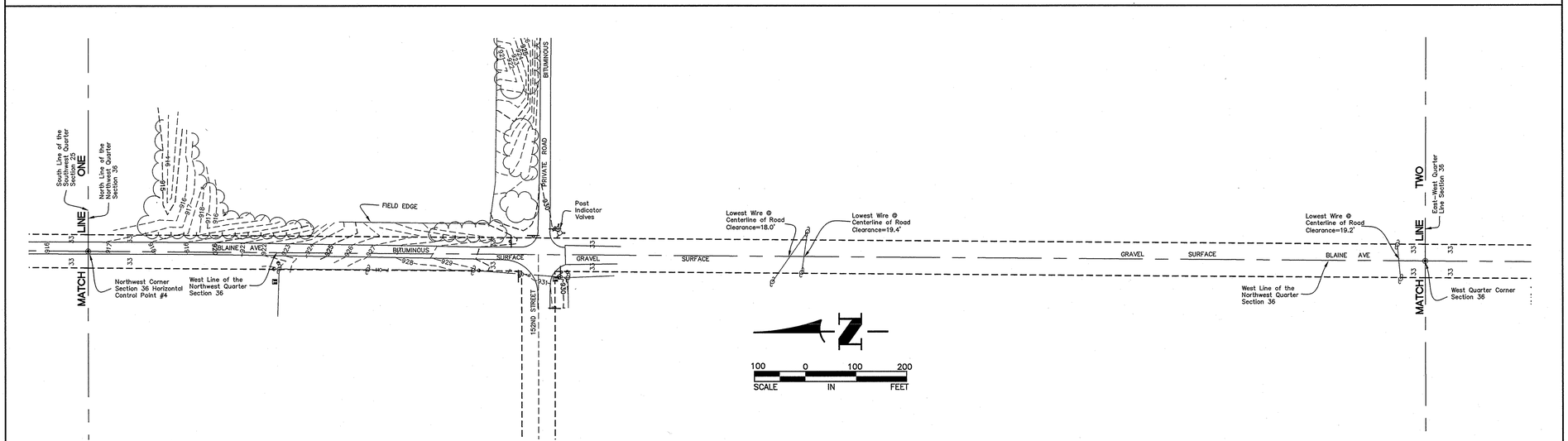

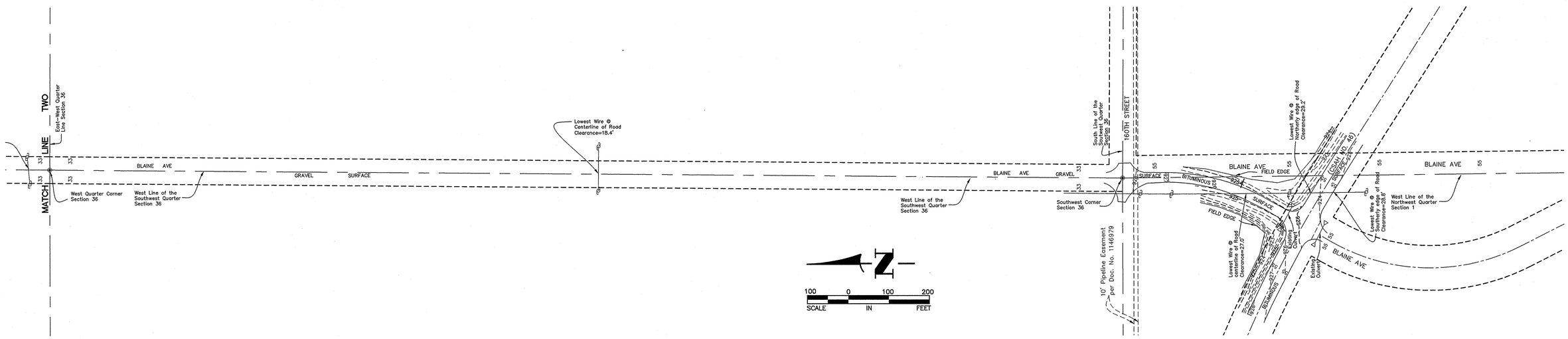

DATE	REVISION	DATE	REVISION
08/24/10	additional topo @ Blaine/CR46 intersection		

Aug 24, 2010 - 11:29am
K:\civil_surv\Land Desktop 2008\2261.126\dwg\2261126BA.dwg

I hereby certify that this survey, plan or report was prepared by me or under my direct supervision and that I am a duly Licensed Professional Land Surveyor under the laws of the State of Minnesota.
Charles R. Christopherson
Date 07/28/10 Lic. No. 18420

DESIGNED BY:	BOOK/PAGE:
BRP	
DRAWN BY:	DATE:
BRP	07/28/10
CHECKED BY:	FILE NO.
CRC	2261.126

Hakanson Anderson Assoc., Inc.
Civil Engineers and Land Surveyors
3601 Thurston Ave., Anoka, Minnesota 55303
763-427-5860 FAX 763-427-0520
www.haa-inc.com

UNIVERSITY OF MINNESOTA

SITE SURVEY
FOR
UNIVERSITY OF MINNESOTA
OF
Wind Energy Research Consortium Project

SHEET 1 OF 2

C-1

SITE SURVEY
~ FOR ~
# UNIVERSITY OF MINNESOTA
~ OF ~
# WIND ENERGY RESEARCH CONSORTIUM PROJECT

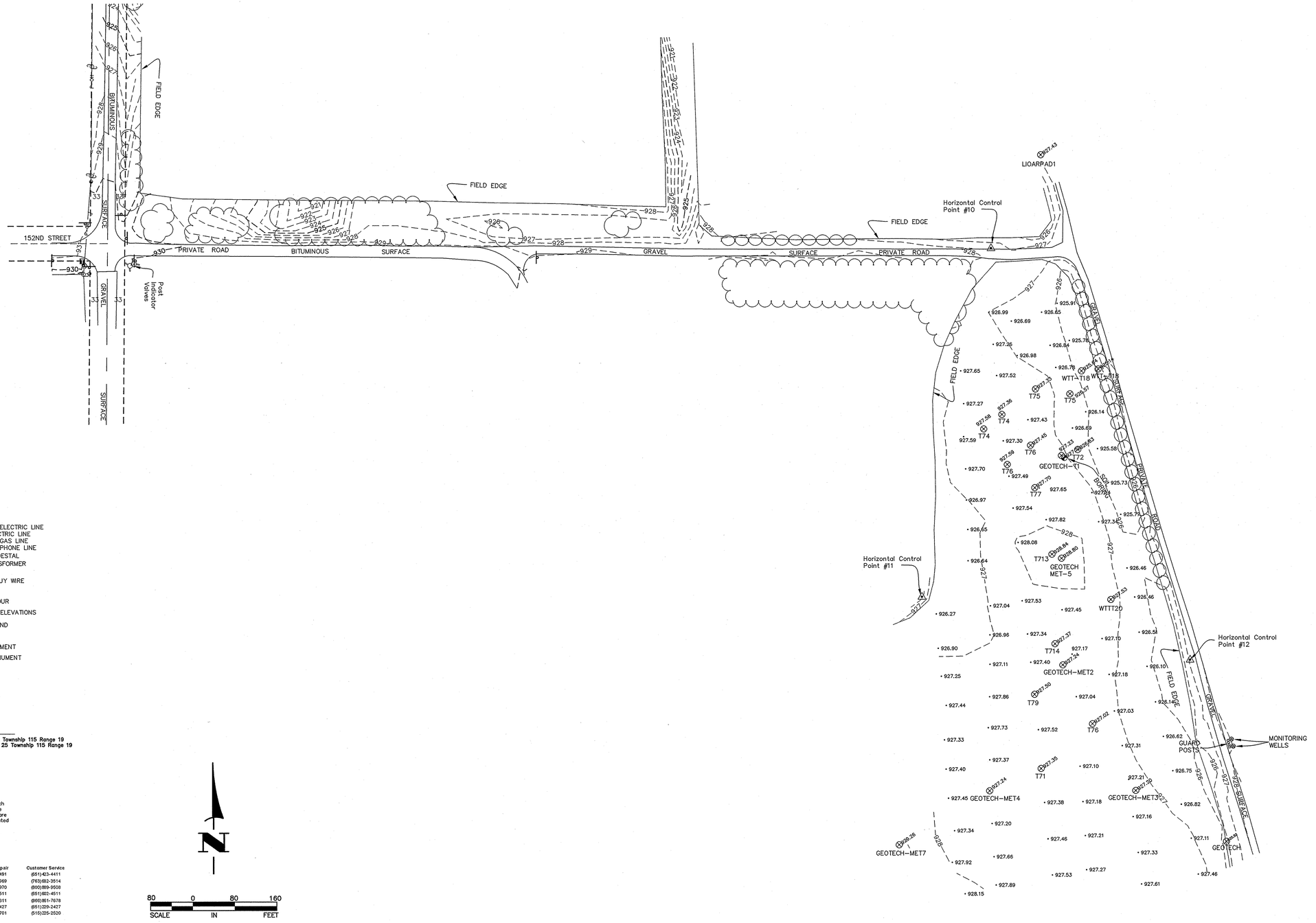

LEGEND

- = HYDRANT
- = MANHOLE
- = ELECTRIC MANHOLE
- = TELEPHONE MANHOLE
- = SANITARY SEWER MANHOLE
- = STORM SEWER MANHOLE
- = CATCH BASIN
- = ELECTRIC BOX
- = LIGHT
- = SIGNAL POLE
- = DENOTES WATER LINE
- = DENOTES SANITARY SEWER LINE
- = DENOTES STORM SEWER LINE
- = DENOTES UTILITY POLE
- = DENOTES LATH SET BY OTHERS
- = DENOTES UNDERGROUND ELECTRIC LINE
- = DENOTES OVERHEAD ELECTRIC LINE
- = DENOTES UNDERGROUND GAS LINE
- = DENOTES UNDERGROUND PHONE LINE
- = DENOTES TELEPHONE PEDESTAL
- = DENOTES ELECTRIC TRANSFORMER
- = DENOTES CABLE TV BOX
- = DENOTES UTILITY POLE GUY WIRE
- = DENOTES GATE VALVE
- = DENOTED EXISTING CONTOUR
- = DENOTED EXISTING SPOT ELEVATIONS
- = DENOTED MONUMENT FOUND
- = DENOTED MONUMENT SET
- = DENOTED CONTROL MONUMENT
- = DENOTES CAST IRON MONUMENT

SITE CONTROL

Dakota County Coordinate System
Horizontal NAD-83 (1986 adjustment)
Vertical NAVD 88

NAME	NORTHING	EASTING	ELEVATION	DESCRIPTION
No. 4	194870.73	568010.96	947.80	Northwest Corner Section 36 Township 115 Range 19
No. 5	197500.36	568035.06	916.60	West Quarter Corner Section 25 Township 115 Range 19
No. 10	193971.60	569684.41	927.79	"HAA" Control Point
No. 11	193307.17	569553.03	928.39	"HAA" Control Point
No. 12	193186.93	570062.21	927.25	"HAA" Control Point

NOTES

1. The underground utilities shown have been located from field survey information and exhibiting drawings. The surveyor makes no guarantees that the underground utilities shown comprise all such utilities in the area, either in service or abandoned. The surveyor further does not warrant that the underground utilities shown are in the exact location indicated although he does certify that they are located as accurately as possible from information available. The surveyor has not physically located the underground utilities. Prior to any excavation, contact Gopher State One Call for an on-site location (612-454-0002). The subsurface utility information on this survey is utility quality level D. This quality level was determined according to the guidelines of CI/ASCE 38-2, entitled "Standard Guidelines for the Collection and Depiction of Existing Subsurface Utility Data.

2. Gopher State One-call Ticket Number 100339768

District Code	Company Name	Marking Concerns	Damage/Repair	Customer Service
CRSMNT01	CITY OF ROSEMOUNT	(651)423-4411	(651)423-4491	(651)423-4411
FRTIER02	FRONTIER COMMUNICATIONS	(763)682-3514	(612)510-7969	(763)682-3514
MERC38	MINNESOTA ENERGY RESOURCES	(800)889-9508	(800)889-4970	(800)889-9508
METWAS01	METRO WASTE COMMISSION	(651)602-4511	(651)602-4511	(651)602-4511
QLNMN14	QWEST	(866)861-7678	(800)573-1311	(866)861-7678
XCEL03	XCEL ENERGY	(651)229-2427	(651)229-2427	(651)229-2427
ZAYC01	ZAYO BANDWIDTH	(518)225-2520	(888)634-7701	(518)225-2520

DATE	REVISION	DATE	REVISION
08/24/10	additional topo @ Blaine/CR46 intersection		

Aug 24, 2010 - 1:45pm
K:\cad_surv\Land Desktop 2008\2261.126\dwg\2261126BA.dwg

I hereby certify that this survey, plan or report was prepared by me or under my direct supervision and that I am a duly Licensed Professional Land Surveyor under the laws of the State of Minnesota.

Charles R. Christopherson
Date 07/28/10 Lic. No. 18420

DESIGNED BY: BRP	BOOK/PAGE:
DRAWN BY: BRP	DATE: 07/28/10
CHECKED BY: CRC	FILE NO. 2261.126

Hakanson Anderson Assoc., Inc.
Civil Engineers and Land Surveyors
3601 Thurston Ave., Anoka, Minnesota 55303
763-427-5860 FAX 763-427-0520
www.haa-inc.com

UNIVERSITY OF MINNESOTA

SITE SURVEY
FOR
UNIVERSITY OF MINNESOTA
OF
Wind Energy Research Consortium Project

SHEET 2 OF 2

12/02/2011
RECORD DRAWING

NO.	BY	CHK.	APP.	DATE	REVISION DESCRIPTION
▲	DMD	DVS	DVS	12/02/11	RECORD DRAWING

I HEREBY CERTIFY THAT THIS PLAN, SPECIFICATION, OR REPORT WAS PREPARED BY ME OR UNDER MY DIRECT SUPERVISION AND THAT I AM A DULY LICENSED PROFESSIONAL ENGINEER UNDER THE LAWS OF THE STATE OF MINNESOTA.
SIGNATURE Dean V. Skallman
PRINTED NAME DEAN V. SKALLMAN
DATE 04/01/2011 REG. NO. 016157

RELEASED TO/FOR	A	B	C	0	1	2	3
CLIENT							
BID				02/23/11			
CONSTRUCTION					04/01/11		
RECORD						12/02/11	
DATE RELEASED							

BARR
Corporate Headquarters:
Minneapolis, Minnesota
Ph: 1-800-632-2277

Project Office:
BARR ENGINEERING CO.
4700 WEST 77TH STREET
MINNEAPOLIS, MN.
55435-4803
Ph: 1-800-632-2277
Fax: (952) 832-2601
www.barr.com

Scale	AS SHOWN
Date	06/07/10
Drawn	DMD
Checked	DVS
Designed	DVS
Approved	

RYAN COMPANIES US, INC.
MINNEAPOLIS, MINNESOTA

UMORE PARK RESEARCH WIND TURBINE
DAKOTA COUNTY, MINNESOTA

SITE MAP

BARR PROJECT No. 23/19-1060
CLIENT PROJECT No.
DWG. No. C-01R
REV. No. 1

12/02/2011
FOR RECORD

NO.	BY	CHK.	APP.	DATE	REVISION DESCRIPTION
▲	DMD	DVS	DVS	12/02/11	RECORD DRAWING

I HEREBY CERTIFY THAT THIS PLAN, SPECIFICATION, OR REPORT WAS PREPARED BY ME OR UNDER MY DIRECT SUPERVISION AND THAT I AM A DULY LICENSED PROFESSIONAL ENGINEER UNDER THE LAWS OF THE STATE OF MINNESOTA.

SIGNATURE Dean V Skallman

PRINTED NAME DEAN V. SKALLMAN

DATE 04/01/2011 REG. NO. 016157

	A	B	C	0	1	2	3
CLIENT							
BID				03/02/11			
CONSTRUCTION					04/01/11		
RECORD						12/02/11	
RELEASED TO/FOR	DATE RELEASED						

BARR
Corporate Headquarters:
Minneapolis, Minnesota
Ph: 1-800-632-2277

Project Office:
BARR ENGINEERING CO.
4700 WEST 77TH STREET
MINNEAPOLIS, MN.
55435-4803
Ph: 1-800-632-2277
Fax: (952) 832-2601
www.barr.com

Scale	AS SHOWN
Date	06/07/10
Drawn	DMD
Checked	DVS
Designed	DVS
Approved	DVS

RYAN COMPANIES US, INC.
MINNEAPOLIS, MINNESOTA

UMORE PARK RESEARCH WIND TURBINE
DAKOTA COUNTY, MINNESOTA

TREE REMOVAL
SITE MAP

BARR PROJECT No. 23/19-1060
CLIENT PROJECT No.
DWG. No. C-04R
REV. No. 1